The Development of PET Techniques to Study the 5-HT_{1A} System

by

Dustin W. Wooten

A dissertation submitted in partial fulfillment of the requirements for the degree of

Doctor of Philosophy

(Medical Physics)

at the

UNIVERSITY OF WISCONSIN-Madison

2013

Date of final oral examination: 4/16/2013

The dissertation is approved by the following members of the Final Oral Committee:

Bradley T. Christian, Associate Professor, Medical Physics

Robert J. Nickles, Professor, Medical Physics

James E. Holden, Professor, Medical Physics

Onofre T. DeJesus, Professor, Medical Physics

Rasmus M. Birn, Assistant Professor, Psychiatry

ACKNOWLEDGEMENTS

First, I would like to thank my advisor Brad Christian. I am honored to have had the privilege and opportunity to study under him, and I thank him for unending support, encouragement, and guidance. He has made this journey enjoyable with his ability to explain complex issues while maintaining focus on the overall picture. I am forever grateful.

Next I want to thank all of my colleagues at the wonderful University of Wisconsin – Madison who have made this body of work possible. I am forever in their debt. Specifically, I would like to thank the Cyclotron Gang for their support. I want to thank Jerry Nickles for his guidance and approachability; Todd Barnhart and Jonathan Engle for their endless supply of ^{18}F, ^{11}C, home brew, and good humor; Dhanabalan Murali for all of his assistance and advice regarding radiochemistry; Jim Holden for keeping me on my toes; and Barb Mueller, the "mom" of the PET group, for her endless support to everyone in the lab. Finally, I am thankful to Onofre DeJesus, Rasmus Birn, Alex Converse, Nick Vandehey, Jeff Moirano, Elizabeth Ahlers, Max Slesarev, Pat Lao, Andrew Higgins, and Julie Larson for all of their assistance.

A special thanks is extended to Ansel Hillmer. He has been there every step of the way offering insight, support, and good humor making the time in the lab enjoyable. The tandem parties and sunny Fridays at the terrace will be missed.

I am also grateful to Jogesh Mukherjee and Neil Saigal at the University of California – Irvine for their supply of mefway precursor and chemistry advice. Without their efforts this work would not have been possible.

Finally, I would like to thank my family and my friends. Their love and support has made this journey possible, and I am deeply indebted to them. I would like to thank my parents, Bill and Barb Wooten, for values that they have instilled upon me including the appreciation for learning.

Next, I would like to thank my sister Janelle Wooten for all of her support throughout the years and the laughter she has provided. Lastly, I want to thank Keslie Stricker for her wonderful and endless inspiration and encouragement.

TABLE OF CONTENTS

LIST OF TABLES

LIST OF FIGURES

ABSTRACT

The serotonin$_{1A}$ (5-HT$_{1A}$) system has been implicated in a wide variety of neuropsychiatric disorders. PET imaging provides an excellent method of analyzing 5-HT$_{1A}$ physiology. This thesis focuses on the development [^{18}F]MeFWAY, laying the groundwork for translation into humans, and two of its isomers for PET assay of the 5-HT$_{1A}$ system. As presented, [^{18}F]MeFWAY exhibits desired in vivo imaging properties similar to the commonly used 5-HT$_{1A}$ PET antagonist [^{11}C]WAY-100635 providing the advantage of the longer lived ^{18}F label and simpler radiosynthesis. Furthermore, the [^{18}F]MeFWAY isomers demonstrate characteristics of potential use for measuring changes in endogenous 5-HT competition. Lastly, results will show the utility of [^{18}F]MeFWAY for in vivo measurement of receptor density (B_{max}) and affinity ($1/K_{Dapp}$) indicating separate measurements of B_{max} and K_{Dapp} are more sensitive to group differences than the widely used binding potential alone.

Chapter 1 Introduction

Positron emission tomography (PET) is a valuable imaging modality capable of measuring physiological and chemical processes in vivo; e.g., fluctuations in receptor systems. [^{18}F]MeFWAY is a PET radiotracer with high specificity and selectivity for the serotonin$_{1A}$ or 5-hydroxytryptamine$_{1A}$ (5-HT$_{1A}$) receptor and is capable of detecting disruptions in the 5-HT$_{1A}$ receptor system (Christian et al., 2013). Disruptions in the 5-HT$_{1A}$ system have been associated with a wide range of neuropsychiatric illnesses, primarily mood and anxiety related disorders such as depression (Heisler et al., 1998; Gingrich and Hen, 2001; Neumeister et al., 2004; Terry et al., 2008). It is important to develop the tools and methodologies necessary to conduct research capable of detecting the underlying characteristics of the 5-HT$_{1A}$ system such as changes in receptor density or affinity states caused by environmental and genetic factors. A better understanding of the 5-HT$_{1A}$ system will aid the development of therapies to target specific ailments attributed to the serotonin system. The work presented in this thesis focuses on development of PET techniques and [^{18}F]MeFWAY to examine distribution of 5-HT$_{1A}$ receptors throughout the brain.

1.1. Physiology of the serotonin system and the 5-HT$_{1A}$ receptor

The serotonin system consists of seven receptor subfamilies and is composed of 14 receptor subtypes. Some 5-HT receptors exhibit an inhibitory response (5-HT_1, 5-HT_5) and others an excitatory response (5-$HT_{(2-4)}$, 5-$HT_{(2-4)}$) (Nichols and Nichols, 2008). The 5-HT_{1A} subtype is expressed presynaptically as somatodentritic autoreceptors in the raphe nuclei located in the brain stem (Azmitia and Whitaker-Azmitia, 1991). Activation of the somatodentritic autoreceptors has an inhibition effect, decreasing cell firing postsynaptically, therefore reducing serotonin synthesis and release throughout the cortex. Postsynaptic 5-HT_{1A} receptors are expressed at high density in areas of the limbic system including the hippocampus and throughout the cortical areas such as the cingulate gyrus, frontal cortex, and temporal cortex.

The serotonin system is believed to play a major role in depression and is often the target of antidepressant drugs such as selective serotonin reuptake inhibitors (SSRIs). The 5-HT_{1A} receptor is a major regulator of functions of the serotonin system including anxiety and panic, food intake, mood, and thermoregulation (Duncan, 2002). The 5-HT_{1A} system has also been associated to the neuropsychiatric illnesses of panic disorder (Neumeister et al., 2004) and post-traumatic stress disorder (Bryant et al., 2010).

1.2. 5-HT_{1A} receptor distribution

In vitro measurements of 5-HT_{1A} receptor density have been performed on postmortem tissue primarily using tritiated forms of 8-OH-DPAT and WAY-100635 (Dillon et al., 1991; Matsubara et al., 1991; Burnet et al., 1997; Hall et al., 1997; Khawaja, 1995; Palego et al., 1997). Both compounds bind selectively to 5-HT_{1A} receptors, however, 8-OH-DPAT behaves as an agonist while WAY-100635 behaves as an antagonist. High to medium 5-HT_{1A} receptor densities have been found in the CA1 field of the hippocampus (113 fmol/mg), raphe nuclei (50.3 fmol/mg),

insula cortex (50.8 fmol/mg), cingulate cortex (73 fmol/mg), frontal cortex (73 fmol/mg), and temporal cortex (78.6 fmol/mg) (Hall et al., 1997).

PET has been used to measure 5-HT_{1A} receptor distribution throughout the brain. The most common 5-HT_{1A} PET tracer, based on WAY-100635, is [Carbonyl-^{11}C]WAY-100635 which is shown in Figure 1-1 (Pike et al., 1996). [^{11}C]WAY-100635 has high affinity and specificity for the 5-HT_{1A} receptor (Kumar and Mann, 2007). Using [^{11}C]WAY-100635 for 5-HT_{1A} receptor

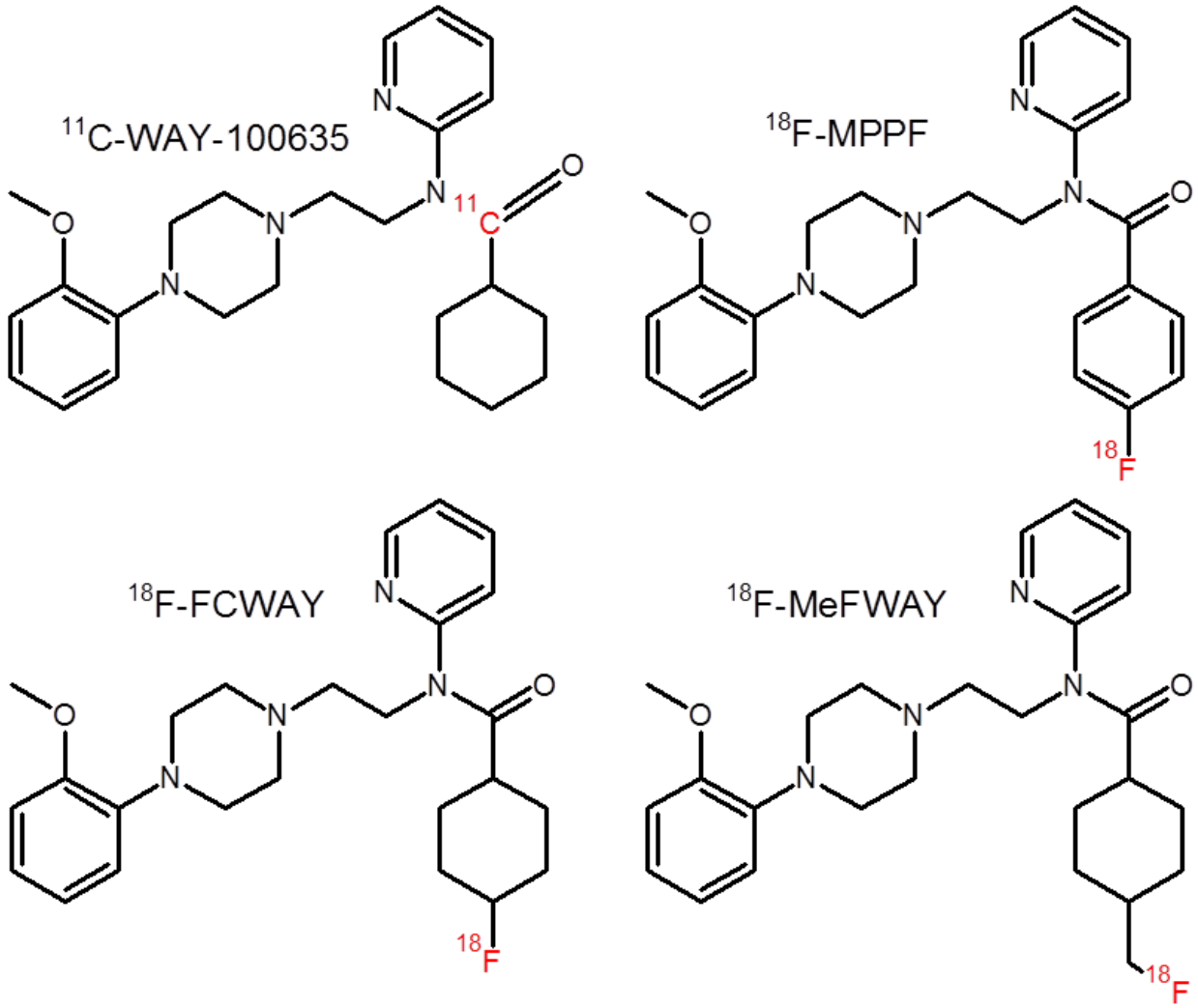

Figure 1-1: 5-HT_{1A} PET radiotracers (top left) [^{11}C]WAY-100635, (top right) [^{18}F]MPPF, (bottom right) [^{18}F]FCWAY, (bottom left) [^{18}F]MeFWAY.

assay, investigations concluded that reference tissue method of estimating binding potential was acceptable designating the cerebellum to be a valid reference region (Gunn et al, 1998). This PET tracer has been used extensively to examine group differences in 5-HT_{1A} expression and the 5-HT_{1A} receptor's relation to neuropsychiatric illness. [^{11}C]WAY-100635 has been used to examine effects of aging and sex-specific differences on binding potential (Meltzer et al., 2001; Parsey et al., 2002; Jovanovic et al., 2008; Stein et al., 2008). It has also been used to examine the relation of 5-HT_{1A} expression and neuropsychiatric diseases of panic disorder (Nash et al., 2008; Neumeister et al., 2004) anxiety (Tauscher et al., 2001) and depression (Drevets et al., 1999, 2007; Sargent et al., 2000; Savitz et al., 2009).

5-HT_{1A} expression measurements found using [^{11}C]WAY-100635 have given binding potential estimates of similar brain-regional rank order to in vitro measurements of 5-HT_{1A} receptor density. A database of [^{11}C]WAY-100635 binding in 61 normal male volunteers showed highest binding in the medial temporal region including the hippocampus, amygdala, and parahippocampus (Rabiner et al., 2002). Medium to high binding was found in the anterior cingulate, frontal cortex, and insula cortex. The raphe nuclei displayed medium to low binding. Comparing in vivo and in vitro results directly, however, are problematic because of methodological differences, inconsistencies in PET region of interest definition and in vitro tissue selection, and irregularities incurred when making in vivo measurements.

1.3. Development of ^{18}F-labeled 5-HT_{1A} PET ligands

The [^{11}C]WAY-100635 radiotracer has demonstrated utility for measuring 5-HT_{1A} expression in PET studies. It suffers, however, from the ^{11}C label which has a short half-life limiting counting statistics toward the end of a 90 minute PET study and requiring an onsite cyclotron for

its production. The fast clearance of [^{11}C]WAY-100635 through the gallbladder, together with the high energy β^+ particle also limit injection activities in human studies. The limitations caused by the ^{11}C-label prompted the development of ^{18}F-labeled analogues of [^{11}C]WAY-100635 which are shown in Figure 1-1. [^{18}F]FCWAY showed great initial promise with similar kinetics to [^{11}C]WAY-100635 in nonhuman primate studies (Carson et al., 2000). When studies were performed in humans, however, [^{18}F]FCWAY defluorinated leading to tracer uptake in bone which confounded the PET measurement (Carson et al., 2003). Similar to [^{18}F]FCWAY, [^{18}F]MPPF was developed to provide an ^{18}F-labeled substitute for [^{11}C]WAY-100635 (Shiue et al., 1997). Initial PET studies with [^{18}F]MPPF performed in cats showed uptake in 5-HT$_{1A}$ receptor rich regions which was blocked by WAY-100635 (Le Bars et al., 1998). Later studies demonstrated [^{18}F]MPPF was a substrate of P-glycoprotein leading to one-tenth the activity in the brain when compared to [^{11}C]WAY-100635 which resulted in lower binding due to increased efflux of [^{18}F]MPPF when compared to [^{11}C]WAY-100635 (Passchier et al., 2000; Kumar and Mann, 2007). [^{18}F]MeFWAY was also developed in response to the problems encountered with [^{11}C]WAY-100635 and is shown in Figure 1-1 (Saigal et al., 2006). Initial work showed high uptake in 5-HT$_{1A}$ specific regions of [^{18}F]MeFWAY, and MeFWAY exhibited similar inhibition constants (IC_{50}) to WAY-100635 (WAY-100635: 23.2 ± 2.8 nmol/L; MeFWAY: 25.7 ± 2.4 nmol/L). This thesis presents work validating the use of [^{18}F]MeFWAY in PET studies for in vivo assay of 5-HT$_{1A}$ receptors.

1.4. PET measurement of 5-HT$_{1A}$ receptor density

The major advantage of in vitro methods for radioligand-receptor analysis is the estimation of receptor density (B_{max}), while PET studies frequently result in nondisplaceable binding potential

(BP_{ND}) estimation which is a composite measure of B_{max} and in vivo K_D (K_{Dapp}). The BP_{ND} is the ratio at equilibrium of specifically bound radioligand to that of nondisplaceable radioligand in tissue (Innis et al., 2007) and can be estimated using a variety of methods (Ichise et al., 1996; Lammertsma and Hume, 1996; Logan et al., 1996). Estimation of binding potential from reference tissue is often appealing due to its simplicity because it requires a single injection of radiotracer and no arterial sampling. BP_{ND} is often referred to as an index of B_{max}; however, BP_{ND} is also influenced by K_D making it susceptible to changes in receptor affinity and endogenous neurotransmitter competition at the receptor site. This makes the BP_{ND} parameter less suitable for studies with the specific goal of examining B_{max}. Multiple injection (MI) PET experiments, when designed correctly, have the potential of measuring B_{max} and K_{Dapp}, in vivo, and provide an excellent alternative to in vitro experiments.

The objective of MI studies for estimation of B_{max} is to uncouple B_{max} and K_D, more specifically k_{on} (via $K_D=k_{off}/k_{on}$), to allow estimation of each parameter separately. A typical two-compartment model used to describe radioligand-receptor binding is shown in Figure 1-2. In the model, K_1 and k_2 represent the bidirectional transport of radioligand across the blood brain

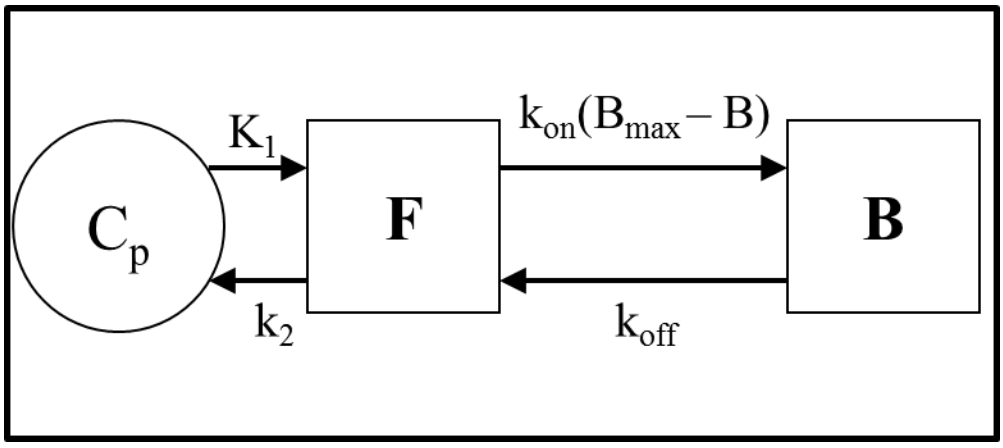

Figure 1-2: Two-compartmental model representing radioligand receptor binding.

barrier and k_{on} and k_{off} represent transfer of radioligand between free (**F**) and bound (**B**) states. In a high specific activity radiotracer study, receptor occupancy is undetectable ($B_{max} >> B$). In turn, B_{max} and k_{on} are completely indistinguishable measures, i.e., a change in k_{on} could be misinterpreted as a change in B_{max}. A MI study significantly alters receptor occupancy over the course of the experiment by introducing multiple radioligand injections at varying specific activities. In altering receptor occupancy, a MI study is able to separately estimate B_{max} and k_{on}.

It is important to distinguish B_{max} from K_{Dapp} when designing experiments with the goal of measuring differences or changes in B_{max}. A measurement of BP_{ND} which contains information about B_{max}, radioligand-receptor affinity, and endogenous neurotransmitter competition, is not necessarily a direct measure of B_{max}. Using [^{11}C]raclopride, changes in endogenous dopamine concentrations have displayed significant effects on binding potential (BP) via in vivo K_D revealing that BP is not necessarily a direct proxy of B_{max} (Doudet et al., 2006). An illustration of how B_{max} and endogenous neurotransmitter concentration changes alter BP_{ND} is shown in Figure 1-3. Figure 1-3 (middle) represents a condition of moderate BP_{ND} caused by medium level of B_{max} and endogenous neurotransmitter competition. Either by increasing B_{max} or decreasing endogenous neurotransmitter competition, BP_{ND} is increased (Figure 1-3 top). Similarly, decreasing B_{max} or increasing endogenous neurotransmitter competition has the opposite effect, a decrease in BP_{ND} (Figure 1-3 bottom).

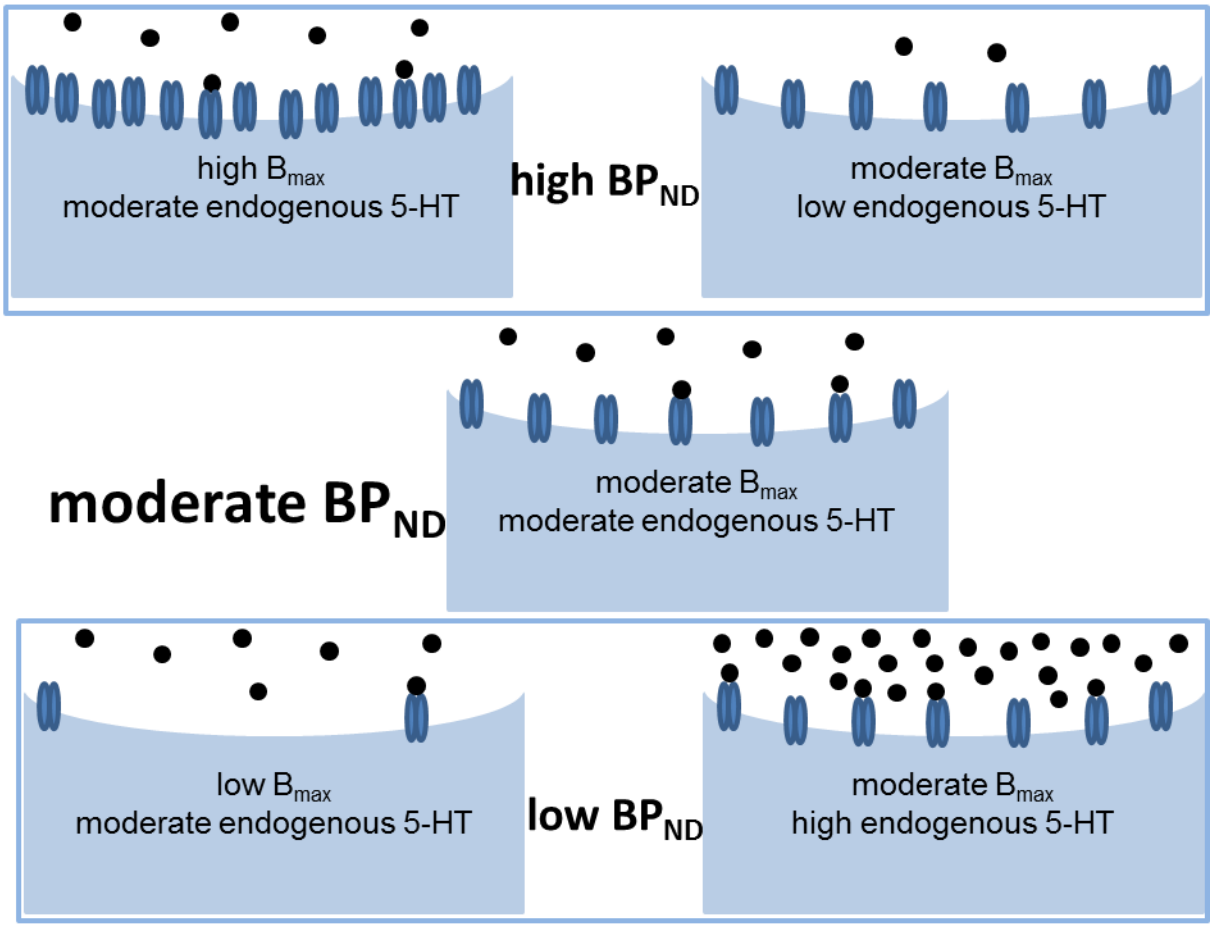

Figure 1-3: Effects of changes in B_{max} and endogenous neurotransmitter concentration on BP_{ND}.

Much has been done with PET to measure 5-HT_{1A} BP_{ND}, however, very little work has been done to measure 5-HT_{1A} B_{max} with PET. Measurement of B_{max} is often problematic, particularly in human studies, because it requires near saturating doses of unlabeled radioligand to alter receptor occupancy. Two previous studies have made in vivo estimates of 5-HT_{1A} B_{max} and K_D. Using [^{18}F]MPPF, estimation of B_{max} and K_D was performed in humans with a two-injection non-equilibrium scheme at varying specific activities (Costes et al., 2002). A second study made estimates of B_{max} and K_D using an equilibrium bolus plus constant infusion method and two-point Scatchard analysis (Spinelli et al., 2010). In both studies however, high levels of intersubject variation were reported for B_{max} (>60%) and K_D (>50%). Part of the work presented

herein use MI experiments to make high precision estimates of 5-HT_{1A} B_{max} and K_{Dapp} in the nonhuman primate. This thesis also presents sex-based differences of 5-HT_{1A} B_{max} and K_{Dapp} in a cohort of rhesus monkeys using the MI technique.

1.5. Thesis organization

The goal of the work presented in this thesis was to develop techniques to study the 5-HT_{1A} system. The remainder of this thesis is organized into five separate chapters presenting studies which address the thesis topic followed by a conclusion. The initial in vivo validation work of [^{18}F]MeFWAY is presented in Chapter 2 in which in vivo kinetics of [^{18}F]MeFWAY were compared to two other commonly used 5-HT_{1A} receptor antagonists [^{11}C]WAY-100635 and [^{18}F]MPPF. Next, Chapter 3 and Chapter 4 examine the effects of isomeric state and labeling position on the in vivo kinetics of [^{18}F]MeFWAY exploring different [^{18}F]MeFWAY analogues with potential application in PET imaging. Chapter 5 describes the development of multiple injection studies using [^{18}F]MeFWAY to estimate B_{max} and other in vivo binding parameters. Results presented in Chapter 6 utilize methods developed in the preceding chapters to examine sex-specific differences in B_{max} and in vivo K_D in a cohort of nonhuman primates. Chapter 7 concludes this thesis with insights gained from this work, the importance of this work, and future direction.

Note: Throughout this thesis, unless otherwise specified, [^{18}F]MeFWAY refers to 4-*trans*-[^{18}F]MeFWAY.

1.6. References

Azmitia E.C., Whitaker-Azmitia P.M., 1991. Awakening the sleeping giant: anatomy and plasticity of the brain serotonergic systems. Journal of Clinical Psychiatry 52, 4–16 Suppl.

Bryant, R.A., Felmingham, K.L., Falconer, E.M., Pe Benito, L., Dobson-Stone, C., Pierce, K.D., Schofield, P.R., 2010. Preliminary evidence of the short allele of the serotonin transporter gene predicting poor response to cognitive behavior therapy in posttraumatic stress disorder. Biological psychiatry 67, 1217–19.

Burnet, P.W., Eastwood, S.L., Harrison, P.J., 1997. [^{3}H]WAY-100635 for 5-HT1A receptor autoradiography in human brain: a comparison with [^{3}H]8-OH-DPAT and demonstration of increased binding in the frontal cortex in schizophrenia. Neurochemistry International 30, 565–74.

Carson, R.E., Lang, L., Watabe, H., Der, M.G., Adams, H.R., Jagoda, E., Herscovitch, P., Eckelman, W.C., 2000. PET evaluation of [^{18}F]FCWAY, an analog of the 5-HT$_{1A}$ receptor antagonist, WAY-100635. Nuclear Medicine and Biology 27, 493–7.

Carson, R.E., Wu, Y., Lang, L., Ma, Y., Der, M.G., Herscovitch, P., Eckelman, W.C., 2003. Brain uptake of the acid metabolites of F-18-labeled WAY 100635 analogs. Journal of Cerebral Blood Flow and Metabolism 23, 249–60.

Christian, B.T., Wooten, D.W., Hillmer, A.T., Tudorascu, D.L., Converse, A.K., Moore, C.F., Ahlers, E.O., Barnhart, T.E., Kalin, N.H., Barr, C.S., Schneider, M.L., 2013.Serotonin transporter genotype affects serotonin 5-HT$_{1A}$ binding in primates. Journal of Neuroscience 33, 2512-16.

Costes, N., Merlet, I., Zimmer, L., Lavenne, F., Cinotti, L., Delforge, J., Luxen, A., Pujol, J.F., Le Bars, D., 2002. Modeling [^{18}F]MPPF positron emission tomography kinetics for the determination of 5-hydroxytryptamine$_{1A}$ receptor concentration with multiinjection. Journal of Cerebral Blood Flow and Metabolism 22, 753–65.

Doudet, D.J., Ruth, T.J., Holden, J.E., 2006. Sequential versus nonsequential measurement of density and affinity of dopamine D_2 receptors with [^{11}C]raclopride: 2: effects of DAT inhibitors. Journal of Cerebral Blood Flow and Metabolism 26, 28–37.

Drevets, W.C., Frank, E., Price, J.C., Kupfer, D.J., Holt, D., Greer, P.J., Huang, Y., Gautier, C., Mathis, C., 1999. PET imaging of serotonin 1A receptor binding in depression. Biological psychiatry 46, 1375–1387.

Drevets, W.C., Thase, M.E., Moses-Kolko, E.L., Price, J., Frank, E., Kupfer, D.J., Mathis, C., 2007. Serotonin-1A receptor imaging in recurrent depression: replication and literature review. Nuclear Medicine and Biology 34, 865–877.

Duncan, J.S., 2002. Neurotransmitters, drugs and brain function. British Journal of Clinical Pharmacology 53, 648.

Gingrich, J.A., Hen, R., 2001. Dissecting the role of the serotonin system in neuropsychiatric disorders using knockout mice. Psychopharmacology 155, 1–10.

Gunn, R.N., Sargent, P.A., Bench, C.J., Rabiner, E.A., Osman, S., Pike, V.W., Hume, S.P., Grasby, P.M., Lammertsma, A.A., 1998. Tracer kinetic modeling of the 5-HT_{1A} receptor ligand [carbonyl-^{11}C]WAY-100635 for PET. NeuroImage 8, 426–440.

Hall, H., Lundkvist, C., Halldin, C., Farde, L., Pike, V., McCarron, J., Fletcher, A., Cliffe, I.., Barf, T., Wikström, H., Sedvall, G., 1997. Autoradiographic localization of 5-HT_{1A} receptors in the post-mortem human brain using [^{3}H]WAY-100635 and [^{11}C]WAY-100635. Brain Research 745, 96–108.

Heisler, L.K., Chu, H.M., Brennan, T.J., Danao, J.A., Bajwa, P., Parsons, L.H., Tecott, L.H., 1998. Elevated anxiety and antidepressant-like responses in serotonin 5-HT_{1A} receptor mutant mice. PNAS 95, 15049–54.

Ichise, M., Ballinger, J.R., Golan, H., Vines, D., Luong, A., Tsai, S., Kung, H.F., 1996. Noninvasive quantification of dopamine D_2 receptors with iodine-123-IBF SPECT. Journal of Nuclear Medicine 37, 513–520.

Innis, R.B., Cunningham, V.J., Delforge, J., Fujita, M., Gjedde, A., Gunn, R.N., Holden, J., Houle, S., Huang, S.C., Ichise, M., Iida, H., Ito, H., Kimura, Y., Koeppe, R.A., Knudsen, G.M., Knuuti, J., Lammertsma, A.A., Laruelle, M., Logan, J., Maguire, R.P., Mintun, M.A., Morris, E.D., Parsey, R., Price, J.C., Slifstein, M., Sossi, V., Suhara, T., Votaw, J.R., Wong, D.F., Carson, R.E., 2007. Consensus nomenclature for in vivo imaging of reversibly binding radioligands. Journal of Cerebral Blood Flow and Metabolism 27, 1533–9.

Jovanovic, H., Lundberg, J., Karlsson, P., Cerin, A., Saijo, T., Varrone, A., Halldin, C., Nordström, A.L., 2008. Sex differences in the serotonin 1A receptor and serotonin transporter binding in the human brain measured by PET. NeuroImage 39, 1408–19.

Dillon, K.A., Gross-Isseroff, R., Israeli, M., Biegon, A., 1991. Autoradiographic analysis of serotonin 5-HT_{1A} receptor binding in the human brain postmortem: effects of age and alcohol. Brain Research 554, 56–64.

Khawaja, X., 1995. Quantitative autoradiographic characterisation of the binding of [^{3}H]WAY-100635, a selective 5-HT_{1A} receptor antagonist. Brain research 673, 217–25.

Kumar, J.S.D., Mann, J.J., 2007. PET tracers for 5-HT_{1A} receptors and uses thereof. Drug discovery today 12, 48–756.

Lammertsma, A.A., Hume, S.P., 1996. Simplified reference tissue model for PET receptor studies. NeuroImage 4, 153–8.

Le Bars, D., Lemaire, C., Ginovart, N., Plenevaux, A., Aerts, J., Brihaye, C., Hassoun, W., Leviel, V., Mekhsian, P., Weissmann, D., Pujol, J.F., Luxen, A., Comar, D., 1998. High-yield radiosynthesis and preliminary in vivo evaluation of p-[^{18}F]MPPF, a fluoro analog of WAY-100635. Nuclear Medicine and Biology 25, 343–50.

Logan, J., Fowler, J., Volkow, N., 1996. Distribution volume ratios without blood sampling from graphical analysis of PET data. Journal of Cerebral Blood Flow and Metabolism 16, 834–40.

Matsubara, S., Arora, R.C., Meltzer, H.Y., 1991. Serotonergic measures in suicide brain: 5-HT$_{1A}$ binding sites in frontal cortex of suicide victims. Journal of Neural Transmission. General Section 85, 181–94.

Meltzer, C.C., Drevets, W.C., Price, J.C., Mathis, C.A., Lopresti, B., Greer, P.J., Villemagne, V.L., Holt, D., Mason, N.S., Houck, P.R., Reynolds III, C.F., DeKosky, S.T., 2001. Gender-specific aging effects on the serotonin 1A receptor. Brain Research 895, 9–17.

Nash, J. R., Sargent, P. A., Rabiner, E. A., Hood, S. D., Argyropoulos, S. V., Potokar, J. P., Grasby, P. M., Nutt, D.J., (2008). Serotonin 5-HT1A receptor binding in people with panic disorder: positron emission tomography study. Brit. J. Psychiat., 193, 229–234

Neumeister, A., Bain, E., Nugent, A.C., Carson, R.E., Bonne, O., Luckenbaugh, D.A., Eckelman, W., Herscovitch, P., Charney, D.S., Drevets, W.C., 2004. Reduced Serotonin Type 1A Receptor Binding in Panic Disorder. The Journal of Neuroscience 24, 589–91.

Nichols, D.E., Nichols, C.D., 2008. Serotonin receptors. Chemical reviews 108, 1614–41.

Palego, L., Marazziti, D., Rossi, A., Giannaccini, G., Naccarato, A.G., Lucacchini, A., Cassano, G.B., 1997. Apparent absence of aging and gender effects on serotonin 1A receptors in human neocortex and hippocampus. Brain Research 758, 26–32.

Parsey, R.V., Oquendo, M.A., Simpson, N.R., Ogden, R.T., Van Heertum, R., Arango, V., Mann, J.J., 2002. Effects of sex, age, and aggressive traits in man on brain serotonin 5-HT$_{1A}$ receptor binding potential measured by PET using [^{11}C]WAY-100635. Brain Research 954, 173–82.

Passchier, J., Van Waarde, A., Doze, P., Elsinga, P.H., Vaalburg, W., 2000. Influence of P-glycoprotein on brain uptake of [^{18}F]MPPF in rats. European journal of pharmacology 407, 273–80.

Pike, V.W., McCarron, J.A., Lammertsma, A.A., Osman, S., Hume, S.P., Sargent, P.A., Bench, C.J., Cliffe, I.A., Fletcher, A., Grasby, P.M., 1996. Exquisite delineation of 5-HT$_{1A}$

receptors in human brain with PET and [carbonyl-^{11}C]WAY-100635. European Journal of Pharmacology 301, R5–7.

Rabiner, E.A., Messa, C., Sargent, P.A., Husted-Kjaer, K., Montgomery, A., Lawrence, A.D., Bench, C.J., Gunn, R.N., Cowen, P., Grasby, P.M., 2002. A database of [^{11}C]WAY-100635 binding to 5-HT$_{1A}$ receptors in normal male volunteers: normative data and relationship to methodological, demographic, physiological, and behavioral variables. NeuroImage 15, 620–32.

Saigal, N., Pichika, R., Easwaramoorthy, B., Collins, D., Christian, B.T., Shi, B., Narayanan, T.K., Potkin, S.G., Mukherjee, J., 2006. Synthesis and biologic evaluation of a novel serotonin 5-HT$_{1A}$ receptor radioligand, ^{18}F-labeled MeFWAY, in rodents and imaging by PET in a nonhuman primate. Journal of nuclear medicine 47, 1697–706.

Sargent, P.A., Kjaer, K.H., Bench, C.J., Rabiner, E.A., Messa, C., Meyer, J., Gunn, R.N., Grasby, P.M., Cowen, P.J., 2000. Brain serotonin$_{1A}$ receptor binding measured by positron emission tomography with [^{11}C]WAY-100635: effects of depression and antidepressant treatment. Archives of general psychiatry 57, 174–80.

Savitz, J., Lucki, I., Drevets, W.C., 2009. 5-HT$_{1A}$ receptor function in major depressive disorder. Progress in Neurobiology 88, 17–31.

Shiue, C.Y., Shiue, G.G., Mozley, P.D., Kung, M.P., Zhuang, Z.P., Kim, H.J., Kung, H.F., 1997. P-[^{18}F]-MPPF: a potential radioligand for PET studies of 5-HT$_{1A}$ receptors in humans. Synapse 25, 147–154.

Spinelli, S., Chefer, S., Carson, R.E., Jagoda, E., Lang, L., Heilig, M., Barr, C.S., Suomi, S.J., Higley, J.D., Stein, E.A., 2010. Effects of early-life stress on serotonin$_{1A}$ receptors in juvenile Rhesus monkeys measured by positron emission tomography. Biological psychiatry 67, 1146–53.

Stein, P., Savli, M., Wadsak, W., Mitterhauser, M., Fink, M., Spindelegger, C., Mien, L.-K., Moser, U., Dudczak, R., Kletter, K., Kasper, S., Lanzenberger, R., 2008. The serotonin-1A receptor distribution in healthy men and women measured by PET and [carbonyl-^{11}C]WAY-100635. European Journal of Nuclear Medicine and Molecular Imaging 35, 2159–68.

Tauscher, J., Bagby, R. M., Javanmard, M., Christensen, B. K., Kasper, S., Kapur, S. (2001). Inverse relationship between serotonin 5-HT(1A) receptor binding and anxiety: a [^{11}C]WAY-100635 PET investigation in healthy volunteers. Am. J. Psychiat., 158, 1326–1328.

Terry, A.V.J., Buccafusco, J.J., Wilson, C., 2008. Cognitive dysfunction in neuropsychiatric disorders: selected serotonin receptor subtypes as therapeutic targets. Behavioural brain research 195, 30–8.

Chapter 2 In Vivo Validation of *trans*-[^{18}F]MeFWAY

2.1. Introduction

Presently, the most commonly used PET radioligand for measuring 5-HT_{1A} expression in the human brain is [^{11}C]WAY-100635. The need for a longer lived 5-HT_{1A} radioligand with similar imaging properties to [^{11}C]WAY-100635 has prompted the development of numerous WAY-100635 analogues with the ^{18}F label. The ^{18}F-labeled radiotracers developed thus far, however, have had shortcomings which are discussed in section 1.3. This chapter focusses on the validation of [^{18}F]MeFWAY as a 5-HT_{1A} PET radioligand by comparing the in vivo kinetics with [^{11}C]WAY-100635 and [^{18}F]MPPF. Validation of the kinetic properties of [^{18}F]MeFWAY is a necessary step in its translation into human studies. Furthermore, these studies lay the ground work for the use of [^{18}F]MeFWAY in more complex experimental protocols, which are impractical with the shorter lived [^{11}C]WAY-100635 radiotracer, that will further depict the 5-HT_{1A} system.

Early studies with [^{18}F]MeFWAY displayed promising characteristics for in vivo PET imaging (Saigal et al., 2006). In vitro binding assays in rat brain slices showed greatest uptake in the region of the hippocampus, revealing a specific to nonspecific binding ratio of 82:1 (using the cerebellum (CB) as a region with negligible specific 5-HT_{1A} binding) (Saigal et al., 2006). High levels of [^{18}F]MeFWAY binding were also seen in the colliculus (46:1) and the frontal cortex (40:1). Additionally, the binding of [^{18}F]MeFWAY was almost completely displaced with competition of 10 μM of WAY-100635, demonstrating high selectivity for the 5-HT_{1A} receptor site. In vitro competition experiments with serotonin yielded IC_{50} values of 170 – 240 nmol/L in the high uptake regions of the rat brain slices. The binding affinity of WAY-100635 (IC_{50} = 23.2 nM) and unlabeled MeFWAY (IC_{50} = 25.7nM) against [^{18}F]MeFWAY were found to be in close

agreement. Also, the lipophilicity of [^{18}F]MeFWAY and [^{11}C]WAY-100635 (logP of 2.62 and 3.28, respectively) (Pike et al., 2000; Saigal et al., 2006), are both within a range that would suggest favorable in vivo uptake in the brain (Kessler et al., 1991).

In this chapter, a direct comparison of the in vivo kinetics of [^{11}C]WAY-100635, [^{18}F]MPPF, and [^{18}F]MeFWAY in rhesus monkeys is described. By performing multitracer studies in the same subjects, it is possible to accurately assess and compare the imaging characteristics of these three 5-HT_{1A} PET radiotracers.

2.2. Materials and Methods

2.2.1. Radiochemical Synthesis

The ^{11}C and ^{18}F radionuclides were produced using either an 11-MeV RDS 112 cyclotron or a 16-MeV GE PETtrace cyclotron.

2.2.1.1. [^{11}C]WAY-100635

[Carbonyl-^{11}C]N-(2-(1-(4-(2-Methoxyphenyl)-piperazinyl)ethyl)-N-pyridinyl) cyclohexanecarboxamide ([^{11}C]WAY-100635) was radiosynthesized similar to a previously reported one-pot procedure (Hwang et al, 1999) and is regarded as one of the most complicated PET radiotracers to synthesize. The $^{11}CO_2$ was produced by a static irradiation of protons on a 1% O_2/N_2 mixture. The radiochemical synthesis is shown in Figure 2-1. First, $^{11}CO_2$ reacts with the Grignard reagent, cyclohexylmagnesium chloride, to produce a carboxylation adduct (1). Thionyl chloride ($SOCl_2$) then reacts with the carboxylation adduct to produce [carbonyl-^{11}C]cyclohexanecarbonylchloride (2). Finally, the precursor, WAY-100634 combines with [carbonyl-^{11}C]cyclohexanecarbonylchloride to yield [^{11}C]WAY-100635.

The [^{11}C]WAY-100635 synthesis must be completed under inert conditions. Therefore a radiosynthesis module (Figure 2-2) was designed to achieve high purity inert conditions by allowing the radiochemistry to be performed under inert conditions. The radiosynthesis module

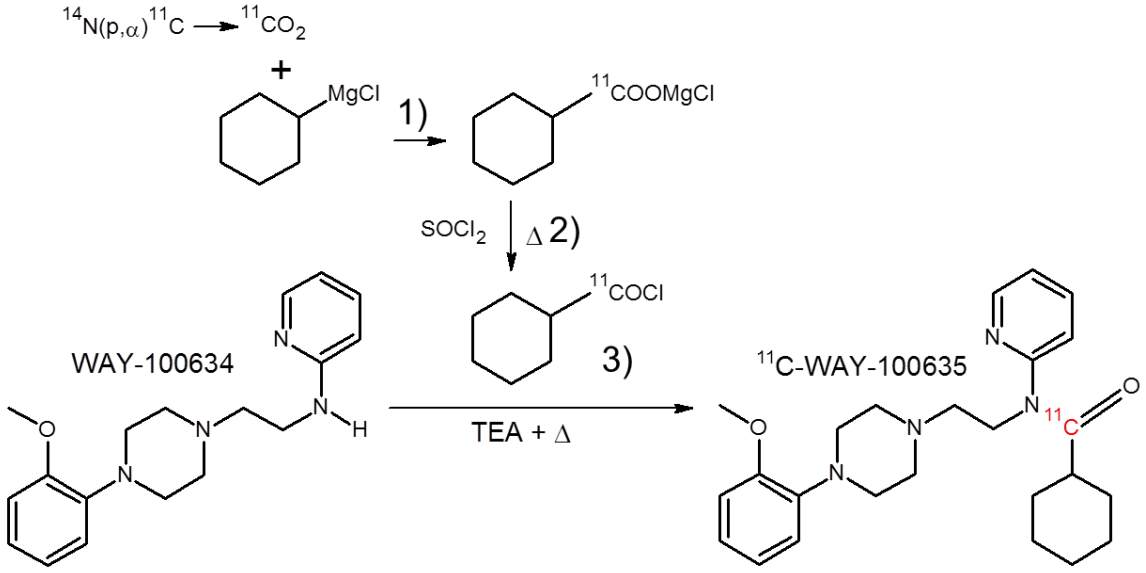

Figure 2-1: Radiochemical synthesis of [^{11}C]WAY-100635.

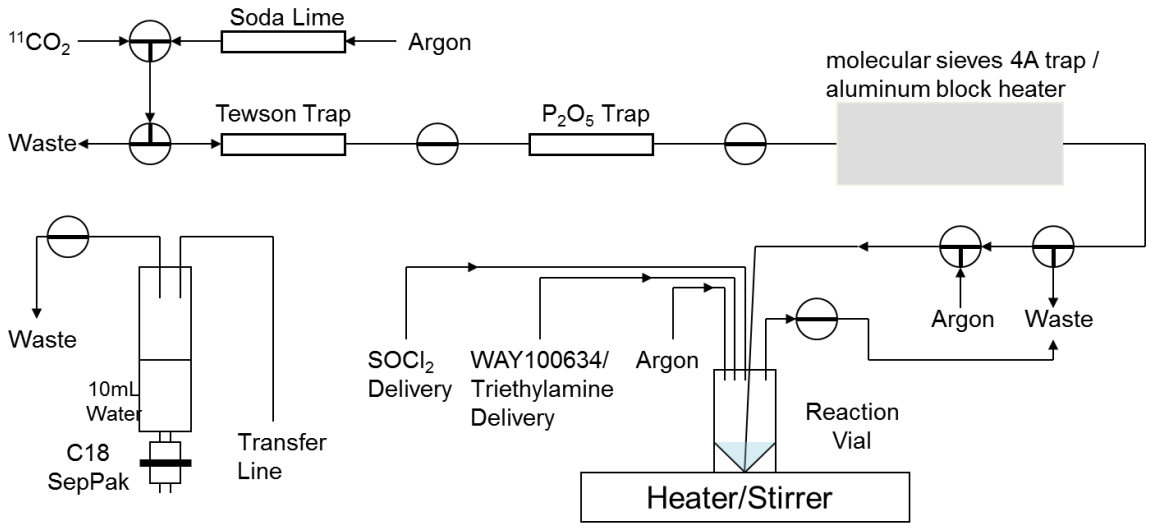

Figure 2-2: Radiosynthesis module for the production of [^{11}C]WAY-100635.

was also designed to reduce radiation exposure. Initially, $^{11}CO_2$ was released from the cyclotron

target and passed through 1) a Tewson trap (Tewson et al, 1989) which removed mono-nitrogen oxides (NO_x) and 2) a phosphorous pentoxide (P_2O_5) trap which removed trace amounts of water. Finally, the $^{11}CO_2$ was trapped in a molecular sieves 4A trap. At room temperature, molecular sieve 4A absorbed CO_2 and allowed other radioactive byproducts produced in the target to pass through, e.g., ^{11}CO. The molecular sieves 4A were then activated or heated to 350 °C to release the trapped gas. The $^{11}CO_2$ was carried out of the trap with high purity Ar gas and bubbled into a Grignard reagent preloaded into a reaction vial. Prior to beginning of synthesis (BOS), the Grignard solution was prepared in an argon bag by mixing 0.5 mL of a 0.2 M solution of cyclohexylmagnesium chloride in ether to 3 mL of anhydrous tetrahydrofuran (THF). For the synthesis, 0.5 mL of the Grignard solution was added to a dry Reacti-vial (Thermo Scientific). The $^{11}CO_2$ bubbled into the Grignard solution for about 3 minutes. Radiation detectors measured radioactivity in both the molecular sieves trap and Reacti-vial which allowed precise monitoring of release time of $^{11}CO_2$ from trap and reaction time in the Grignard solution. When maximum radioactivity was reached in the Grignard solution, the reaction was stopped by ending the flow of Ar through the molecular sieves trap leaving a mixture containing the carboxylation adduct as shown in step 1 of Figure 2-1. Next, 0.22 mL of a $SOCl_2$ solution, prepared by adding 0.2 mL of $SOCl_2$ to 2 mL of anhydrous THF, was added to the Reacti-vial. The reaction proceeded under a slow Ar flow cooking at 75 °C for about 1 minute. After 1 minute the Ar flow was increased gradually to aid in the complete dry down of the mixture which typically took an additional 3 minutes. When the mixture was dry, Ar flow was reduced. Next, the precursor solution, prepared by adding 2 mg of WAY-100634 (ABX, Raderberg, Germany) to a solution containing 0.6 mL of anhydrous THF and 0.02 mL of triethylamine

(NEt_3), was added to the Reacti-vial. The reaction proceeded for 5 minutes at 75 °C under a slow Ar flow to produce a product mixture containing [^{11}C]WAY-100635.

Following the reaction, 1 mL of acetonitrile (MeCN) was added to the Reacti-vial to aid in the transfer of the [^{11}C]WAY-100635 containing mixture to the Sep-Pak unit pre-loaded with 10 mL of water for initial purification. The C18 Sep-Pak trapped lipophilic molecules (including [^{11}C]WAY-100635 and allowed more polar molecules to pass through. Following the trapping of [^{11}C]WAY-100635, the Sep-Pak was rinsed with aqueous solutions of hydrochloric acid (HCl), methanol (MeOH), and sodium hydroxide (NaOH). The product was then eluted from the Sep-Pak with 1 mL of ethanol (EtOH) and injected onto high performance liquid chromatography (HPLC) for further purification. The HPLC setup is shown in Figure 2-3. The mobile phase consisted of 3% 0.1 M ammonium formate, 70% MeOH, and 0.3% of NEt_3 at a flow rate of 8 mL/minute. The solid phase consisted of a Prodigy 10 µm, 250 x 10 mm (Phenomenex) column. A uv absorbance meter and radiation detector was used to detect the elution of product from the column. As seen in Figure 2-4, [^{11}C]WAY-100635 begins eluting at about 500 seconds. The [^{11}C]WAY-100635 peak was then collected, diluted with 60 mL of H_2O for final formulation, and was then trapped on another C18 Sep-Pak cartridge. The C18 Sep-Pak was subsequently eluted with 1 mL of EtOH for injection, diluted with 9 mL of sterile saline, and passed through a sterile filter into a sterile empty vial. A 100µL sample was held back for analytic HPLC analysis. Analytic HPLC was performed using a Prodigy 5micron, 250 x 4.60mm ODS3 100Å (Phenomenex) and a mobile phase consisting of 55% 0.1M ammonium formate solution and 45% acetonitrile. A representative analytic HPLC chromatogram for [^{11}C]WAY-100635 is shown in Figure 2-5. At end of synthesis, radiochemical purity was > 95%, with specific activity of 34 – 92 GBq/micromol providing a batch yield of 370 – 740 MBq.

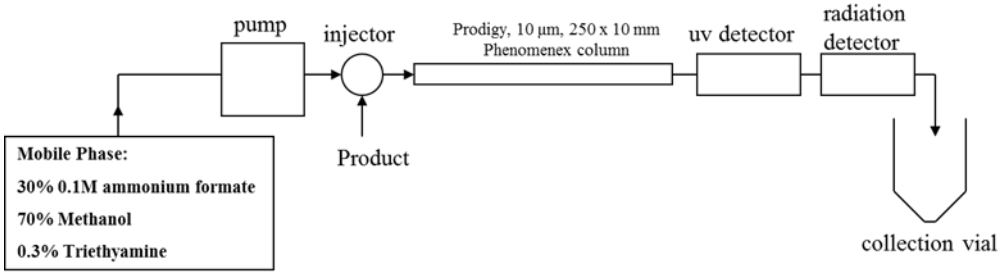

Figure 2-3: Semi Preperative HPLC setup for the production of [^{11}C]WAY-100635.

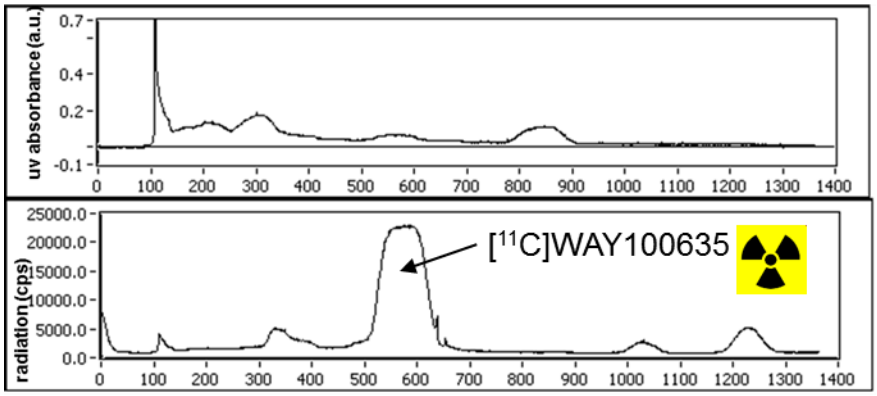

Figure 2-4: Semi preperative HPLC chromatogram for the production of [^{11}C]WAY-100635.

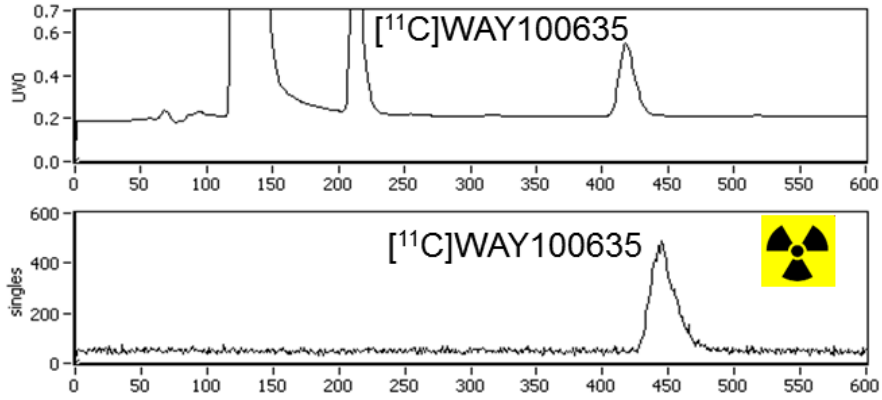

Figure 2-5: Analytic HPLC chromatogram of [^{11}C]WAY-100635.

2.2.1.2. [^{18}F]MeFWAY

N-{2-[4-(2-methoxyphenyl)piperazinyl]ethyl}-N-(2-pyridyl)-N-(4-[^{18}F]-fluoromethylcyclohexane)carboxamide (^{18}F-MeFWAY) was synthesized by a nucleophilic

substitution of the tosylate precursor similar to a previously reported method (Saigal et al., 2006). Production of ^{18}F was performed by bombardment of protons on $H_2{}^{18}O$. At the end of bombardment (EOB), the target water was passed through an anion exchange QMA cartridge which captured the fluorine and allowed the $H_2{}^{18}O$ water to pass through. The fluorine was then eluted from the QMA cartridge with an aqueous solution of potassium carbonate and Kryptofix 222 into a vial. The synthesis of ^{18}F-MeFWAY (shown in Figure 2-6) was performed using a computer process control unit (CPCU). Using the CPCU, azeotropic distillation was first

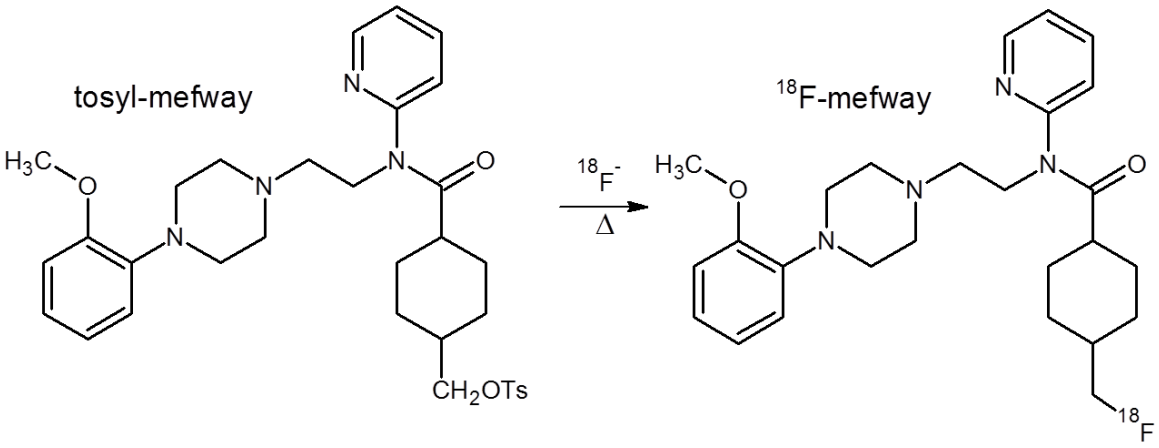

Figure 2-6: Radiochemical synthesis of [^{18}F]MeFWAY.

performed to remove water. Acetonitrile was added to the vial and the solution was then transferred to a reaction vessel in the CPCU. The solution was azeotropically distilled at 120˚C with an argon bubble for 5 minutes. Anhydrous acetonitrile was added to the vessel and dried at 120˚C with an argon bubble for 5 minutes and then again repeated to ensure no water remained in the reaction vessel. The tosylate precursor, which was dissolved in 500µL of anhydrous acetonitrile, was then added to the reaction vessel and heated at 96˚C for 10 minutes. The product was then dissolved in 3mL of methanol and passed through a preconditioned alumina Sep-Pak (Waters) which trapped the unreacted ^{18}F. The solution was then dried by a rotary

evaporator and prepared for injection onto reverse phase preparative HPLC. HPLC purification consisted of a C18 Econosil column (250 x 10 mm; Alltech) and a mobile phase of 60% acetonitrile, 40% sterile water, and 0.1% triethylamine at a flow rate of 2.5mL/min. The product was then dissolved in 1.5 mL of mobile phase and injected into the HPLC system. The product eluted at 10.5 minutes and was collected into a rotary evaporator vial. HPLC solvents were removed from the product by a rotary evaporator and the dried product was dissolved in 1 mL of ethanol and 9 mL of saline. The [^{18}F]MeFWAY solution was then passed through a 0.2 micron sterile Millipore filter into a sterile empty vial. A 100µL sample was held back for analytic HPLC analysis. Analytic HPLC was performed using a Prodigy 5micron, 250 x 4.60mm ODS3 100Å (Phenomenex) and a mobile phase consisting of 60% 0.1 M ammonium formate solution and 40% acetonitrile. Reference standard was purchased from Huayi Isotopes. A representative analytic HPLC chromatogram for [^{18}F]MeFWAY is shown in Figure 2-7. Non decay corrected radiochemical yields were typically 4-7% with the final product having a radiochemical purity >95% and specific activities between 74 – 111 GBq/µmol.

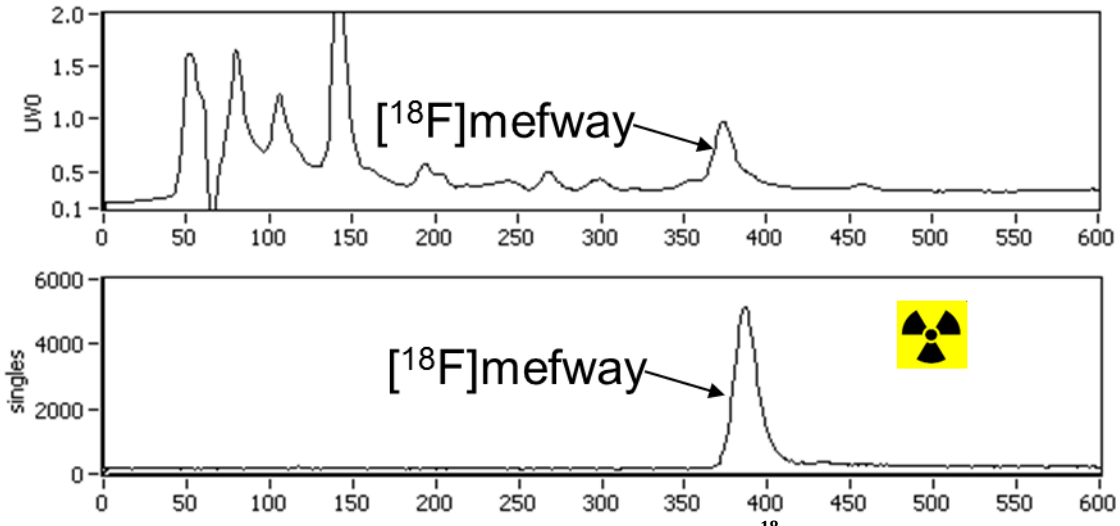

Figure 2-7: Analytic HPLC chromatogram of [^{18}F]MeFWAY.

2.2.1.3. [^{18}F]MPPF

4-Fluoro-N-[2-[4-(2-methoxyphenyl)piperazin-1-yl]ethyl]-N-pyridin-2-ylbenzamide ([^{18}F]MPPF) was synthesized by nucleophilic substitution of the nitro precursor by Dr. Dhanabablan Murali. In short, the [^{18}F]F^{-} was heated with 1-2mg of nitro MPPF derivative (ABX, Raderberg, Germany) dissolved in 0.45ml solvent at 135°C for 30 minutes. Following the reaction, HPLC was performed using Prevail C18, 5 micron, 250 x 10 mm column (Alltech) and mobile phase of 18% THF: 27% MeOH: 55% 0.05M NaOAc, pH=5 (by volume) at a flow rate of 3ml/min. The [^{18}F]MPPF was collected at approximately 17 minutes and roto-evaporated to dryness. The final product was then diluted in 0.9% saline for injection and passed through a 0.22 μm millipore filter. The radiochemical purity was > 95% and the specific activity of the [^{18}F]MPPF was 84 - 102 GBq/micromol at the end of synthesis providing a batch yield of 185 – 370 MBq.

2.2.2. Subjects

A total of 4 macaca mulatta (rhesus) (4 male; 7.8 ± 1.7 kg) underwent PET scans with [^{18}F]MeFWAY, [^{11}C]WAY-100635, and [^{18}F]MPPF. The age of the subjects at the time of the first scan was 4.6 ± 0.3 years and the repeated scans were performed between 1 week and 7 months following the first scan. For the imaging procedures, the subjects were first anesthetized with ketamine (15 mg/kg IM) and maintained on 0.75% - 1.5% isoflurane for the duration of the experiment. Atropine sulfate (0.27 mg IM) was administered to minimize secretions during the course of the experiment. During the length of the scans, body temperature, breathing rate, heart rate, and SpO_2 levels were monitored and recorded. A catheter was placed in the femoral artery for arterial plasma sampling and the saphenous vein for administration of radiotracer. After data

acquisition, subjects were removed from anesthesia and returned to their cages when swallowing reflex was restored, then continuously monitored until fully alert. The subjects were housed at the Harlow Primate Laboratory at the University of Wisconsin and all housing and experimental procedures were in accordance with institutional guidelines.

2.2.3. Data Acquisition

PET scans were acquired using a Concorde microPET P4 scanner. The scanner has an axial field of view of 7.8 cm, a transaxial field of view of 19 cm, and an in-plane spatial resolution of 1.8 mm (Tai et al., 2001). The heads of the subjects were positioned in a stereotaxic headholder to maintain a consistent orientation for all scans on all subjects. Prior to injection of radiotracer, a 518 second transmission scan was acquired using a Co-57 point source. Emission data collection was started at the time of bolus injection of radiotracer of 161 ± 41 MBq, 101 ± 35 MBq, 47 ± 20 MBq for [^{11}C]WAY-100635, [^{18}F]MPPF and [^{18}F]MeFWAY, respectively. The injected mass for each radiotracer was 1.15 ± 0.50 nmol/kg, 0.18 ± 0.16 nmol/kg, 0.14 ± 0.18 nmol/kg for [^{11}C]WAY100635, [^{18}F]MPPF and [^{18}F]MeFWAY, respectively. One of the subjects (M2) did not receive a [^{11}C]WAY100635 scan due to low radioactivity yields in the radiotracer synthesis. An acquisition of 120 minutes was acquired for the [^{18}F]MPPF and [^{18}F]MeFWAY studies, and 90 minutes for the [^{11}C]WAY100635 studies. Arterial blood samples were acquired throughout the course of the study ranging from every 5 seconds immediately after injection to every 10 minutes toward the end of the study. Whole blood samples were taken in volumes of ~0.5mL, mixed with heparinized saline and counted using a NaI(Tl) well counter which was cross calibrated in units of kBq/mL with the PET scanner. The blood samples were then centrifuged for 5 minutes, 250 µL of plasma was drawn and added to 50 µL of sodium bicarbonate, and then

the plasma was immediately assayed. Ethyl acetate extraction was performed (2 times, 500 µL each) on the plasma samples to separate the lipophilic parent compound from the polar metabolites using previously reported methods (Saigal et al., 2006). The lipophilic fraction was assayed for radioactivity to provide the input function for tracer kinetic analysis. The same procedure for arterial sampling was performed in all of the studies.

2.2.4. Data Analysis

Raw list mode data from all scans were binned into temporal frames of 4 x 1 minute, 3 x 2 minutes, and either 16 x 5 minutes ([^{11}C]WAY-100635) or 22 x 5 minutes ([^{18}F]MPPF and [^{18}F]MeFWAY) with corrections applied for scanner deadtime and random coincidence events. Sinograms of the emission scan were reconstructed using filtered backprojection (0.5 cm^{-1} ramp filter) with corrections to account for attenuation, scatter, radioactive decay, and scanner normalization to a final matrix size of 128 x 128 x 63 and voxel dimensions of 1.90 x 1.90 x 1.21 mm^3. The multitracer time series were realigned into common space for each subject using the Linear Image Registration Tool, which is part of the FMRIB Software Library (Jenkinson and Smith, 2001), to obtain the rigid body transformation matrix obtained from the coregistration of the integrated (i.e summed) data over the entire study. Circular regions of interest (ROIs) were drawn in various regions of the brain to extract time-activity curves (TACs) of the radiotracer in the tissue, which included the brain regions of the CB (1.02 cm^3), caudal anterior cingulate gyrus (ACG) (0.82 cm^3), insula cortex (IC) (0.66 cm^3), raphe nuclei (RN) (0.08 cm^3) and mesial temporal cortex (MTC) (0.70 cm^3) which includes the hippocampus.

The time series data were analyzed using two separate methods for estimation of the in vivo behaviors of the radiotracers. In the CB, the PET signal is dominated by nondisplaceable tracer

(i.e. radiotracer that is not specifically bound to the 5-HT_{1A} receptors) and this region is frequently used as a reference for radiotracer behavior in regions without specific binding. To explore the presence of small but significant specific binding, the data from the cerebellar region were analyzed using the two-tissue compartment model, described by the state equations:

$$\textbf{(2-1)}\quad \frac{dC_{ND}}{dt} = K_1 C_P - (k_2 + k_3) C_{ND} + k_4 C_S$$

$$\textbf{(2-2)}\quad \frac{dC_S}{dt} = k_3 C_{ND} - k_4 C_S$$

where C_{ND} and C_S represent the radioactive concentration of radiotracer in the nondisplaceable (free and nonspecifically bound) and specifically bound states, respectively. The concentration of parent radiotracer in the arterial plasma is C_p, K_1 (mL/mL/min) and k_2 (min^{-1}) represent the bidirectional transport of radiotracer across the blood-brain barrier. The specific binding of the radiotracer to the receptor site is given by a bimolecular association parameter k_3 ($=k_{on}B_{max}$ in units of min^{-1}) and dissociation rate k_4 ($=k_{off}$)(min^{-1}). The decay corrected, measured PET signal in a tissue region represents: $C_T(t) = C_{ND} + C_S + f_V C_{WB}$, in units of kBq/mL, assuming the fractional blood volume (f_V) and concentration of radioactivity in the whole blood of C_{WB}. For this work, a value of 0.04 was assumed for f_V. There was no attempt to estimate the fraction of radiotracer bound to plasma proteins or nonspecifically bound in the brain. A single-compartment model was also examined by fixing $k_3 = k_4 = 0$ to assess if the data could be adequately described without a compartment for specific binding. COMKAT software (Muzic and Cornelius, 2001) was used for obtaining the parameter estimates with the model configurations. The data were weighted according to the reciprocal of the variance of the PET data (weight = frame duration / PET concentration) and the standard deviation of the parameter estimates were derived from the covariance matrix (Mazoyer et al., 1986). The results of the one-

and the two-compartment models were compared using the Akaike information criteria (AIC) and the appropriate model was selected based upon the lowest AIC (Akaike, 1974).

The two-compartment model was not used for regions of the brain with medium to high 5-HT_{1A} receptor density (ACG, IC, RN, MTC) due to the lack of parameter identifiability (i.e. large covariance between the kinetic parameter estimates) as is frequently observed when attempting to estimate four or more parameters from a single bolus injection study (Delforge et al., 1990). The Logan graphical method was used in these brain regions with the CB time course serving as the reference region (Logan et al., 1996) to obtain an index of specific 5-HT_{1A} binding. A period of linearization of t* = 40 minutes was used to obtain an estimate of the distribution volume ratio (DVR) for each brain region. A fixed value of k_2 was used for each radiotracer (averaged over the 4 subjects) as obtained by the cerebellar compartment analysis. Estimates of the nondisplaceable binding potential (BP_{ND}) were obtained by the relationship: $BP_{ND} = DVR - 1$. Estimates of BP_{ND} bias due to small amounts of specific binding in the CB were investigated based upon the k_3 and k_4 terms in the two-compartment analysis of the cerebellar data.

Parametric images of DVR were generated to provide a visual comparison of the binding profile for each radiotracer. Voxel based estimates of DVR were calculated using the same graphical based algorithm described above and the same period of linearization on the dynamic time series. The parametric images display DVR values (rather than BP_{ND}) to illustrate the presence of radiotracer uptake in regions outside the brain (e.g. scalp, sinuses) which would not be evident with using a threshold to eliminate negative BP_{ND} values.

2.3. Results

2.3.1. Plasma Kinetics

The radioactive decay corrected time courses of the arterial plasma radioactivity and parent radiotracer concentrations in plasma are shown in Figure 2-8. Following the period of rapid clearance from the blood (>30 minutes), the tracers cleared from the arterial plasma at a rate of 0.0031 min-1 ([^{18}F]MeFWAY), 0.0078 min-1 ([^{18}F]MPPF) and 0.0069 min-1 ([^{11}C]WAY-100635). The fraction of radioactivity in the plasma due to the parent radiotracer at 30 minutes after injection was 19% ([^{18}F]MeFWAY), 28% ([^{18}F]MPPF) and 29% ([^{11}C]WAY-100635).

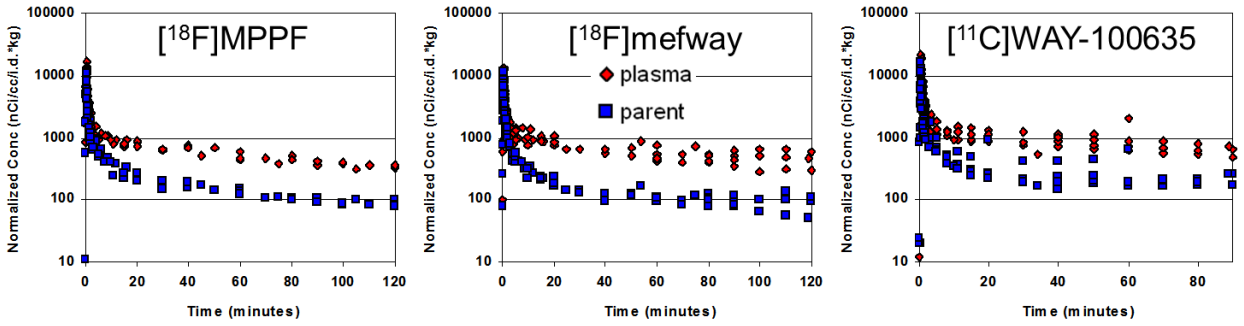

Figure 2-8: Arterial time courses of total radioactivity (♦) and parent compound radioactivity (■) in plasma for [^{18}F]MPPF (left), [^{18}F]MeFWAY (middle), and [^{11}C]WAY-100635 (right).

2.3.2. Cerebellar Kinetics

The cerebellar TACs of the radiotracers through the CB are shown in Figure 2-9. Similar to the

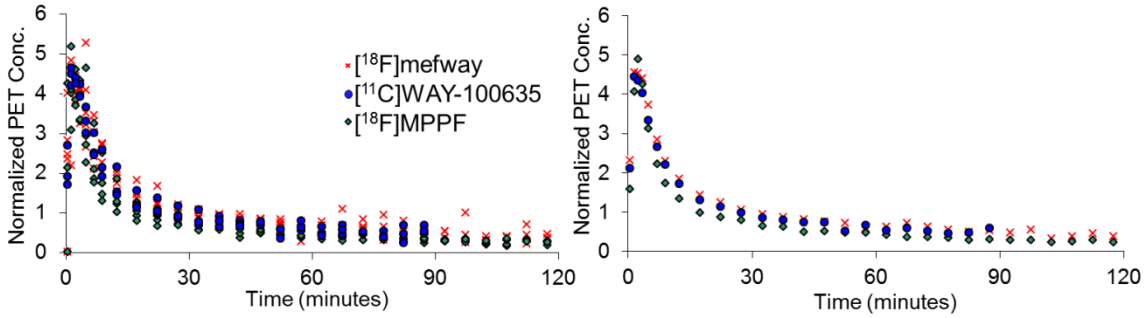

Figure 2-9: (Left) Cerebellar time-activity curves for [^{18}F]MeFWAY (x), [^{11}C]WAY-100635 (●), and [^{18}F]MPPF (♦). (Right) Data for each radiotracer averaged all over subjects.

plasma TACs, the plots demonstrate fast and slow components of clearance. An exponential fit to the slow component (t > 30 minutes) reveals a clearance rate of 0.010 min^{-1} ([^{18}F]MeFWAY), 0.011 min^{-1} ([^{18}F]MPPF) and 0.014 min^{-1} ([^{11}C]WAY-100635), which is the same rank order as the plasma clearance for each radiotracer. The cerebellar data were modeled as single-tissue compartment and two-tissue compartment (k_3, k_4) configurations. For all of the studies, the single-tissue compartment model was selected as the most appropriate model to describe the cerebellar TACs based upon the AIC. The parameter estimates for the single-compartment model fitting are shown in Table 2-1. Also given in the table are the nondisplaceable distribution volumes ($V_{ND} = K_1/k_2$), these values did not change by more than 10% when the two-tissue compartment parameter estimates were used indicating that the potential presence of small levels of specific binding in this region left the measure of V_{ND} largely unchanged.

Table 2-1: Compartment modeling estimates for K1, k2, and K1/k2.

RadioLigand	Subject	K_1 (min^{-1})	k_2 (min^{-1})	K_1/k_2
[^{18}F]MPPF	M1	******No Bloods		
	M2	0.9	0.29	3.1
	M3	1.32	0.45	3.0
	M4	0.76	0.27	2.9
	Average	**0.99**	**0.33**	**3.0**
	S.D.	**0.29**	**0.1**	**0.1**
[^{18}F]Mefway	M1	0.58	0.12	4.8
	M2	1.36	0.39	3.5
	M3	1.13	0.27	4.3
	M4	**0.63**	**0.16**	**3.9**
	Average	**0.93**	**0.23**	**4.1**
	S.D.	0.38	0.12	0.6
[^{11}C]WAY-100635	M1	0.58	0.16	3.6
	M3	1.07	0.41	2.6
	M4	0.62	0.23	2.7
	Average	**0.76**	**0.27**	**3.0**
	S.D.	**0.27**	**0.13**	**0.6**

2.3.3. Kinetics in Regions with Specific Binding

The brain regions with the highest specific binding of the radiotracers were the MTC and the ACG as shown in Figure 2-10. Intermediate binding was seen in the temporopolar cortex and dorsal lateral prefrontal cortex and the RN. Significant binding was seen throughout the cortical regions, including the IC, temporal and frontal cortex. A comparison of the time course for the radiotracers in the MTC and IC regions is shown in Figure 2-11. The time course is also plotted as a ratio with the CB concentration to provide an indication of when the psuedoequilibrium between bound-to-nondisplaceable binding occurs. For [^{18}F]MPPF, a plateau is reached in this ratio by approximately 30 minutes in the high binding regions. The target to CB ratios are very similar for [^{11}C]WAY-100635 and [^{18}F]MeFWAY, reaching a plateau by approximately 60 minutes in the IC, but not reaching a plateau within the 2 hour scanning period in the high uptake regions. The regional estimates of BP_{ND} for each of the radiotracers are given in Table 2-2.

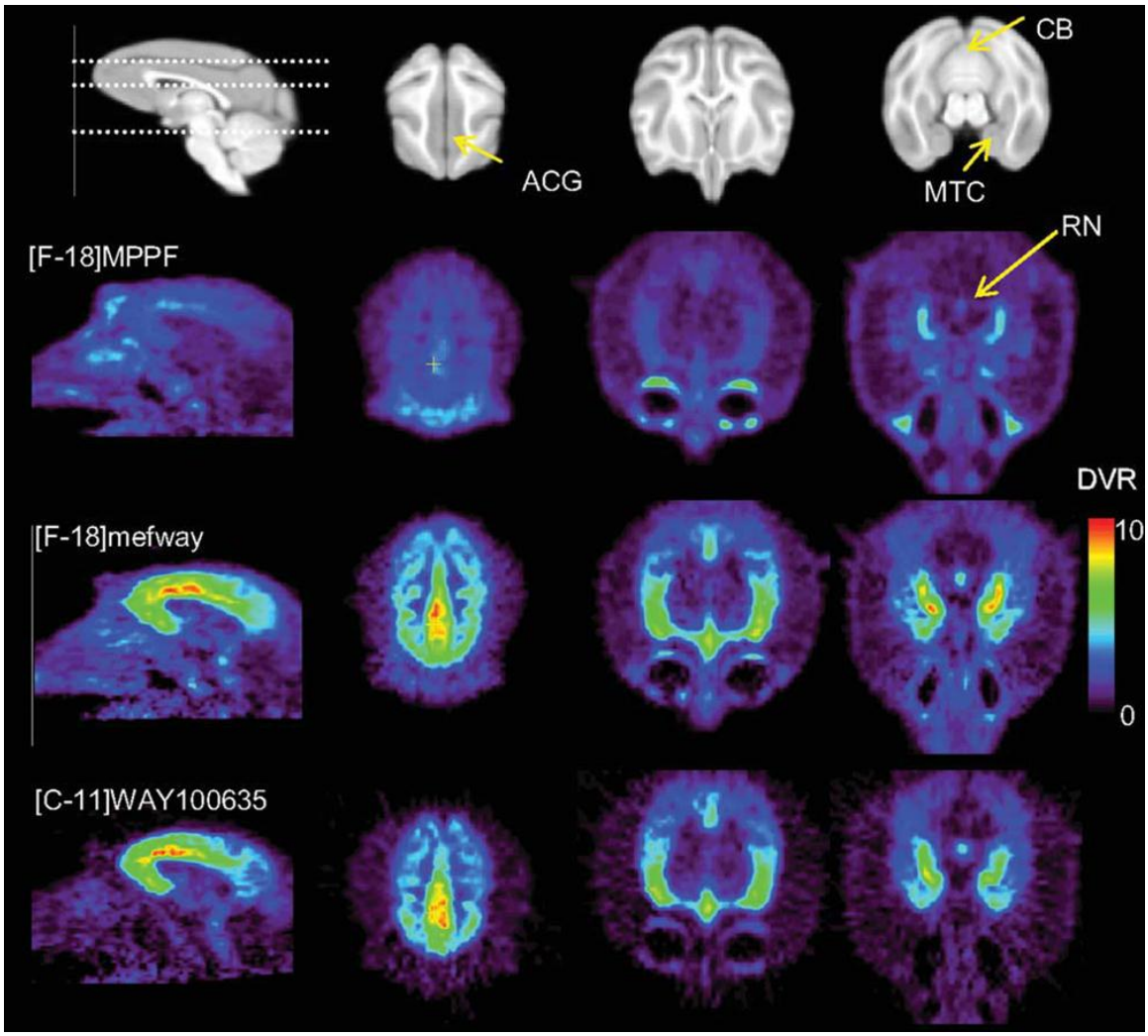

Figure 2-10: Parametric DVR comparisons of [^{18}F]MPPF, [^{18}F]MeFWAY, and [^{11}C]WAY-100635 in the rhesus monkey brain (M1). The top row is a skull stripped T1 magnetic resonance image, with the dotted line illustrating the planes of the 3 transaxial slices highlighting radiotracer binding.

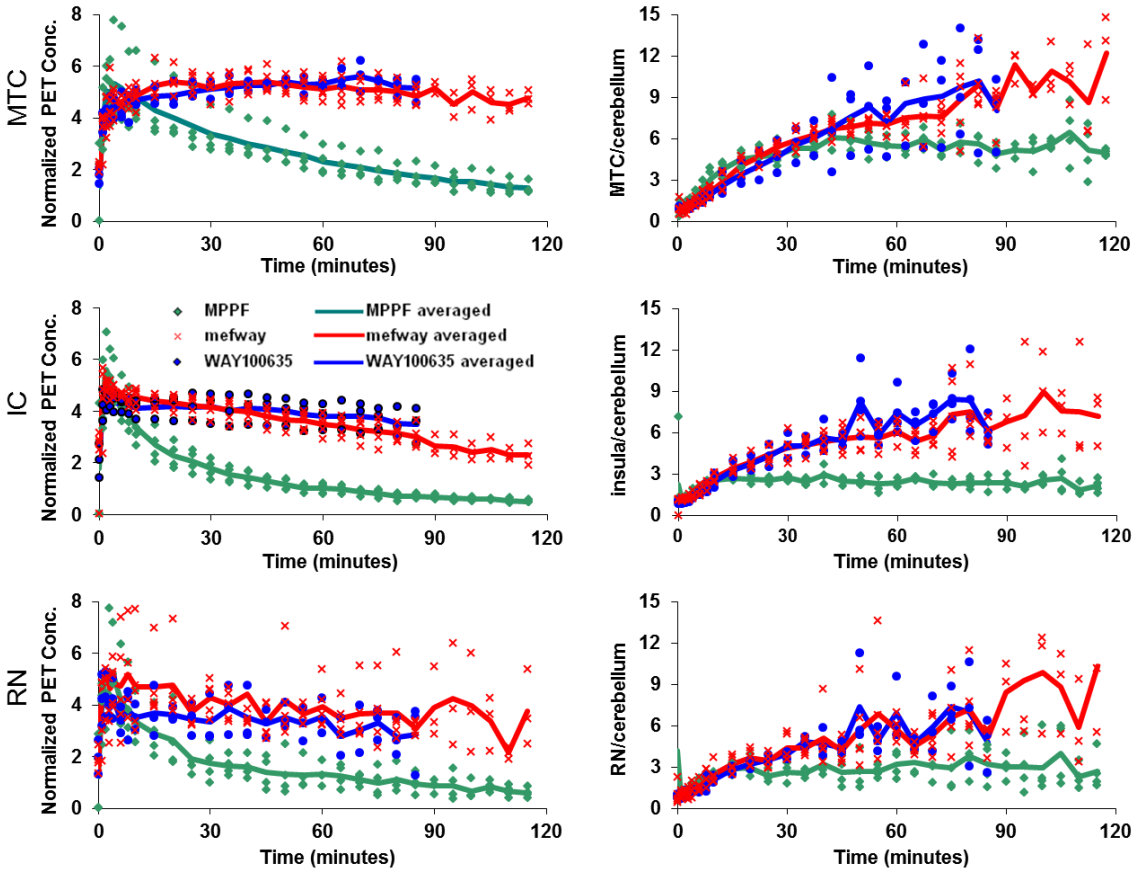

Figure 2-11: Time-activity curves for MTC (top) and IC (bottom) with [^{18}F]MPPF (♦), [^{18}F]MeFWAY (x), and [^{11}C]WAY-100635 (●). The left panel shows the time course for all the studies, normalized to injected dose and multiplied by the animal weight (kBq/cc/i.d.*kg*1000). The right panel shows the time course of the ratio of the regions to the CB. The lines represent the averages over all subjects for [^{18}F]MPPF (green), [^{18}F]MeFWAY (red), and [^{11}C]WAY-100635 (blue).

Table 2-2: Regional BP_{ND} estimates.

Radiotracer	Subject	MTC	ACG	RN	IC
[^{18}F]Mefway	M1	7.23	6.92	4.06	4.51
	M2	8.25	7.00	4.00	3.57
	M3	7.17	5.87	2.85	3.72
	M4	6.77	8.82	3.84	4.83
	mean ± s.d.	**7.36 ± 0.63**	**7.15 ± 1.23**	**3.69 ± 0.57**	**4.16 ± 0.61**
[^{18}F]MPPF	M1	3.01	2.05	1.49	1.24
	M2	3.67	2.19	1.71	1.11
	M3	2.99	1.93	0.98	0.98
	M4	2.88	2.30	1.18	1.28
	mean ± s.d.	**3.14 ± 0.36**	**2.12 ± 0.16**	**1.34 ± 0.32**	**1.15 ± 0.14**
[^{11}C]WAY-100635	M1	5.97	6.90	3.97	4.08
	M2	--	--	--	--
	M3	8.37	7.64	2.66	4.11
	M4	6.66	9.21	3.17	5.77
	mean ± s.d.	**7.00 ± 1.24**	**7.91 ± 1.18**	**3.27 ± 0.66**	**4.65 ± 0.97**

2.4. Discussion

This study compares the in vivo kinetics of three 5-HT_{1A} antagonist PET radiotracers in the rhesus monkey. The results indicate that [^{18}F]MeFWAY and [^{11}C]WAY-100635 have very similar in vivo kinetics throughout the regions of the brain and provides specific-to-nonspecific binding ratios of 2-3 times greater than [^{18}F]MPPF in the rhesus monkey.

2.4.1. Considerations in Plasma and Cerebellar Kinetics

The time course of parent radioligand in the arterial plasma was very similar for all three compounds. A rapid decrease over the first several minutes was followed by a slow clearance of the compound out to the end of the study. The radioligand [^{18}F]MeFWAY cleared from the arterial plasma at approximately half the rate of the other two compounds, however, in all cases the mean clearance time was of the same order as period of measurement (30 – 90 minutes) for the exponential component thus reducing the precision of this parameter estimate. The assay of

parent compound was performed by ethyl acetate extraction and this fraction could have also included lipophilic metabolites. No attempt was made to further characterize lipophilic species using HPLC or thin layer chromatography, as previous measurements revealed only a small fraction (<10%) of radiolabeled lipophilic metabolites of [^{18}F]MeFWAY in the rhesus monkey (Saigal et al., 2006) and conclude that only a small portion of the CB PET signal may be due to nonparent compound.

The CB is frequently used as a reference region for 5-HT$_{1A}$ PET studies to provide information of the radiotracer's kinetics in the absence of specific binding. In humans, there have been several reports on the presence of small, yet significant, levels of specific 5-HT$_{1A}$ binding in the CB (Parsey et al., 2005; Hirvonen et al., 2007). CB TACs were analyzed with both a one- and two-compartment model to determine if additional parameters (k_3, k_4) were needed to account for specific binding. Of the 10 studies acquired with arterial blood samples, only one study ([^{18}F]MPPF in M4) showed a significant improvement in the data description with the two-compartment model. However, for this study only the k_3 parameter was significantly larger than zero and this additional term may be attributed to imprecision in the measurement of metabolites. There are examples with PET radiotracers (e.g. [^{11}C]tropanyl benzilate) where the binding and dissociation are sufficiently rapid that a two-compartment model cannot resolve the binding and delivery processes (Koeppe et al., 1994). However, based upon the similarities of the in vivo kinetics of [^{18}F]MeFWAY with [^{11}C]WAY-100635 in the high binding regions and the reported in vivo rate constants of [^{11}C]WAY-100635 (Gunn et al., 1998), it is not likely that the delivery and the binding processes are being coupled in the single-compartment description of these data. The potential levels of specific 5-HT$_{1A}$ binding in the CB of the rhesus monkey are below the

threshold of detection for the methodologies employed in this work and these data suggest that the CB is a reasonable reference region for [^{18}F]MeFWAY.

In comparing the nondisplaceable distribution volume ($V_{ND} = K_1/k_2$), these data indicate a rank order of [^{18}F]MeFWAY > [^{18}F]MPPF > [^{11}C]WAY-100635. The tissue to plasma transport (K_1) is approximately equal for MeFWAY and MPPF, but the efflux constant (k_2) is larger for MPPF, resulting in a faster clearance from the tissue for this radiotracer. MPPF has been shown to be a substrate for p-glycoprotein (Pgp) (Passchier et al., 2000), and the presence of this transmembrane efflux pump increases the k_2. Neither MeFWAY nor WAY-100635 have been found to be Pgp substrates. Of the three compounds, [^{11}C]WAY-100635 displayed the smallest K_1 and, in turn, the lowest V_{ND}.

2.4.2. Considerations in Regions with Specific 5-HT$_{1A}$ Binding

The CG and the MTC were the brain regions demonstrating the highest levels of 5-HT$_{1A}$ binding for all three radiotracers. The region of highest focal binding was observed in the anterior hippocampus (within the region of the MTC), with elevated uptake seen throughout the entire hippocampal structure. There was no attempt to define the boundaries or subregions of the hippocampus without MRI scans for each individual. Many of the cortical areas were visually distinguishable on the [^{11}C]WAY-100635 and [^{18}F]MeFWAY scans, with elevated binding seen throughout the entire cingulate gyrus, orbitofrontal gyrus, central gyrus, superior and medial frontal gyri, temporal gyrus, and insula cortex. Reduced but detectable binding was observed in the occipital cortex. These cortical regions were not as visually distinct on the [^{18}F]MPPF data. The RNs were clearly defined with all three radiotracers as seen in Figure 2-10.

Figure 2-11 displays the target to CB ratios for the radiotracers during the course of the study. A plateau of this ratio represents a psuedoequilibrium of the two regions, a point at which the concentration in the free and the bound states are changing at the same rate. It is often desirable to acquire time series data until this plateau is reached to avoid possible flow dependent biases in the estimation of specific binding. It can be seen that in a region of the intermediate binding (IC), pseudoequlibrium is reached by 60 minutes for [^{11}C]WAY-100635 and [^{18}F]MeFWAY and by approximately 20 minutes for [^{18}F]MPPF. In the high binding region of the MTC, a plateau is not reached within the total time of acquisition for [^{11}C]WAY-100635 and [^{18}F]MeFWAY. Although the presence of psuedoequilibrium is not a necessary condition for accurate estimation of specific binding when using the Logan graphical method, it does suggest that a longer period may be required for linearization of the functional equations to avoid underestimation (i.e. negative bias) of the DVR parameter. For all four subjects it was found that the functional equation was linear starting at 40 minutes (i.e. t*=40) when the mean efflux term was excluded from the functional equation (i.e. $C_{ref}/\bar{k}_2 = 0$) for [^{11}C]WAY-100635 and [^{18}F]MeFWAY and a scanning duration of 90 minutes provided an adequate period for stable BP_{ND} estimation. For the [^{18}F]MPPF studies, the functional equations were linear within several minutes following injection and a shorter scanning duration is allowable for stable parameter estimation. An example of the Logan plot is shown in Figure 2-12in the region of the ACG for subject M4.

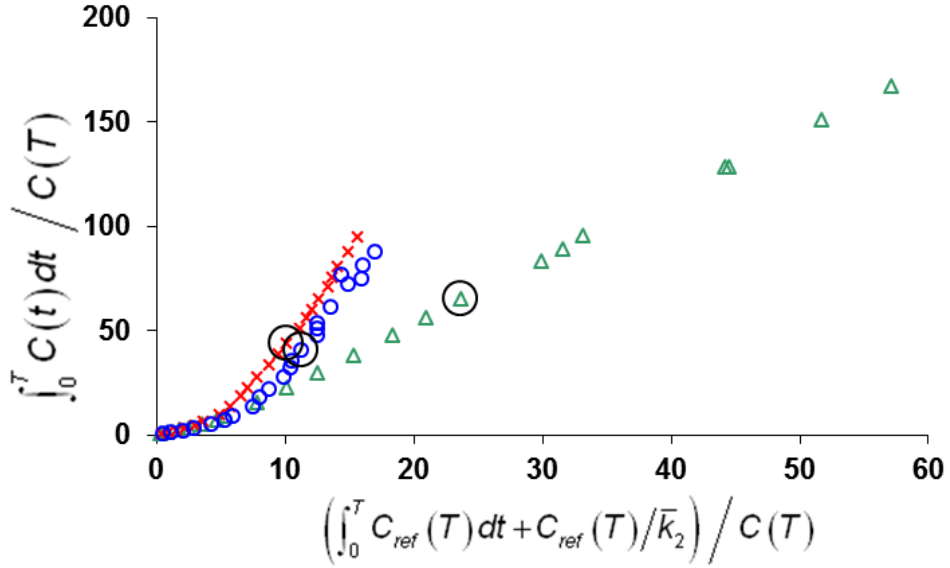

Figure 2-12: Logan DVR plots for [^{18}F]MPPF (Δ), [^{18}F]MeFWAY (x), and [^{11}C]WAY100635 (o) in the ACG. For these curves, the term $C_{ref}/\bar{k}_2$ was set to 0 to illustrate the period of linearization with no a priori assumptions of the mean $\bar{k}_2$ parameter. The circles around the three points correspond to the 40 minute data point. The data for [^{18}F]MeFWAY displays only the first 90 minutes to be consistent with the [^{11}C]WAY-100635 and the [^{18}F]MPPF displays only 80 minutes to scale the axes for enhanced visualization.

2.4.3. Potential Mass Effects from WAY-100635

Because there was a large variation in the injected mass of the three ligands, the potential effects of reduced specific binding due to competing unlabeled ligand must be closely examined. The shorter half-life of the ^{11}C radiolabel resulted in a larger amount of injected mass for the [^{11}C]WAY-100635 studies because of the decrease in specific activity due to the transport time needed to deliver the radioligand to the animal imaging facility. For the three studies reported herein there was an injected WAY-100635 mass of 1.0, 1.7 and 0.7 nmol/kg, for M1, M3 and M4, respectively. Hume and colleagues performed detailed experiments in rats using [^{3}H]WAY-100635 and reported an ED_{50} of 4.78 nmol/kg (Hume et al., 1994). The ED_{50} represents a measure of the injected dose required to reduce the maximal binding by one-half. Using this value and the relation for receptor occupancy and ED_{50} (Hume et al., 1998), it can be estimated

that the occupancies of the WAY-100635 at the 5-HT_{1A} receptor sites are 18% (M1), 26% (M3) and 13% (M4) for these [^{11}C]WAY-100635 studies. The increased receptor occupancy by the unlabeled drug will result in a decreased PET measured BP_{ND} due to the competition between the radiolabeled and unlabeled drugs. However, the measured BP_{ND} values in Table 2 do not scale inversely with the injected mass of [^{11}C]WAY-100635. For example, if we consider the region of the ACG, the BP_{ND} of M3 study ranks in the middle for [^{11}C]WAY-100635 and lowest for the [^{18}F]MPPF and [^{18}F]MeFWAY studies despite having the highest WAY100635 mass injection. We speculate that the ED_{50} (and apparent K_D) may be higher in rhesus monkeys than rats and that the significance of competing unlabeled WAY-100635 mass may not be detectable in this small sample size. However, it is not possible to measure the effects of competing mass for the [^{11}C]WAY-100635 studies without performing additional multi-dose scans on each animal. Therefore, a caveat must be issued that the average BP_{ND} values of [^{11}C]WAY-100635 reported here may be underestimated by an upper limit of 20% due to nontracer conditions. For the sake of comparison, if a comparable ED_{50} is assumed for [^{18}F]MPPF and [^{18}F]MeFWAY, then the occupancy of the unlabeled drug is less than 3% for both radiotracers.

2.5. Summary

[^{18}F]MeFWAY has similar in vivo kinetic behavior to [^{11}C]WAY-100635, with both being highly selective PET radiotracers for 5-HT_{1A} receptor binding. [^{18}F]MeFWAY and [^{11}C]WAY-100635 provide a greater dynamic range in BP_{ND} measurement compared to [^{18}F]MPPF, but require a longer study duration to achieve stable BP_{ND} estimates. [^{18}F]MeFWAY offers the advantage of increased 5-HT_{1A} detection sensitivity over [^{18}F]MPPF throughout the brain regions with low, intermediate, and high 5-HT_{1A} expression. Additionally, [^{18}F]MeFWAY

provides an improvement of counting statistics compared to [^{11}C]WAY-100635, due to the 110 minute half-life of the ^{18}F radiolabel. This chapter demonstrates [^{18}F]MeFWAY's utility in the nonhuman primate for in vivo assay of 5-HT_{1A} binding laying the ground work for its use in more complex PET protocols and its translation into human studies.

2.6. References

Akaike, H., 1974. A new look at the statistical model identification. IEEE Transactions on Automatic Control 19, 716–23.

Christian, B.T., Vandehey, N.T., Floberg, J.M., Mistretta, C.A., 2010. Dynamic PET Denoising with HYPR Processing. Journal of Nuclear Medicine 51, 1147–54.

Gunn, R.N., Sargent, P.A., Bench, C.J., Rabiner, E.A., Osman, S., Pike, V.W., Hume, S.P., Grasby, P.M., Lammertsma, A.A., 1998. Tracer kinetic modeling of the 5-HT_{1A} receptor ligand [carbonyl-^{11}C]WAY-100635 for PET. NeuroImage 8, 426–40.

Hirvonen, J., Kajander, J., Allonen, T., Oikonen, V., Någren, K., Hietala, J., 2007. Measurement of serotonin 5-HT_{1A} receptor binding using positron emission tomography and [carbonyl-^{11}C]WAY-100635-considerations on the validity of cerebellum as a reference region. Journal of Cerebral Blood Flow and Metabolism 27, 185–95.

Hume, S.P., Ashworth, S., Opacka-Juffry, J., Ahier, R.G., Lammertsma, A.A., Pike, V.W., Cliffe, I.A., Fletcher, A., White, A.C., 1994. Evaluation of [O-methyl-^{3}H]WAY-100635 as an in vivo radioligand for 5-HT_{1A} receptors in rat brain. European Journal of Pharmacology 271, 515–23.

Hume, S.P., Gunn, R.N., Jones, T., 1998. Pharmacological constraints associated with positron emission tomographic scanning of small laboratory animals. European Journal of Nuclear Medicine 25, 173–6.

Hwang, D.R., Simpson, N.R., Montoya, J., Man, J.J., Laruelle, M., 1999. An improved one-pot procedure for the preparation of [^{11}C-carbonyl]WAY-100635. Nuclear Medicine and Biology 26, 815–9.

Jenkinson, M., Smith, S., 2001. A global optimisation method for robust affine registration of brain images. Medical image analysis 5, 143–156.

Kessler, R.M., Ansari, M.S., De Paulis, T., Schmidt, D.E., Clanton, J.A., Smith, H.E., Manning, R.G., Gillespie, D., Ebert, M.H., 1991. High affinity dopamine D_2 receptor radioligands. 1. Regional rat brain distribution of iodinated benzamides. Journal of Nuclear Medicine 32, 1593–600.

Koeppe, R.A., Frey, K.A., Mulholland, G.K., Kilbourn, M.R., Buck, A., Lee, K.S., Kuhl, D.E., 1994. [^{11}C]tropanyl benzilate-binding to muscarinic cholinergic receptors: methodology and kinetic modeling alternatives. Journal of Cerebral Blood Flow and Metabolism 14, 85–99.

Kumar, J.S.D., Mann, J.J., 2007. PET tracers for 5-HT_{1A} receptors and uses thereof. Drug discovery today 12, 748–56.

Logan, J., Fowler, J., Volkow, N., 1996. Distribution volume ratios without blood sampling from graphical analysis of PET data. Journal of Cerebral Blood Flow and Metabolism 16, 834–40.

Mazoyer, B.M., Huesman, R.H., Budinger, T.F., Knittel, B.L., 1986. Dynamic PET data analysis. Journal of computer assisted tomography 10, 645–53.

Muzic, R.F., Cornelius, S., 2001. COMKAT: Compartment model kinetic analysis tool. Journal of Nuclear Medicine 42, 636–45.

Parsey, R. V, Arango, V., Olvet, D.M., Oquendo, M.A., Van Heertum, R.L., Mann, J.J., 2005. Regional heterogeneity of 5-HT_{1A} receptors in human cerebellum as assessed by positron emission tomography. Journal of Cerebral Blood Flow and Metabolism 25, 785–93.

Passchier, J., Van Waarde, A., Doze, P., Elsinga, P.H., Vaalburg, W., 2000. Influence of P-glycoprotein on brain uptake of [^{18}F]MPPF in rats. European journal of pharmacology 407, 273–80.

Pike, V.W., Halldin, C., Wikström, H., Marchais, S., McCarron, J.A., Sandell, J., Nowicki, B., Swahn, C.G., Osman, S., Hume, S.P., Constantinou, M., Andrée, B., Farde, L., 2000. Radioligands for the study of brain 5-HT_{1A} receptors in vivo--development of some new analogues of way. Nuclear Medicine and Biology 27, 449–455.

Saigal, N., Pichika, R., Easwaramoorthy, B., Collins, D., Christian, B.T., Shi, B., Narayanan, T.K., Potkin, S.G., Mukherjee, J., 2006. Synthesis and biologic evaluation of a novel serotonin 5-HT_{1A} receptor radioligand, ^{18}F-labeled MeFWAY, in rodents and imaging by PET in a nonhuman primate. Journal of Nuclear Medicine 47, 1697–706.

Tai, C., Chatziioannou, A., Siegel, S., Young, J., Newport, D., Goble, R.N., Nutt, R.E., Cherry, S.R., 2001. Performance evaluation of the microPET P4: a PET system dedicated to animal imaging. Physics in Medicine and Biology 46, 1845–62.

Tewson, T.J., Banks, W., Franceschini, M., Hoffpauir, J., 1989. A trap for the removal of nitrogen oxides from carbon-11 carbon dioxide. Applied Radiation Isotopes 40, 765–8.

Chapter 3 In vivo comparison of *cis*- and *trans*- [^{18}F]MeFWAY in the nonhuman primate

3.1. Introduction

Previous work presented in Chapter 2 validated the use of *trans*-[^{18}F]MeFWAY for in vivo assay of the 5-HT$_{1A}$ system in the nonhuman primate. [^{18}F]MeFWAY can be radiolabeled as two different isomeric forms at the 4-cyclohexyl position, representing *cis*-[^{18}F]MeFWAY and *trans*-[^{18}F]MeFWAY, which are shown in Figure 3-1. Binding affinity of isomeric forms of another closely related PET radioligand, 4-[^{18}F]FCWAY, has been previously examined (Lang et al., 2000). The conformation of *trans*- and *cis*- [^{18}F]FCWAY displayed a dramatic difference in 5-

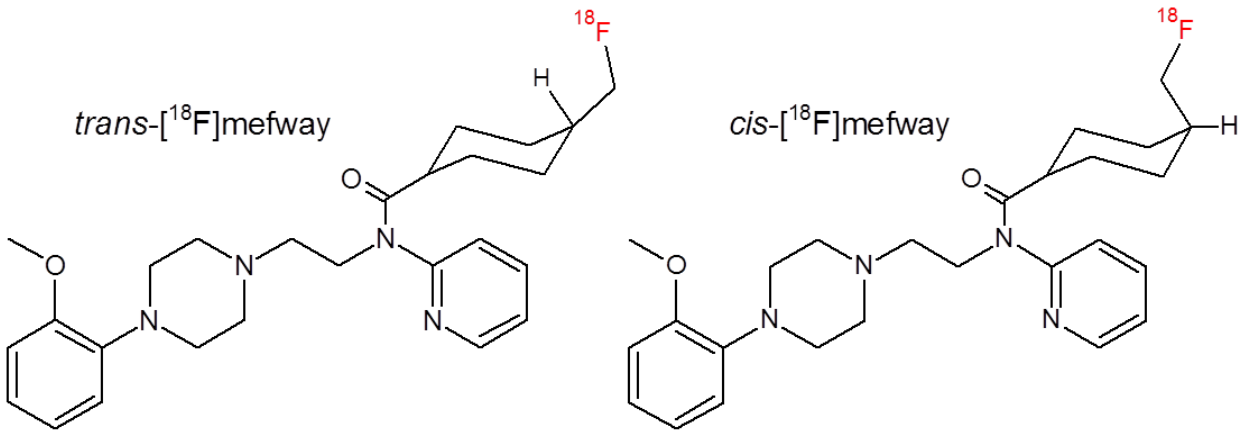

Figure 3-1: Molecular structure of *trans*- and *cis*-[^{18}F]MeFWAY.

HT$_{1A}$ binding with reported IC$_{50}$ values of 1.7nM and 21nM, respectively. In vivo PET measures revealed similar blood metabolic profiles, but hippocampus to cerebellum ratios were 19.3 and 3.6 for *trans*- and *cis*- [^{18}F]FCWAY, respectively (Lang et al., 1999). Similarly, binding of 4-methoxy WAY-100635 analogues were shown to have different binding depending upon isomeric state (Wilson et al, 1999). Preliminary in vitro measures have also been made for [^{18}F]MeFWAY, which have indicated that the *cis*- isomer has lower affinity for the 5-HT$_{1A}$ receptor than the *trans*- isomer (Saigal et al, 2006b). The goal of this work was to investigate the

in vivo behavior of *cis*-[^{18}F]MeFWAY and assess its potential as a moderate affinity 5-HT_{1A} radiotracer for yielding shortened equilibration times (~30 minutes) and sufficiently high target to background binding (>1.5) for PET imaging applications. This was accomplished by comparing the in vivo kinetics of *cis*-[^{18}F]MeFWAY and *trans*-[^{18}F]MeFWAY in rhesus monkeys and is described in this chapter.

3.2. Methods

3.2.1. Separation of *cis*- and *trans*-tosyl MeFWAY precursor

The tosylate precursor (N-{2-[4-(2-methoxyphenyl)piperazinyl]ethyl}-N-(2-pyridyl)-N-(4-tosyloxymethylcyclohexane)carboxamide) for the radiochemical synthesis of [^{18}F]MeFWAY and MeFWAY reference standard were purchased as a mixture of geometric isomers from a commercial vendor (Huayi Isotopes Co.). The isomeric separation of the tosyl MeFWAY precursor was performed using HPLC methods. Reverse phase HPLC utilized a C18 Econosil 10 µm 250 x 10 mm column (Alltech) and mobile phase consisting of 60% acetonitrile, 40% water, and 0.1% triethylamine (by volume) at a flow rate of 2.5 mL/min. The two isomeric peaks eluted from the column at 19 and 23 minutes for the *trans*- and *cis*- tosylate MeFWAY, respectively. The *cis*- and *trans*- tosylates were isolated from the corresponding HPLC fractions using liquid-liquid extraction. The acetonitrile was first removed from the individual eluted samples using rotoevaporation. The remaining portion was then added to 15-20 mL of methylene chloride in a separatory funnel and mixed. Once adequate separation was achieved, the liquid layer volumes were separated into two different flasks. The portion containing the methylene chloride and precursor was then further dried with magnesium sulfate and filtered. The methylene chloride was then evaporated by rotoevaporation. The product was further dried by azeotropic distillation

with anhydrous acetonitrile. After separation, analytic HPLC was performed on the samples to ascertain isomeric purity. Separation was not performed on the MeFWAY standard.

3.2.2. Analytic Validation

Isomeric purity of the separated forms was measured using HPLC and mass spectroscopy methods. Analytic HPLC was performed using a mobile phase consisting of 45% acetonitrile and 55% 0.1M aqueous ammonium formate at a flow rate of 2.5 mL/min. The analytic column was a C18 Prodigy 5 µm 4.6 x 250 mm ODS 3 100Å (Phenomenex). The *cis*- and *trans*- mass peaks were quantitatively assayed with a uv/vis absorption detector (Waters Model 2489) at 254 nm.

Mass spectrometry (MS) was conducted on the original commercially purchased compounds (MeFWAY standard and tosyl precursor) and on the tosylate precursor following separation. The MS was acquired using an Agilent ESI-TOF mass spectrometer in positive ion electrospray mode. Liquid chromatography mass spectrometry (LCMS) was performed on a ThermoFinnigan LTQ mass spectrometer with an Eksigent 2DnanoLC pump. The pump was setup in gradient mode with two solvents. Solvent A consisted of 0.1% formic acid in water and solvent B consisted of 50% acetonitrile, 50% ethanol, and 0.1% formic acid. The flow rate through the column was 300 nL/min consisting of initially 2% solvent B, and increasing solvent B from 2% to 90% from 2-20 minutes, then holding solvent B at 90% for 3 minutes. The column was a C18 Magic 5 µm 100 x 0.1 mm 300Å (Michrom) and a C8 Zorbax 5 µm 300SB 300 Å (Agilent) loading trap. The MS consisted of positive nanoESI spray at 3000 V using full MS scan in the range of 200 to 1000 m/z. LCMS was performed on isolated samples of *trans*-tosylate MeFWAY, *cis*-tosylate MeFWAY and the *cis*-, *trans*-MeFWAY standard.

3.2.3. Radiochemical synthesis

The ^{18}F radiolabel was produced by a 16-MeV GE PETtrace cyclotron. The radiochemical synthesis was performed similar to methods in presented in section 2.2.1.2. In brief, 1 mg of precursor (either *trans*- or *cis*-) dissolved in 400 µL of anhydrous acetonitrile was added to the dry ^{18}F then heated at 95˚C for 10 minutes. The mixture was then dissolved in 3 mL of methanol and passed through a preconditioned alumina cartridge. The eluted methanol was then dried and dissolved in 1.5 mL of HPLC mobile phase and injected onto HPLC. HPLC consisted of a C18 Econosil 10 µm 250 x 10 mm column (Alltech) and mobile phase consisting of 50% acetonitrile, 50% water, and 0.1% triethylamine (by volume) at a flow rate of 5 mL/min. *Trans*-[^{18}F]MeFWAY eluted from the column at 11.0 minutes and *cis*-[^{18}F]MeFWAY eluted from the column at 12.2 minutes. The eluted product was then diluted and passed through a C18 Sep-Pak for final formulation. The radiosynthesis was completed in 1.5 hours, yielding specific activities of 111-130 GBq/mCi (3-3.5 Ci/µmol) and batch yields of 1.48-2.96 GBq (40-80 mCi).

3.2.4. Subjects

PET scans with *cis*- and *trans*-[^{18}F]MeFWAY were performed on each of two Macaca mulattas (rhesus)(one male, one female; 14 kg, 7.7 kg). The ages of the subjects were 12.3 and 13.6 years and both radiotracers were scanned within two weeks of each other. Subject preparation and care was similar to methods in section 2.2.2. Radiotracer was administered through the saphenous vein and venous plasma samples were acquired on the opposite limb.

3.2.5. Data acquisition

The PET scans were acquired on a microPET P4 scanner similar to methods in section 2.2.3. Data collection was initiated with the bolus injection of radiotracer of 120 ± 4.4 MBq (3.24 ± 0.12 mCi) and continued for a total acquisition time of 90 minutes. Venous blood samples were

acquired for the *cis*-[^{18}F]MeFWAY studies beginning at 30 minutes, with 0.5 mL withdrawn at 10 minute intervals. The whole blood samples were assayed for radioactivity and then centrifuged for the extraction of plasma. Lipophilic species were extracted from the plasma by liquid-liquid extraction with ethyl acetate using methods described in Chapter 2 (see also Wooten et al., 2011). Thin layer chromatography (TLC) was performed using aluminum backed silica gel plates with a mobile phase of 50% methanol and 50% solution of 10% ammonium acetate in water. The plates were then dried and exposed on an autoradiographic phosphor plate to determine the presence of radiolabeled lipophilic species.

3.2.6. Data analysis

Raw list mode emission data for each individual scan were binned into temporal frames of 4 x 1 minute, 3 x 2 minutes, and 16 x 5 minutes. Corrections for scanner deadtime and random coincidence events were performed. The sinograms were reconstructed using filtered back projection with a 0.5 cm^{-1} ramp filter and corrections were applied for attenuation, scatter, radioactive decay, and scanner normalization. Reconstructed voxel dimensions were 1.90 x 1.90 x 1.21 mm^3 with a total matrix size of 128 x 128 x 63 voxels. Dynamic PET images for each subject were realigned into common space by using a rigid body transformation matrix calculated by SPM5 software (http://www.nitrc.org/projects/spm/) based upon the first six minutes of integrated data from each study. Time activity curves (TACs) were extracted by drawing circular regions of interest (ROIs) in the areas of the brain including the mesial temporal cortex (MTC), anterior cingulate gyrus (aCG), insula cortex (IC), raphe nuclei (RN) and cerebellum (CB).

A multilinear Logan reference region method was used to obtain an index of specific binding in the specified regions of the brain using the cerebellum as a reference region and a period of linearization t* of 40 minutes (Logan et al., 1996). A value of 0.27 min^{-1} was used for $\bar{k}_2$ in all of the distribution volume ratio (DVR) estimates. DVR was converted to nondisplaceable binding potential (BP_{ND} = DVR – 1) which is the equilibrium ratio of specifically bound to nondisplaceable radioligand in tissue (Innis et al., 2007). For visual comparison, parametric BP_{ND} images were generated at the voxel level using the same multilinear Logan method as used above.

3.3. Results

3.3.1. Analytic identification of *cis*- and *trans*-tosyl MeFWAY and MeFWAY

Shown in Figure 3-2 are the chromatographic spectra of the MeFWAY standard. The MS

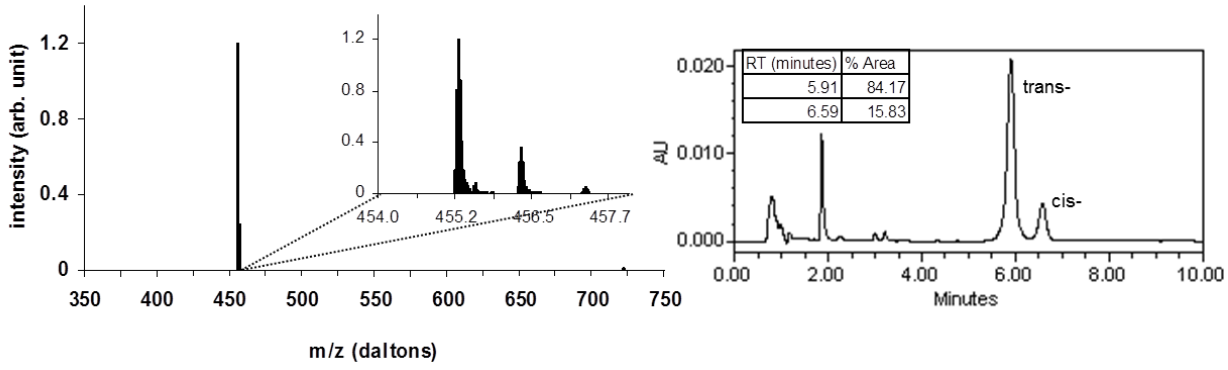

Figure 3-2: MS spectrum (left) and HPLC chromatogram (right) of the isomeric mixture of reference MeFWAY standard. The magnified view of MS displays the main peak along with corresponding ^{13}C peaks.

spectrum reveals the presence of only a single mass peak of 455 daltons, along with the corresponding peaks containing fractions of ^{13}C. The HPLC chromatogram illustrates the presence of two absorption peaks, corresponding to the *trans*- and *cis*- MeFWAY forms, indicating the presence of an 84:16 mixture of *trans*- to *cis*- MeFWAY.

The analytic spectra for the isomerically separated tosyl MeFWAY precursors are shown in Figure 3-3. LCMS performed on the isolated samples of *trans*-tosylate MeFWAY and *cis*-tosylate MeFWAY resulted in masses of 607 daltons for both tosylate MeFWAY samples indicating there is no mass difference between the two samples. Also seen are mass fragments at

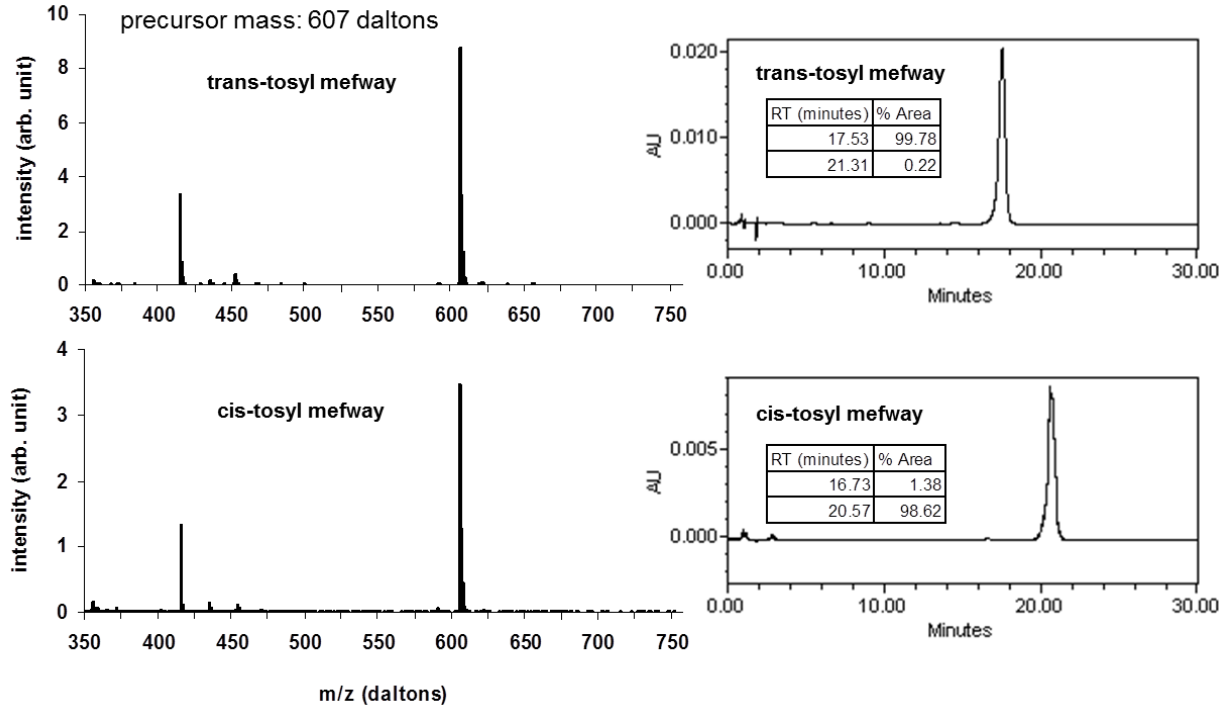

Figure 3-3: Isomeric validation of tosyl MeFWAY. The left column shows the LCMS spectra for *trans*-(top) and *cis*-(bottom) tosyl MeFWAY. The right column shows the corresponding HPLC chromatograms of the individual separated *trans*- and *cis*- tosyl MeFWAY isomers.

approximately 420 daltons indicating a breakdown of compound during processing with identical fragments seen in both samples. Prior to the HPLC separation, the tosyl MeFWAY contained a 64:36 mixture of *trans*- to *cis*- tosyl MeFWAY. Following separation, the HPLC chromatograms

in Figure 3-3 reveal a greater than 99% isomeric purity for the isolated *trans*-tosyl MeFWAY and greater than 98% for the isolated *cis*-tosyl MeFWAY. The radiochemical labeling of ^{18}F to the individual *cis*- and *trans*- MeFWAY precursors resulted in isomeric radiochemical purities of 99.0% for *trans*-[^{18}F]MeFWAY and 98.4% for *cis*-[^{18}F]MeFWAY.

3.3.2. Blood data

Venous blood draws were performed on the *cis*-[^{18}F]MeFWAY studies during the period of 30-90 minutes post-injection. The presence of parent compound, based upon the component in the ethyl acetate fraction, could be described by a single exponential function, with an average decay constant of 0.016 min^{-1} (0.014, 0.018 min^{-1}). This is in close agreement with similar measures made on separate, same age subjects using *trans*-[^{18}F]MeFWAY, yielding a washout constant of 0.016 min^{-1} (0.017, 0.013, 0.018 min^{-1}). The TLC performed on the ethyl acetate fraction showed only one radioactive peak which was consistent with the *cis*-[^{18}F]MeFWAY standard.

3.3.3. PET data

Cerebellar time-activity curves for *cis*- and *trans*- [^{18}F]MeFWAY are shown in Figure 3-4. The CB time courses of the two isomers show close consistency. Following the passage of the bolus activity, there is a fast and a slow component in the clearance of the tracer from the CB. At time greater than 30 minutes, the clearance rates for each tracer were 0.012 min^{-1} (0.011, 0.014 min^{-1}) for *trans*-[^{18}F]MeFWAY and 0.012min^{-1} (0.012, 0.013 min^{-1}) for *cis*- [^{18}F]MeFWAY. Also shown in Figure 3-4 are early (first 5 minutes) and late (≥45 minutes) integrated PET images in the region of the CB for both *cis*- and *trans*- [^{18}F]MeFWAY studies in one of the subjects. Significant binding of only the *trans*-[^{18}F]MeFWAY in the vermis of the cerebellum can be seen in the late image.

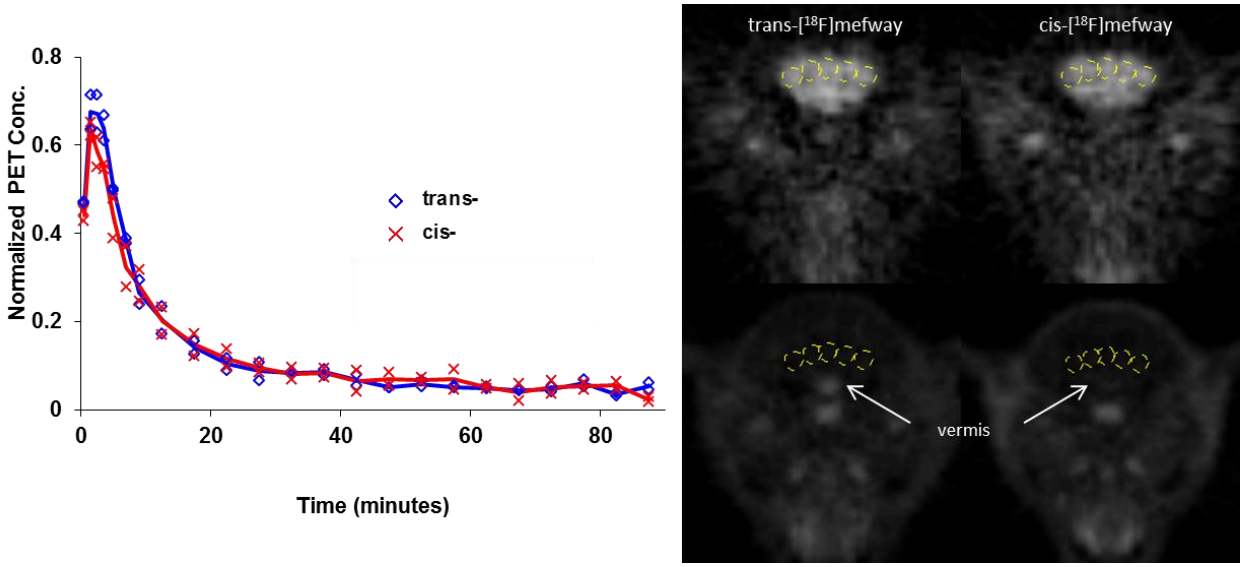

Figure 3-4: PET CB time course. (Left) CB time activity curves for *trans*-[^{18}F]MeFWAY (◊) and *cis*-[^{18}F]MeFWAY (x) averaged over the two studies in units of (kBq/cc/i.d. x kg)*100. (Right) CB regions of interest displayed on the early (0 – 5 minutes) (top row) and late (45 – 90 minutes) (bottom) PET images.

Similar to data presented in Chapter 2, elevated uptake of *trans*-[^{18}F]MeFWAY was detected across the cortical and midbrain regions. In comparison, only small amounts of uptake could be detected with *cis*-[^{18}F]MeFWAY. Figure 3-5 illustrates comparative time activity curves for *cis*- and *trans*- [^{18}F]MeFWAY in the MTC and IC. Also shown are target-to-CB ratio plots for the two radiotracers. A plateau of the curve is not reached in the MTC with *trans*-[^{18}F]MeFWAY, whereas *cis*- reaches a plateau of roughly 1.9 averaged across each monkey at approximately 10 minutes. An earlier plateau is reached in the IC with *trans*-[^{18}F]MeFWAY at a ratio of 6.7 after 60 minutes compared to 1.3 at 5 minutes for *cis*-[^{18}F]MeFWAY. Table 3-1 shows *trans*- and *cis*-[^{18}F]MeFWAY BP_{ND} estimates for the regions of the MTC, aCG, IC and RN, along with the ratio of BP_{ND} for the two radiotracers. Parametric BP_{ND} images of *trans*- and *cis*- [^{18}F]MeFWAY are shown in Figure 3-7 highlighting specific binding in the MTC. Elevated binding is evident with *cis*-[^{18}F]MeFWAY in this region, but at considerably lower levels than *trans*-

[^{18}F]MeFWAY. Logan plots in the MTC of *trans*- and *cis*- [^{18}F]MeFWAY in one subject are shown in **Error! Reference source not found.**.

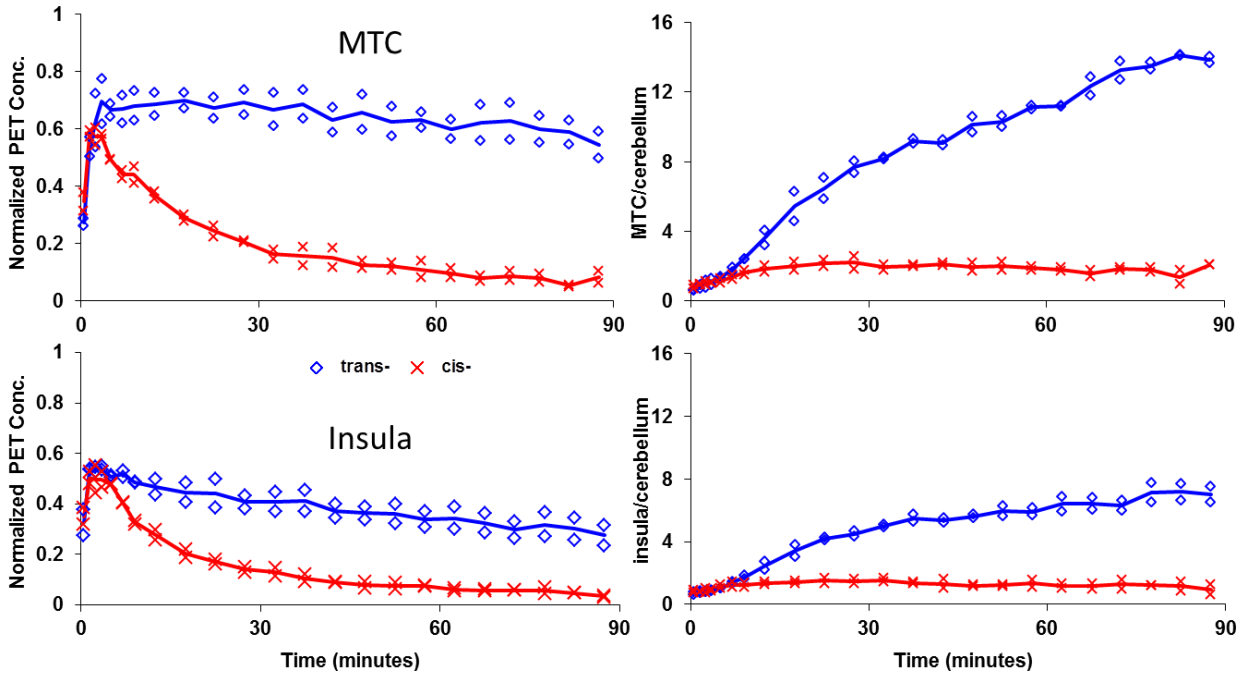

Figure 3-5: (Left) Time activity curves in the MTC (top) and IC (bottom) for *trans*-[^{18}F]MeFWAY (◊) and *cis*-[^{18}F]MeFWAY (x). The lines represent the average of the two subjects and are normalized to (kBq/cc/i.d. x kg)*100. (Right) Target to CB time course for the MTC (top) and IC (bottom). The CB data was modeled as a 2-exponential function for times greater than 5 minutes.

Table 3-1: BP_{ND} estimates in the regions with specific 5-HT_{1A} binding.

Region	[^{18}F]mefway	M1	M2	Mean	Ratio
MTC	*trans*-	8.14	7.25	**7.70**	**13.2**
	cis-	0.46	0.71	**0.58**	
CG	*trans*-	5.13	4.77	**4.95**	**15.5**
	cis-	0.22	0.42	**0.32**	
IC	*trans*-	3.65	2.89	**3.27**	**15.9**
	cis-	0.10	0.31	**0.21**	
RN	*trans*-	2.88	3.23	**3.05**	**23.7**
	cis-	0.07	0.19	**0.13**	

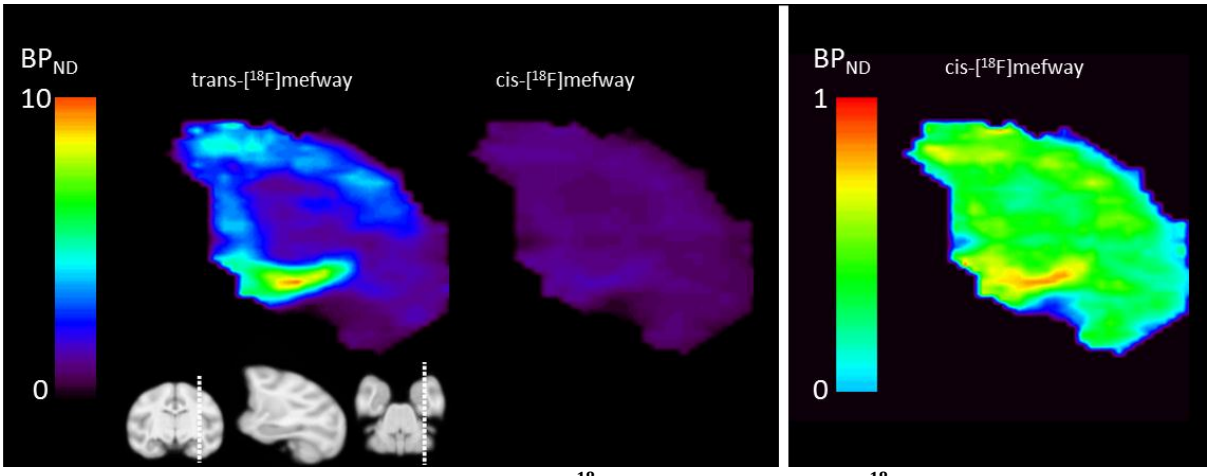

Figure 3-6: (Left) BP_{ND} PET images of *trans*-[^{18}F]MeFWAY and *cis*-[^{18}F]MeFWAY highlighting binding in the MTC in subject M2. The MRI illustrates the sagittal slice of the PET image. (Right) BP_{ND} image of *cis*-[^{18}F]MeFWAY with the threshold adjusted to enhance visualization of binding in the MTC.

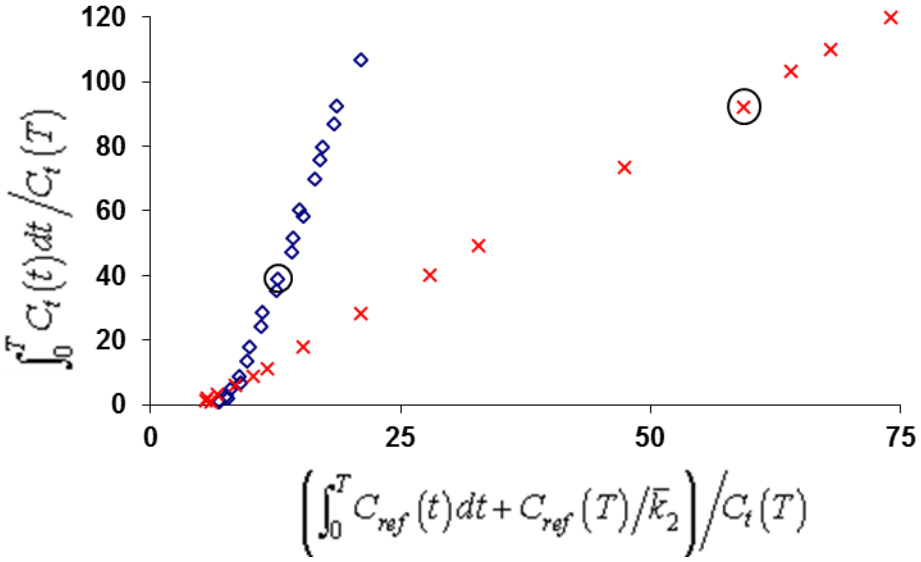

Figure 3-7: Logan DVR plots in the MTC for trans-[^{18}F]MeFWAY (◊) and cis-[^{18}F]MeFWAY (x) in one subject. The circles around the two points represent the 40 minute time points. To enhance the visualization of the trans-[^{18}F]MeFWAY plot, only the first 55 minutes of data was shown for cis-[^{18}F]MeFWAY to allow a scaling of the axis.

3.4. Discussion

Validation studies of *trans*-[^{18}F]MeFWAY in the nonhuman primate have demonstrated its high specificity for the 5-HT_{1A} receptor site and favorable PET imaging properties, providing a

valuable ^{18}F labeled alternative to [^{11}C]WAY100635 (Saigal, 2006a; Wooten et al., 2011). The reported BP_{ND} values were 7.4 ± 0.6 in the 5-HT_{1A} receptor-rich region of the hippocampus (included in the MTC) and elevated specific binding in many of the temporal and frontal cortical regions in the brain. To provide a stable estimate of specific binding in the receptor rich regions of the brain, it was reported that approximately 90 minutes of dynamic PET data acquisition would be required to avoid flow dependent variations in BP_{ND} measurement. The motivation for exploring the use of *cis*-[^{18}F]MeFWAY as a biomarker for 5-HT_{1A} binding was driven by the desire for a radiotracer with "faster" kinetics, permitting a shorter scanning session and making it a candidate ligand for measuring endogenous 5-HT competition. For example, under certain conditions a larger (i.e. faster) ligand-receptor dissociation constant (k_{off}) may result in an earlier time of equilibration, and in turn, a shorter scanning period. The purpose of this investigation was to examine if *cis*-[^{18}F]MeFWAY would yield more rapid equilibration and retain a sufficiently large BP_{ND} value for PET research applications.

An isomeric mixture of *cis*- and *trans*- tosylate precursor was used as the starting material for these studies. The chromatographic separation of the *cis*- and *trans*- tosylate precursors provided high purity starting materials (>98%) for radiochemistry of both radioligands. Following the radiochemical syntheses, only small amount of radiolabeled isomeric impurities could be detected, the formulated *trans*-[^{18}F]MeFWAY contained 1.0% *cis*-[^{18}F]MeFWAY and the formulated *cis*-[^{18}F]MeFWAY contained 1.6% *trans*-[^{18}F]MeFWAY. The effects of these impurities on interpreting the results are discussed below.

Venous blood samples were acquired for only the *cis*-[^{18}F]MeFWAY studies to provide an indication of the plasma concentration and the possible presence of radiolabeled metabolites. The clearance rate of radioligand from the venous plasma was found to be in close agreement with

the measured clearance from previous *trans*-[^{18}F]MeFWAY studies (using venous samples) in separate subjects of similar age. TLC analysis performed on the *cis*-[^{18}F]MeFWAY ethyl acetate extractions revealed only one radioactive peak, which corresponded to the parent compound. Ma and colleagues reported extensive blood analysis on the *cis*- and *trans*- isomers of 3-[^{18}F]FCWAY (Ma et al., 2006). Using cynomolgus monkey hepatocytes, it was found the profile of radiolabeled metabolites were uniform between the isomeric compounds. Although similar studies would be required to fully characterize the metabolic profiles of *cis*- and *trans*-[^{18}F]MeFWAY, these preliminary data suggest the presence of radiolabeled metabolism will be comparable between them.

The PET data demonstrate close agreement in the *trans*port of compounds across the blood-brain barrier. As seen in Figure 3-4, the time course of *cis*-[^{18}F]MeFWAY and *trans*-[^{18}F]MeFWAY in the cerebellum are almost indistinguishable. Assuming only negligible cerebellar 5-HT$_{1A}$ binding and the similar time course of the radiotracers in the plasma, approximately equivalent nondisplaceble volumes of distribution (V_{ND}) for *cis*-[^{18}F]MeFWAY and *trans*-[^{18}F]MeFWAY can be assumed. In the 5-HT$_{1A}$ receptor-rich regions of the brain, the time required for a plateau of the target to cerebellum ratio, i.e., psuedoequilibrium, was approximately 10 minutes in the highest binding region of the mesial temporal cortex, suggesting shorter PET scanning sessions could be used for *cis*-[^{18}F]MeFWAY assay of 5-HT$_{1A}$ binding. However, the level of specific binding was dramatically reduced compared to the *trans*-[^{18}F]MeFWAY measures and not detectable in low binding regions such as the cerebellar vermis (shown in Figure 3-4). The ratio of *cis*- and *trans*-[^{18}F]MeFWAY BP_{ND} values was approximately 15 when averaged across the cortical regions reported in Table 3-1. These differences in specific binding of *cis*- and *trans*- compounds follow those reported for *cis*- and

trans- 4-[^{18}F]FCWAY and *cis*- and *trans*- 3-[^{18}F]FCWAY, with ratios in hippocampal specific binding between isomers of 5 (*trans*-/*cis*-), and 3 (*trans*-/*cis*-), respectively, based upon biodistribution studies at 30 minutes in rats (Lang et al., 2006). By assuming that both *cis*- and *trans*-[^{18}F]MeFWAY compounds target the identical receptor pool and have equal nonspecific binding in the brain, this difference can be attributed to the apparent (in vivo) equilibrium dissociation constant, K_D. Measures of apparent K_D have not been made for *cis*- or *trans*-[^{18}F]MeFWAY. Comparative studies in nonhuman primates suggest the apparent K_D of *trans*-[^{18}F]MeFWAY is of the same order as [^{11}C]WAY100635, which is approximately 1 nM based on data reported by Farde et al.(Farde et al., 1997), which would scale to an estimate of 10-20 nM for *cis*-[^{18}F]MeFWAY (Wooten et al., 2011).

Given the low levels of specific binding of the *cis*-[^{18}F]MeFWAY studies, the presence of the 1.6% *trans*-[^{18}F]MeFWAY contamination on the estimated BP_{ND} cannot be discounted. Scaling the BP_{ND} from the *trans*-[^{18}F]MeFWAY studies would result in a BP_{ND} contribution of 7.7*(1.6%) = 0.12 in the MTC due to the this compound in the *cis*-[^{18}F]MeFWAY studies. Thus, this radiochemical impurity in the *cis*-[^{18}F]MeFWAY studies may contribute to a fractional component of the binding measure (0.12/0.58 = 21% in MTC), however, it cannot discount the presence of measurable *cis*-[^{18}F]MeFWAY specific binding. There is also the possibility that a metabolite of *trans*- or *cis*- [^{18}F]MeFWAY, *trans*- or *cis*-[^{18}F]fluoromethylcyclohexanecarboxylic acid, may confound the estimate of BP_{ND}. Carson et al. closely examined the effect of the analogous [^{18}F]FCWAY metabolite, [^{18}F]fluorocyclohexanecarboxylic acid on measures of binding in the rhesus monkey (Carson et al., 2000). Direct injection of [^{18}F]fluorocyclohexanecarboxylic acid revealed a rapid defluorination and subsequent accumulation of the ^{18}F radiolabel in the bone, which was found

to bias the measure of uptake in the neighboring tissue. The experiments reported herein were not sensitive to detecting low levels of uptake in the bone and made no attempt to account for their potential presence.

3.5. Summary

The in vivo behavior of *cis*-[^{18}F]MeFWAY was compared with *trans*-[^{18}F]MeFWAY in nonhuman primates to investigate its potential as a PET marker of 5-HT$_{1A}$ receptors. While the time required for PET 5-HT$_{1A}$ binding assay is shorter for *cis*-[^{18}F]MeFWAY compared to *trans*-[^{18}F]MeFWAY, the lower target to cerebellar ratios severely limit its use in brain regions outside the MTC. It is possible that *cis*-[^{18}F]MeFWAY could have utility for measuring endogenous 5-HT competition in the MTC, however, additional validation studies are required for such an application.

3.6. References

Carson, R.E., Lang, L., Watabe, H., Der, M.G., Adams, H.R., Jagoda, E., Herscovitch, P., Eckelman, W.C., 2000. PET evaluation of [^{18}F]FCWAY, an analog of the 5-HT$_{1A}$ receptor antagonist, WAY-100635. Nuclear Medicine and Biology 27, 493–7.

Innis, R.B., Cunningham, V.J., Delforge, J., Fujita, M., Gjedde, A., Gunn, R.N., Holden, J., Houle, S., Huang, S.-C., Ichise, M., Iida, H., Ito, H., Kimura, Y., Koeppe, R.A., Knudsen, G.M., Knuuti, J., Lammertsma, A.A., Laruelle, M., Logan, J., Maguire, R.P., Mintun, M.A., Morris, E.D., Parsey, R., Price, J.C., Slifstein, M., Sossi, V., Suhara, T., Votaw, J.R., Wong, D.F., Carson, R.E., 2007. Consensus nomenclature for in vivo imaging of reversibly binding radioligands. Journal of Cerebral Blood Flow and Metabolism 27, 1533–9.

Lang, L., Jagoda, E., Schmall, B., Sassaman, M., Ma, Y., Eckelman, W.C., 2000. Fluoro analogs of WAY-100635 with varying pharmacokinetics properties. Nuclear Medicine and Biology 27, 457–62.

Farde, L., Ginovart, N., Ito, H., Lundkvist, C., Pike, V.W., McCarron, J.A., Halldin, C., 1997. PET-characterization of [carbonyl-^{11}C]WAY-100635 binding to 5-HT$_{1A}$ receptors in the primate brain. Psychopharmacology 133, 196–202.

Lang, L., Jagoda, E., Schmall, B., Sassaman, M., Magata, Y., Eckelman, W.C., 1999. Comparison of ^{18}F-labeled *cis*- and *trans*- 4-fluorocyclohexane derivatives of WAY-100635. Journal of Nuclear Medicine 40, 37P–38P.

Lang, L., Jagoda, E., Ma, Y., Sassaman, M.B., Eckelman, W.C., 2006. Synthesis and in vivo biodistribution of ^{18}F-labeled 3-*cis*-,3-*trans*-, 4-*cis*-, and 4-*trans*-fluorocyclohexane derivatives of WAY-100635. Bioorganic & Medicinal Chemistry 14, 3737–48.

Logan, J., Fowler, J., Volkow, N., 1996. Distribution volume ratios without blood sampling from graphical analysis of PET data. Journal of Cerebral Blood Flow and Metabolism 16, 834–40.

Ma, Y., Lang, L., Kiesewetter, D., Jagoda, E., Eckelman, W.C., 2006. Species differences in metabolites of PET ligands: serotonergic 5-HT$_{1A}$ receptor antagonists 3-*trans*-FCWAY and 3-*cis*-FCWAY. Nuclear Medicine and Biology 33, 1013–9.

Saigal, N., Pichika, R., Easwaramoorthy, B., Collins, D., Christian, B.T., Shi, B., Narayanan, T.K., Potkin, S.G., Mukherjee, J., 2006. Synthesis and biologic evaluation of a novel serotonin 5-HT$_{1A}$ receptor radioligand, ^{18}F-labeled MeFWAY, in rodents and imaging by PET in a nonhuman primate. Journal of Nuclear Medicine 47, 1697–706.

Saigal, N., Pichika, R., Easwaramoorthy, B., Collins, D., Mukherjee, J., 2006. Serotonin competition with the new 5-HT_{1A} receptor PET radiotracer: ^{18}F-MeFWAY. Journal of Nuclear Medicine 47, 281P.

Tai, C., Chatziioannou, A., Siegel, S., Young, J., Newport, D., Goble, R.N., Nutt, R.E., Cherry, S.R., 2001. Performance evaluation of the microPET P4: a PET system dedicated to animal imaging. Physics in Medicine and Biology 46, 1845–62.

Wilson, A.A., Garcia, A., Li, J., Dasilva, J.N., Houle, S., 1999. Analogues of WAY-100635 as radiotracers for in vivo imaging of 5-HT_{1A} receptors. Journal of Labelled Compounds and Radiopharmaceuticals 42, 611–20.

Wooten, D.W., Moraino, J.D., Hillmer, A.T., Engle, J.W., Dejesus, O.J., Murali, D., Barnhart, T.E., Nickles, R.J., Davidson, R.J., Schneider, M.L., Mukherjee, J., Christian, B.T., 2011. In vivo kinetics of [^{18}F]MEFWAY: a comparison with [^{11}C]WAY100635 and [^{18}F]MPPF in the nonhuman primate. Synapse 65, 592–600.

Chapter 4 An in vivo comparison of 3- and 4- [^{18}F]MeFWAY in the nonhuman primate

4.1. Introduction

As discussed in Chapter 2, 4-*trans*-[^{18}F]MeFWAY (4-[^{18}F]MeFWAY) has demonstrated high affinity for the 5-HT$_{1A}$ receptor and pseudoequilibration times similar to [^{11}C]WAY-100635. Previous studies utilizing [^{11}C]WAY-100635 have shown binding levels to be unaltered by drug induced changes in endogenous 5-HT competition (see Paterson et al., 2010 for review). The insensitivity of [^{11}C]WAY-100635 is possibly due to its high affinity for the 5-HT$_{1A}$ receptor. The comparable kinetics of 4-[^{18}F]MeFWAY and [^{11}C]WAY-100635 suggests, similarly, 4-[^{18}F]MeFWAY may not be susceptible to drug induced changes in endogenous 5-HT competition. It has been suggested that a radioligand with lower affinity will allow detection of changes in endogenous neurotransmitter concentrations (Endres and Carson, 1998). Previous work examining binding of analogues of [^{18}F]FCWAY reported positioning of the ^{18}F label on 3 position of the cyclohexane ring affected the kinetics (Lang et al., 2006). Therefore, [^{18}F]CH_2F was placed on the 3 position of the cyclohexane ring to determine if 3-[^{18}F]MeFWAY (shown in Figure 4-1 along with 4-[^{18}F]MeFWAY) also possessed a lower 5-HT$_{1A}$ affinity or faster kinetic properties.

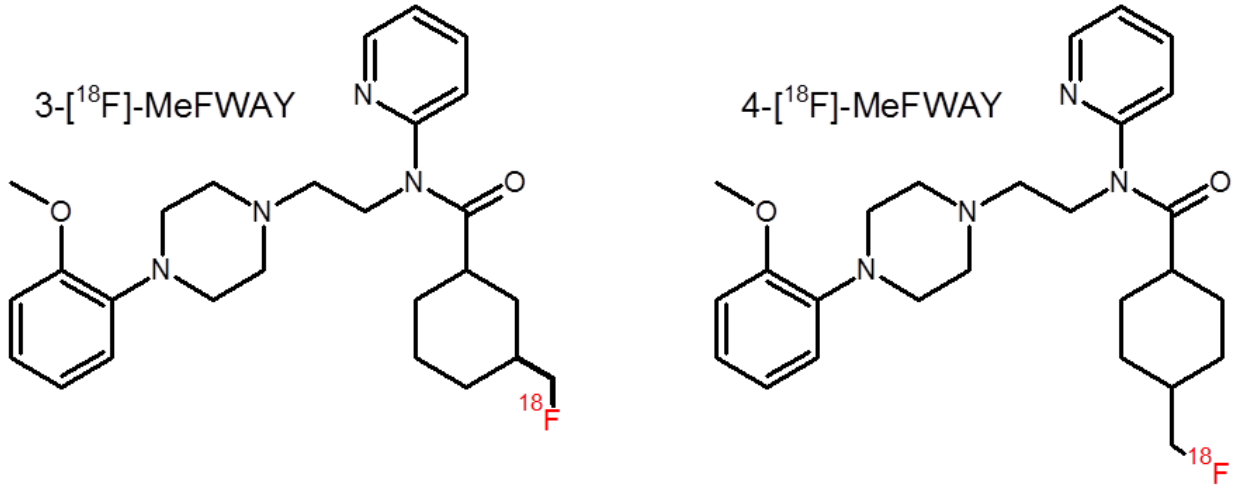

Figure 4-1: Molecular structure of 3- and 4- [^{18}F]MeFWAY

4.2. Methods

The PET procedures and data analysis closely follow the methods used in Chapter 2 and Chapter 3 and are only briefly discussed this chapter.

4.2.1. Radiochemistry

The chemical synthesis of 3- and *trans*-4- [^{18}F]MeFWAY was performed via nucleophilic substitution with their respective precursors similar to methods discussed in Chapter 2. The precursor for the production of 3-[^{18}F]MeFWAY was provided by Professor Jogeshwar Mukherjee from the University of California-Irvine. The radiochemical yield of 3-[^{18}F]MeFWAY was ~1% (non decay corrected) with a specific activity at end of synthesis of 740 GBq/μmol (20 Ci/μmol).

4.2.2. PET scans

PET scans were acquired using a Concorde microPET P4 scanner. With the bolus injection of either 3-[^{18}F]MeFWAY (80.5 MBq, 2.2 mCi) or 4-*trans*-[^{18}F]MeFWAY (104.83 MBq, 2.8 mCi) collection of emission data was initiated and collected for 90 minutes. Arterial blood samples

were acquired throughout the course of the study ranging from every 5 seconds immediately after injection to every 10 minutes toward the end of the study. The lipophilic fraction was separated from plasma using two ethyl acetate liquid-liquid extractions and was assayed for radioactivity of 3- or 4- [^{18}F]MeFWAY concentration to provide the input function for tracer kinetic analysis.

4.2.3. Data analysis

Raw list mode data were binned into time frames of 4 x 1 minute, 3 x 2 minutes, and 16 x 5 minutes. Sinograms were reconstructed using filtered backprojection and a 0.5 cm^{-1} ramp filter. Corrections were applied for attenuation, scatter, radioactive decay, and scanner normalization to result in a final reconstructed image of matrix size of 128 x 128 x 63 and voxel dimensions of 1.90 x 1.90 x 1.21 mm^3. Regions of interest (ROIs) were drawn in various regions of the brain to extract time-activity curves (TACs) of the radiotracer. Regions examined included the cerebellum (CB) (1.02 cm^3), mesial temporal cortex (MTC) (0.70 cm^3), caudal anterior cingulate gyrus (ACG) (0.82 cm^3), and raphe nuclei (RN) (0.08 cm^3).

Nondisplaceable kinetics of 3- and 4- *trans*-[^{18}F]MeFWAY between plasma and free tissue (CB) were analyzed using a single tissue compartmental model. Estimates of K_1, k_2, and V_{ND} were performed using COMKAT software (Muzic and Cornelius, 2001). The MRTM method was used to estimate binding potential (BP_{ND}) in the MTC, ACG, and RN using the CB as a reference region which was validated for 4-[^{18}F]MeFWAY as a reference region in Chapter 2 (Ichise et al., 1996).

4.3. Results

4.3.1. Blood data

The radioactive time course curves of arterial plasma and parent radiotracer concentrations in plasma are shown in Figure 4-2. At 30 minutes after bolus injection of radiotracer, the fraction of parent compound in plasma was 30% (3-[^{18}F]MeFWAY) and 28% (4-[^{18}F]MeFWAY). Following initial rapid clearance of tracer from plasma (time > 30 minutes) exponential clearance of radiotracer from plasma was 0.015 min^{-1} (3-[^{18}F]MeFWAY) and 0.014 min^{-1} (4-[^{18}F]MeFWAY).

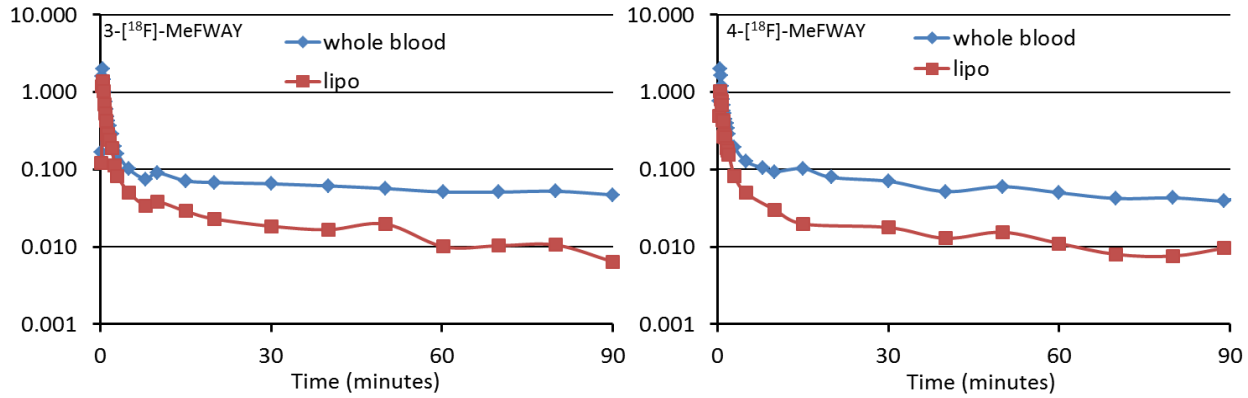

Figure 4-2: Arterial time courses of total radioactivity in plasma (♦) and parent compound radioactivity in plasma (■) for 3-[^{18}F]MeFWAY (left) and 4-[^{18}F]MeFWAY (right).

4.3.2. Cerebellum kinetics

Radioactive time course of activity in the CB for 3- and 4-[^{18}F]MeFWAY are shown in Figure 4-3. The CB TACs were modeled as a single compartmental model revealing transport kinetics of radiotracer from plasma to CB tissue of K_1: 0.69, 0.77 mL/mL/min; k_2: 0.11, 0.13 min^{-1}; and V_{ND}: 6.4, 6.2 for 3-[^{18}F]MeFWAY and 4-[^{18}F]MeFWAY, respectively.

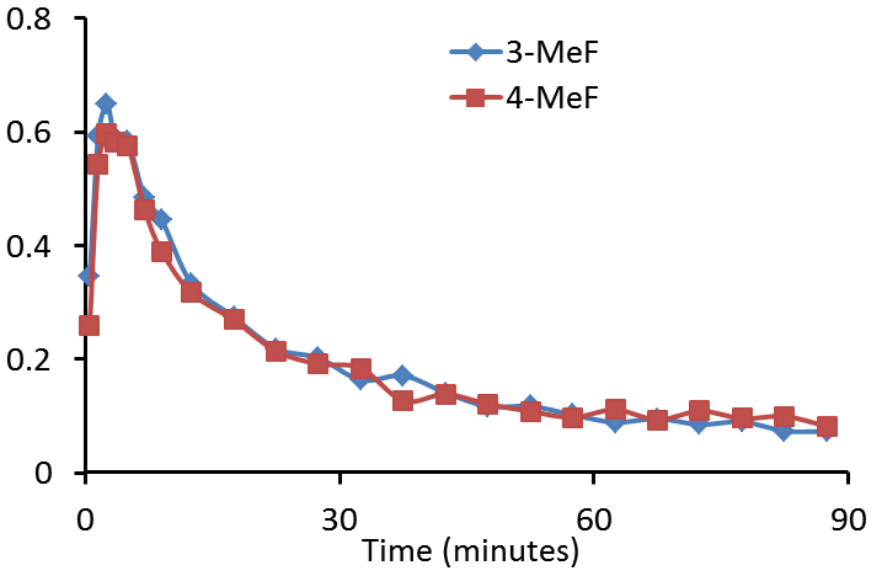

Figure 4-3: Cerebellum time activity curves for 3-[^{18}F]MeFWAY (♦) and 4-[^{18}F]MeFWAY (■).

4.3.3. Kinetics in the 5-HT$_{1A}$ receptor regions

A comparison of 3- and 4-[^{18}F]MeFWAY specific binding is shown in the parametric BP_{ND} images in Figure 4-5. Higher binding was observed with 4-[^{18}F]MeFWAY in the MTC, dACg,

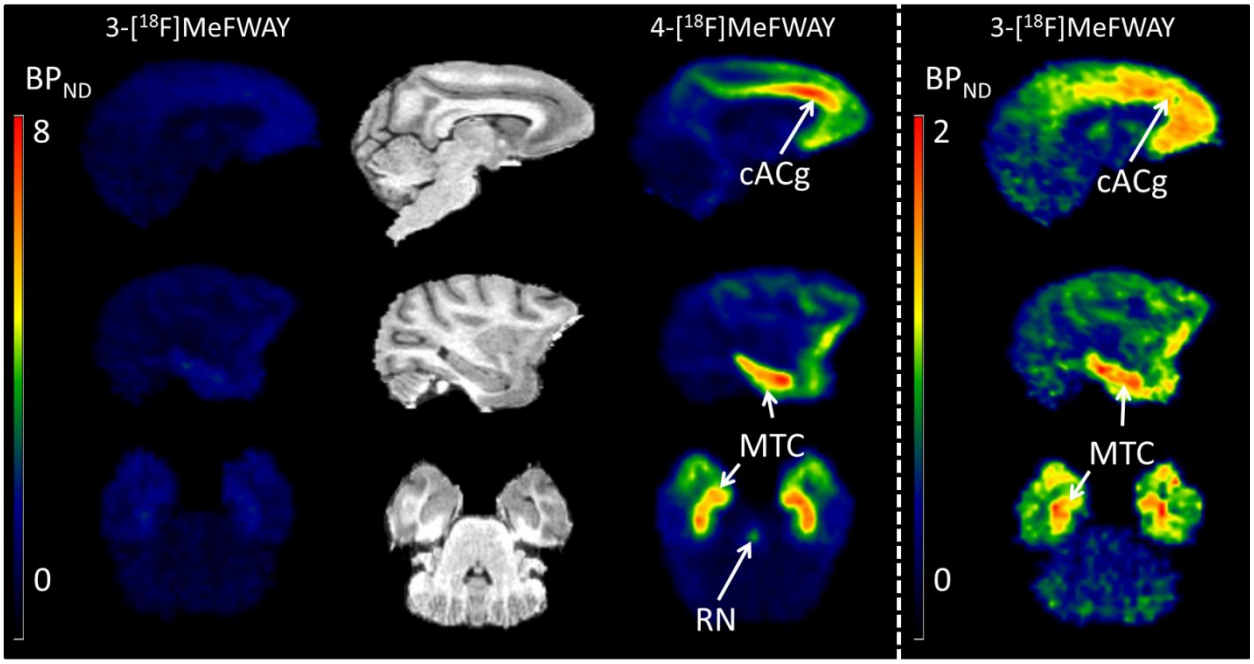

Figure 4-4: (Left) Parametric BP_{ND} images of 3-[^{18}F]MeFWAY and 4-[^{18}F]MeFWAY along with corresponding T1 MRIs. (Right) BP_{ND} images of 3-[^{18}F]MeFWAY with the threshold adjusted to enhance visualization of binding.

and RN. To enhance visualization of the 3-[^{18}F]MeFWAY binding, threshold level was decreased and is shown in the right panel of Figure 4-5. Uptake is essentially undetectable in the RN for 3-[^{18}F]MeFWAY. TACs and bound to free ratio plots in the MTC and cACg are shown in Figure 4-4. 3-[^{18}F]MeFWAY reaches a plateau of about 2.7 by 40 minutes in the MTC and 2.3 by 30 minutes in the cACg. In the MTC, 4-[^{18}F]MeFWAY did not reach a plateau by the end

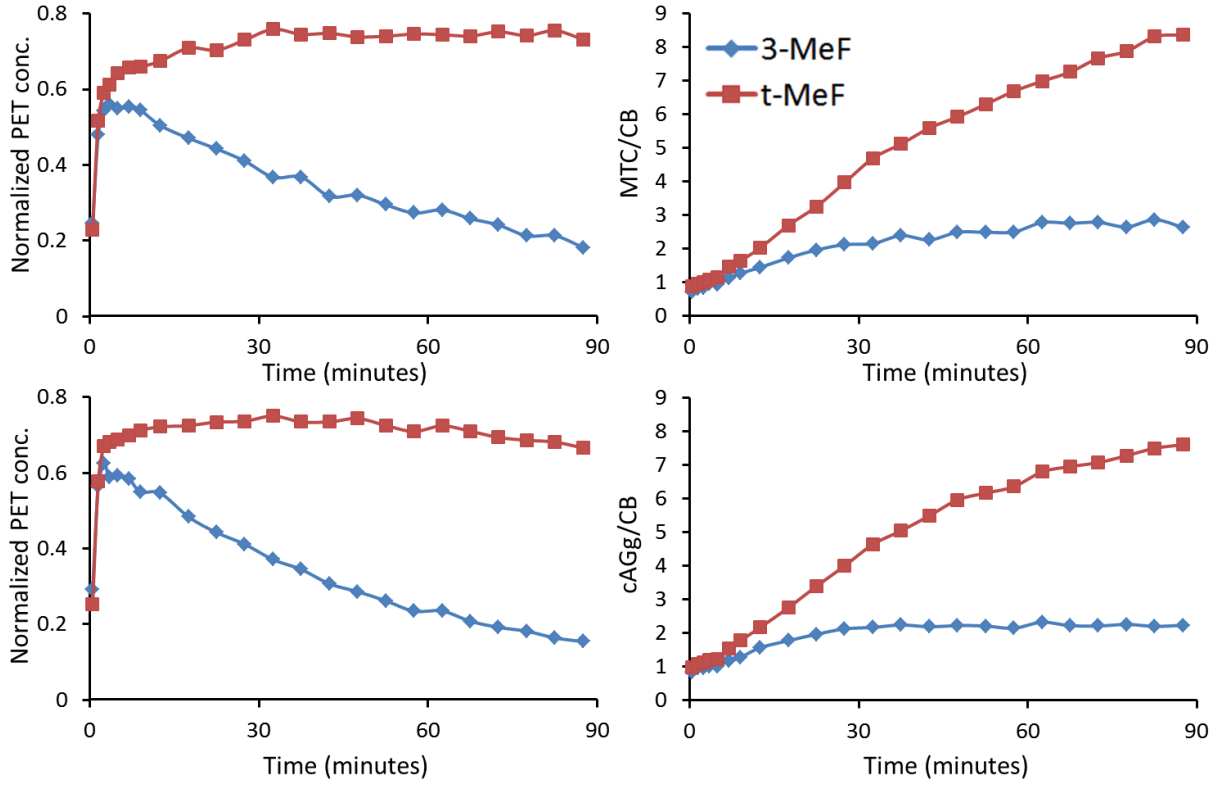

Figure 4-5: TACs (left) and CB ratio plots (right) of 3- (♦) and 4- (■) [^{18}F]MeFWAY in the MTC (top) and cACg (bottom).

of the 90 minute scan period in the MTC or cACg. Highest regional BP_{ND} values were found in the MTC (3.8) and cACg (3.5) for 4-[^{18}F]MeFWAY and lower BP_{ND} was measured in the RN (2.2). Similarly, highest BP_{ND} was measured in the MTC (1.04) and cACg (0.85) for 3-[^{18}F]MeFWAY and lower binding was detected in the RN (0.3).

4.4. Discussion

Validation studies performed using 4-[^{18}F]MeFWAY, discussed in Chapter 2, demonstrated its usefulness as a PET radiotracer for measuring the 5-HT_{1A} receptor. The high specific binding levels of 4-[^{18}F]MeFWAY to 5-HT_{1A} receptor throughout the cortical regions make it an excellent ^{18}F-labeled alternative to the [^{11}C]WAY-100635 compound. 4-[^{18}F]MeFWAY and [^{11}C]WAY-100635 however, require longer scan times (>90 minutes) to reach a psueudoequilibrium. Radiotracers with faster kinetics are often desired to reduce scan times. Additionally, both 4-[^{18}F]MeFWAY and [^{11}C]WAY-100635 demonstrate high affinity to the 5-HT_{1A} receptor which is believed to attribute to their insensitivity to endogenous competition with 5-HT (Paterson et al., 2010). Lower affinity radioligands are desired when the objective is measuring changes in endogenous neurotransmitter competition (Endres and Carson, 1998). The goal of this work was to determine if 3-[^{18}F]MeFWAY possessed the properties of a lower affinity 5-HT_{1A} radioligand.

Both 3- and 4- [^{18}F]MeFWAY exhibited similar in vivo kinetics in the nondisplaceble binding region of the CB. One-compartment modeling in one primate revealed similar estimates of plasma to free tissue bidirectional transport kinetics (K_1, k_2, and V_{ND}). Major differences, however, were observed between the specific binding of the two radiotracers. The similarities in nondisplaceable kinetics suggest the differences in specific 5-HT_{1A} binding are due to lower affinity for 3-[^{18}F]MeFWAY. The low affinity 3-[^{18}F]MeFWAY make it a potential radioligand for detecting changes in endogenous levels of 5-HT, however, 5-HT depletion and competition studies will be needed to determine the extent of these effects on binding.

The radioligand, 4-[^{18}F]MeFWAY, demonstrates a large dynamic range in uptake, capable of detecting 5-HT_{1A} receptors in lower density regions. Similar to [^{11}C]WAY-100635, 4-[^{18}F]MeFWAY takes >90 minutes to reach pseudoequilibrium in high 5-HT_{1A} receptor density

regions. In certain studies, however, radiotracers allowing shorter scan times are desired. Pseudoequilibrium was reached within 30-50 minutes for 3-[^{18}F]MeFWAY in the high 5-HT_{1A} receptor binding regions. The faster equilibration times and adequate uptake in the 5-HT_{1A} binding regions of 3-[^{18}F]MeFWAY make it suitable for use in studies requiring shorter scanning durations with a focus on studying the higher 5-HT_{1A} binding regions.

Figure 4-5 shows similar distribution of 3- and 4- [^{18}F]MeFWAY uptake throughout the cortical areas indicating 3-[^{18}F]MeFWAY is binding selectively to 5-HT_{1A} receptors. Previous studies examining kinetic properties of 3-*cis*-, 3-*trans*-, 4-*cis*-, and 4-*trans*- [^{18}F]FCWAY showed the isomer state and placement of ^{18}F on the cyclohexane ring had significant effects on specific 5-HT_{1A} uptake (Lang et al., 2006). Highest hippocampus to cerebellum ratio was found using *trans*-4-[^{18}F]FCWAY, which was similarly observed with *trans*-4-[^{18}F]MeFWAY. Additionally, 3-*cis*-[^{18}F]FCWAY showed a lower affinity to the 5-HT_{1A} receptor with faster kinetics, while 3-*trans*-[^{18}F]FCWAY displayed affinity for the α_1 adrenoreceptor. Blocking studies were not performed in this work to test for specific binding to α_1 adrenoreceptor. Therefore, the extent of 3-[^{18}F]MeFWAY binding to the α_1 adrenoreceptor can only be speculated. High levels of α_1 adrenoreceptor density are found in the thalamus of nonhuman primates (Palacios et al., 1987). Thus, levels of 3- and 4-[^{18}F]MeFWAY uptake were examined in this region finding low levels of uptake for 3-[^{18}F]MeFWAY ($BP_{ND} < 0.6$) and 4-[^{18}F]MeFWAY ($BP_{ND} < 1.0$) indicating limited if any significant binding to the α_1 adrenoreceptor. Furthermore, the use of the thalamus for detection of α_1 adrenoreceptor binding may not be valid because a previous study reported significant 5-HT_{1A} receptor density in the thalamus (Pazos et al., 1987; Dillon et al., 1991).

4.5. Summary

The in vivo behavior of 3-[^{18}F]MeFWAY was compared with 4-[^{18}F]MeFWAY in the nonhuman primate to preliminarily investigate its use as a 5-HT_{1A} receptor antagonist. The lower affinity of 3-[^{18}F]MeFWAY may make it useful for measuring changes in endogenous 5-HT levels. Additionally, the shorter equilibration and sufficiently high binding of 3-[^{18}F]MeFWAY make it a potential 5-HT_{1A} PET radiotracer for studies requiring a shorter scan time.

4.6. References

Endres, C.J., Carson, R.E., 1998. Assessment of dynamic neurotransmitter changes with bolus or infusion delivery of neuroreceptor ligands. Journal of cerebral blood flow and metabolism 18, 1196–1210.

Dillon, K.A., Gross-Isseroff R., Israeli, M., Biegon, A., 1991. Autoradiographic analysis of serotonin 5-HT_{1A} receptor binding in the human brain postmortem" effects of age and alcohol. Brain Research 554, 56–64.

Ichise, M., Ballinger, J.R., Golan, H., Vines, D., Luong, A., Tsai, S., Kung, H.F., 1996. Noninvasive quantification of dopamine D_2 receptors with iodine-123-IBF SPECT. Journal of Nuclear Medicine 37, 513–20.

Lixin Lang, Elaine Jagoda, Ying Ma, Mark B. Sassaman, William C. Eckelman, 2006. Synthesis and in vivo biodistribution of F-18 labeled 3-cis-,3-trans-, 4-cis-, and 4-trans-fluorocyclohexane derivatives of WAY 100635. Bioorganic Medicinal Chemistry 14, 3737–48.

Muzic, R.F., Cornelius, S., 2001. COMKAT: Compartment model kinetic analysis tool. Journal of Nuclear Medicine 42, 636–645.

Palacios, J.M., Hoyer, D., Cortés, R., 1987. alpha 1-Adrenoceptors in the mammalian brain: similar pharmacology but different distribution in rodents and primates. Brain Research 419, 65–75.

Paterson, L.M., Tyacke, R.J., Nutt, D.J., Knudsen, G.M., 2010. Measuring endogenous 5-HT release by emission tomography: promises and pitfalls. Journal of cerebral blood flow and metabolism 30, 1682–1706.

Pazos, A., Probst, A., Palacios, J.M., 1987. Serotonin receptors in the human brain--III. Autoradiographic mapping of serotonin-1 receptors. Neuroscience 21, 97–122.

Chapter 5 Measurement of 5-HT_{1A} receptor density and in vivo binding parameters of [^{18}F]MeFWAY in the nonhuman primate

5.1. Introduction

The similar in vivo kinetics of [^{18}F]MeFWAY to the commonly used [^{11}C]WAY-100635 and longer lived radioactive half-life of the ^{18}F label makes it appropriate for use in complex multiple injection (MI) PET protocols for in vivo estimation of 5-HT_{1A} receptor density (B_{max}). In vitro measurements of B_{max} have been reported using [^{11}C]WAY-100635 and validated by comparison with its tritiated form (Hall et al., 1997), finding high levels of 5-HT_{1A} receptor expression throughout the frontal, temporal, parietal, and cingulate cortices with the highest receptor density in the hippocampus (including regions CA1, subiculum, uncus). In vivo measurements of 5-HT_{1A} B_{max} have been limited to one study using [^{11}C]WAY-100635 due to the complexity of the chemical synthesis and short radioactive half-life (Farde et al, 1997). Using [^{18}F]MPPF, in vivo estimates of 5-HT_{1A} B_{max} have been made in five human subjects finding similar rank order in 5-HT_{1A} receptor expression across brain regions as in vitro studies (Costes et al., 2002). [^{18}F]MeFWAY holds an advantage over [^{18}F]MPPF of higher sensitivity to the 5-HT_{1A} receptor and a greater dynamic range of binding as discussed in Chapter 2.

The MI PET technique used in this work is a nonequilibrium approach and involves performing serial injections with varying levels of unlabeled ligand, with the intent of occupying a significant fraction of the receptors (Delforge et al, 1990). This strategy permits the estimation of B_{max}, separated from the ligand-receptor specific binding parameters (k_{on}, k_{off}). The MI method provides a measure of B_{max} that is independent of the characteristics of the radioligand, unlike the BP metric obtained with tracer-only PET studies, which represent a composite function of B_{max} and ligand-receptor affinity (Innis et al., 2007). Additionally, MI methods have

also been implimented for the measurement of B_{max} in the peripheral benzodiazepine (Delforge et al., 1996), beta adrenergic (Muzic et al., 2000; Salinas et al, 2007), dopamine transporter (Morris et al., 1996; Poyot et al., 2001), dopamine D2 (Christian et al., 2004; Delforge et al., 1999; Mauger et al., 2005; Vandehey et al., 2010), and nicotinic acetylcholine (Gallezot et al., 2008) receptor systems. This chapter presents work on the development of MI PET methods using [^{18}F]MeFWAY for estimation of 5-HT_{1A} B_{max} and K_{Dapp} in the nonhuman primate.

5.2. Methods

5.2.1. Chemical synthesis

The synthesis of [^{18}F]MeFWAY (N-{2-[4-(2-methoxyphenyl)piperazinyl]ethyl}-N-(2-pyridyl)-N-(4-*trans*-[^{18}F]-fluoromethylcyclohexane)carboxamide) was performed similar to the method presented in Chapter 2. The average specific activity at time of first injection of the PET scan was 77 GBq/μmol. The unlabeled MeFWAY used for the MI studies was purchased from a commercial vendor (Huayi Isotopes Co.) as an 85:15 isomeric mixture of *trans*:*cis*-MeFWAY. The injected mass for the partial saturation administrations (injection #2) was calculated based upon the fractional mass of the *trans*-MeFWAY and the pharmacological effects of the *cis*-MeFWAY component were assumed to be negligible based upon work previously presented in Chapter 3 (see also Wooten et al., 2011b).

5.2.2. Design of the multiple injection experiments

The MI experiments were designed to optimize the precision of the parameter estimates of B_{max} and the ligand-specific binding parameters (k_{on}, k_{off}). A requirement was placed on the experimental design to limit the first injection to tracer-only doses of [^{18}F]MeFWAY and a duration of 90 minutes before the subsequent injection. This design permits the comparison of

[^{18}F]MeFWAY BP_{ND} with other subjects using single injection protocols. Experimental designs were investigated for 2- and 3-injection studies to select the amount of unlabeled MeFWAY and the injection time for each administration. The experimental design was selected using the D-optimal criterion, which minimizes the correlation between the kinetic parameters (described in (Salinas et al., 2007)). The inverse determinant of the reduced Hessian ($\det(H_R)^{-1}$) is proportional to the volume of the indifference region for the parameter estimates. In minimizing this region, the parameter precision is increased. Only k_{on}, k_{off}, and B_{max} were considered for the optimization. The experimental designs were simulated using the COMKAT software (Muzic and Cornelius, 2001) based upon previously measured arterial input functions presented in Chapter 2 (see also Wooten et al., 2011a) and a range of B_{max} (40-100 pmol/mL), k_{off} (0.01-0.1 min^{-1}) and k_{on} (0.004-0.04 min^{-1}) values estimated using previous studies and literature values with comparable ligands (Hall et al., 1997; Gunn et al., 1998). As a validation of the selected experimental designs, simulated noise was added to each data point of the simulated ROIs similar to a reported method (Logan et al., 2001) using the equation:

$$\textbf{(5-1)}\quad C_R^* = C_{R(fit)} + \left(G_{(0,1)}c_1\sqrt{C_{R(fit)}} + G_{(0,1)}c_2\right)$$

where C_R^* is the noise-added time activity curves (TACs) in the different brain regions, $C_{R(fit)}$ is the noise free TACs, $G_{(0,1)}$ is the noise addition which was a pseudorandom number from a normal distribution with a mean of zero and a standard deviation of 1, and the constants c_1(1.5-2.5) and c_2(0-60) represent scaling factors to approximate noise found in the original TACs (using 50 realizations). Parameter estimates were performed on these simulated TACs to examine the parameter identifiability. The optimization was repeated following the first several experiments to incorporate the newly measured parameters in the design of the later experiments.

5.2.3. PET scans

MI PET experiments were conducted on a total of 6 *Macaca mulatta* (rhesus) subjects (2m, 4f; 8.2 ± 1.6 kg; 13.0 ± 3.9 y). Subject preparation and care were performed similar to procedures used in Section 2.2.2.

The PET scans were acquired using a Concorde microPET P4 scanner (Tai et al., 2001), similar to methods described in Section 2.2.3. The collection of three hours of emission data was initiated with the first bolus injection of [^{18}F]MeFWAY.

5.2.4. Measurement of the arterial input function

Arterial samples were collected to provide an input function for kinetic modeling of [^{18}F]MeFWAY. Arterial samples were collected in volumes of 0.5 mL every 10-15 seconds for 2 minutes immediately following each injection to every 10-20 minutes toward the end of each injection segment. The 0.5 mL whole blood samples were processed for estimation of [^{18}F]MeFWAY concentration in plasma using a similar method already described in Section 2.2.3.

As implemented, the MI model requires the [^{18}F]MeFWAY arterial time course to be separated and uniquely defined for each of the 3 injections. This requires the mathematical removal of radioactivity of the first injection from the second and third injections (and the second injection from the third injection). The first injection was parameterized by fitting the data from 5-90 minutes post-injection to a bi-exponential function and extrapolating the curve to the end of the study (3 hrs) for subtraction from the subsequent injections. The same method was used to parameterize the second injection which was then subtracted from the third injection. The individual time courses of [^{18}F]MeFWAY were then decay corrected and divided by the specific

activity (at the time of each injection) to yield units of molar concentration (pmol/mL) of MeFWAY that are unaffected by radioactive decay.

5.2.5. Data analysis

5.2.5.1. Image reconstruction

The dynamic list mode emission data were binned into 2 minute sinograms and reconstructed with a filtered back projection algorithm using a 0.5 cm^{-1} ramp filter with corrections applied for attenuation, scatter, and scanner normalization. The final matrix size was 128x128x63, with voxel dimensions of 1.90x1.90x1.21 mm^3.

5.2.5.2. Regions of interest selection

Regions of interest (ROIs), shown in Figure 5-1, were selected from the PET images in cortical areas with uniform 5-HT_{1A} binding. Multiple, circular ROIs were placed within the regions of the mesial temporal cortex (MTC)(0.28 cm^3), superior temporal cortex (sTC)(0.91 cm^3), parietal cortex (PC)(0.91 cm^3), dorsal anterior cingulate cortex (dACC)(0.73 cm^3) and the cerebellum (CB)(0.92 cm^3) to extract time activity curves. ROIs were also applied to the subcortical region of the raphe nuclei (RN)(0.08 cm^3), guided by the focal uptake of [^{18}F]MeFWAY binding. A denoising algorithm was applied to the dynamic PET images prior to the extraction of the time activity curves (Christian et al., 2010).

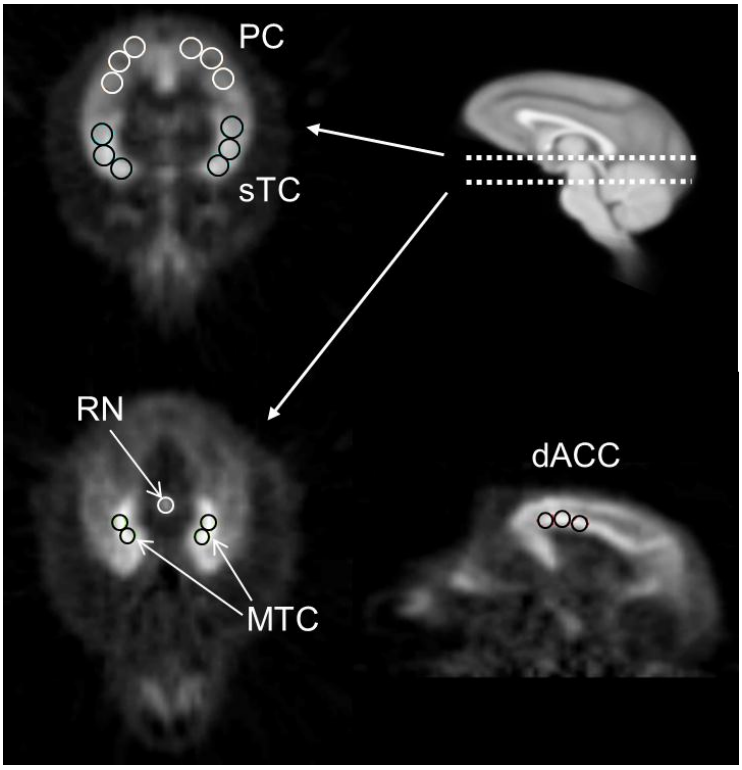

Figure 5-1: Regions of interest (ROIs) in the areas of the mesial temporal (MTC), dorsal anterior cingulate (dACC), superior temporal (sTC), parietal (PC) cortices, and raphe nuclei (RN) drawn on summed dynamic frames (20-90 minutes). The top right sagittal MRI illustrates the transaxial planes shown in the two PET images in the left panel and is in the same space as the sagittal PET image (bottom right).

5.2.5.3. Parameter estimation

The in vivo kinetic behavior of [^{18}F]MeFWAY was analyzed using a two-compartment model, as shown in Figure 5-2, to account for ligand in the free (F) (pmol/mL), including unbound and nondisplaceably bound, and specifically bound (B) (pmol/mL) states. C_{pi} represents the molar concentration of MeFWAY in the plasma (pmol/mL) and serves as the input function. For studies with multiple injections, B and F compartments are created for each injection (i) (Delforge et al., 1990; Muzic et al., 2000; Christian et al., 2004; Morris et al., 2004), as described by the differential equations:

$$\textbf{(5-2)}\quad \frac{dF_i}{dt} = K_1 C_{pi} - k_2 F_i + k_{off} B_i - k_{on} F_i \left(B_{max} - \sum_i B_i \right)$$

$$\textbf{(5-3)}\quad \frac{dB_i}{dt} = k_{on} F_i \left(B_{max} - \sum_i B_i \right) - k_{off} B_i$$

The bidirectional transport of radiotracer across the blood brain barrier, represented by K_1

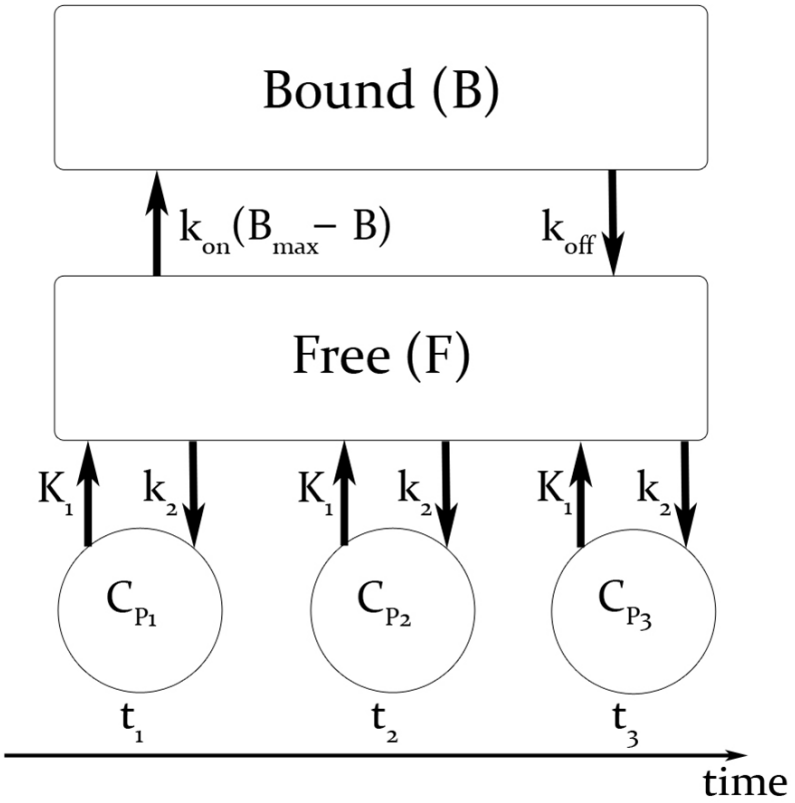

Figure 5-2: Two-compartment model describing a three injection protocol. $t_{1\text{-}3}$ represent the injection times, $C_{P1\text{-}3}$ represent the molar ligand concentration (pmol/mL) in the arterial plasma and bi-directionally exchanged between the free (F) and bound (B) states

(mL/min/mL) and k_2 (min^{-1}), dissociation rate constant (k_{off}) (min^{-1}), association rate constant (k_{on}) (mL/pmol/min), and receptor density (B_{max}) (pmol/mL), are common between each of the injections. The modeled PET signal is obtained by converting the absolute molar concentrations (F_i and B_i) into Bq/cm^3 by multiplication with the time decaying specific activities ($sa_i(t)$) of

each injection. The data are then normalized by the frame duration and can be expressed by the following model:

$$\textbf{(5-4)}\quad C_{PET}(t) = \frac{1}{t_j - t_{j-1}} \int_{t_{j-1}}^{t_j} \left\{ \sum_i sa_i(t)(1 - f_V)(F_i(t) + B_i(t)) + f_V A_i \right\} dt$$

The fractional blood volume (f_V) accounts for the vascular component of radioactivity measured in the decaying whole blood (A_i) and was fixed to a value of 0.04 for all brain regions. Thus, the model sums the radioactivity concentration for each injection (i) to obtain the PET signal, C_{PET}, which is not corrected for radioactive decay to be consistent with the acquired PET data.

The parameter estimation for each subject was performed using COMKAT (Muzic and Cornelius, 2001). The following assumptions were implemented to permit the simultaneous estimation of all the regional parameters for [^{18}F]MeFWAY throughout the brain:

1. Nondisplaceable distribution volume,
2. $V_{ND} = K_1/k_2$, is uniform across all ROIs, whereas K_1 can vary between ROIs to account for regional differences in blood flow.
3. The specific binding association and dissociation rate constants, k_{on} and k_{off}, are uniform across all ROIs, whereas B_{max} can vary between ROIs.
4. The blood flow within each ROI does not change throughout the course of the experiment, so the radiotracer influx and efflux constants, K_1 and k_2, are time invariant.

With these assumptions, estimates of k_{on}, k_{off}, and V_{ND} were made uniform for all ROIs and estimates of K_1 and B_{max} were unique for each ROI. For the CB, the compartment for specific binding (B) was not included and only K_1 was uniquely measured for this region. Thus for each subject, a total of 14 parameters were simultaneously estimated from the time series data of 6

brain regions (MTC, sTC, PC, dACC, RN, and CB). The apparent equilibrium dissociation constant, K_{Dapp}, was calculated as: $K_{Dapp} = k_{off}/k_{on}$

The parameter estimates were obtained by minimizing the least squares objective function (o) between $C_{PET}(t)$ and the corresponding ROI measurement (r) for each time frame (j) of the PET scan scaled by a weighting factor (w). Uniform weighting was selected for these data as it has been shown to minimize bias for parameter estimates in PET compartment analysis (Muzic and Christian, 2006). The objective function is described as:

$$\textbf{(5-5)} \quad o = \sum_{r=1}^{R}\sum_{j=1}^{J} w_{r,j}\left(PET_{r,j} - C_{PETr,j}\right)^2$$

with 6 ROIs (R=6) and 180 minutes of PET data in 2 minute time frames (J=90).

Estimation of uncertainties in the parameter estimates were performed similar to a method used by Salinas et al (2007) and Vandehey et al (2010). The parameter estimates obtained from the PET data were used to generate a noise free simulated data set for each subject. Noise was then added to the simulated data using the noise model described in equation 1, with 50 noise trials for each subject. Parameter estimates were then obtained for each trial and the standard deviation of each parameter was calculated from the population obtained from the 50 noise trials. The coefficient of variation (*cov* = s.d./mean*100%) was then measured for each parameter and mean coefficients of variation were reported for each parameter as the average *cov* over the 6 subjects.

For comparison with the B_{max} estimates, measurements were also made for nondisplaceable binding potential, BP_{ND} (Innis et al., 2007), using the data from 0-90 minutes, consisting of only the high specific activity first injection. BP_{ND} was estimated using the CB as a reference region with the Logan distribution volume ratio (DVR) method and calculated as $BP_{ND} = DVR - 1$

(Logan et al, 1996)BP_{ND} = DVR-1, using a period of linearization of t*=40 min and a $\bar{k}_2$ value obtained from the compartmental modeling.

5.3. Results

5.3.1. Optimization of MI protocol

The optimization of the MI protocol focused on selecting the unlabeled dose of MeFWAY for the second and third injections and the timing of the third injection. It was found that identifiability of B_{max}, k_{on}, and k_{off} was most sensitive to the MeFWAY dose for the second injection and much less sensitive to the timing and dose of the third injection (see Discussion and Figure 5-3). Figure 5-3 illustrates the dependence of the $\det(H_R)^{-1}$ on the MeFWAY dose for the second injection, suggesting the optimal dose is approximately 100-200 nmol. Also shown is the B_{max} correlation with k_{on} and k_{off}, demonstrating the high correlation is reduced at an optimal range of unlabeled mass doses for the second injection. The sensitivity curves in the region of the MTC for B_{max}, k_{on}, and k_{off} (shown in Figure 5-3), illustrates the decoupling of the parameters over the duration of the experiment.

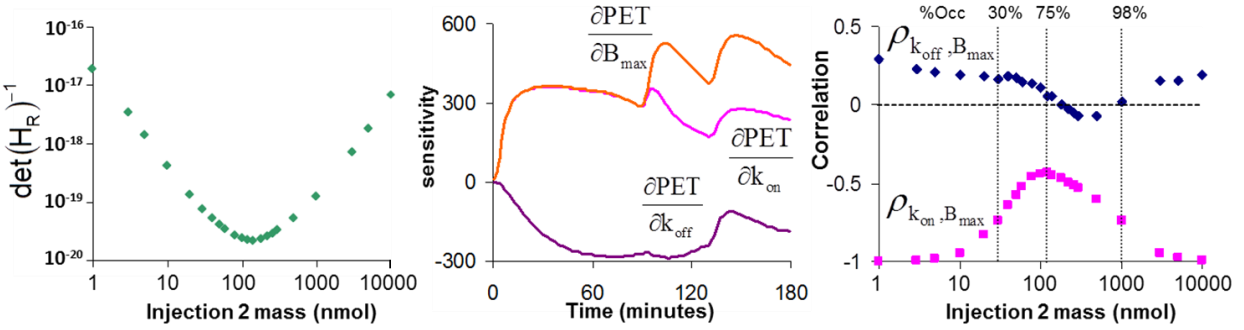

Figure 5-3: Experimental Design – effects of mass in the second injection. (Left) D-optimal ($\det(H_R)^{-1}$) criterion as a function of injected mass. (Middle) Correlations between B_{max} with k_{on} and k_{off} as a function of injected mass. (Right) Sensitivity curves for k_{on}, k_{off}, and B_{max} in the MTC in which the second injection consists of unlabeled MeFWAY mass that occupies ~75% of the available receptors.

The experimental protocols for subjects M1-M6 are shown in Table 5-1. It should be noted that the initial optimizations were based upon a K_{Dapp} that was approximately 70% lower than the newly measured values. Analysis from the first subject showed that optimal parameter estimation needed only a high mass dose in injection 2 and low mass in injection 3, which was then implemented in the following studies. As the experiments progressed, the most recent parameter estimates were incorporated into the optimization and resulted in increasing the MeFWAY mass for the second injection.

Table 5-1: Injection parameters for MI experiments.

Injection #	Parameter	Subject					
		M1	M2	M3	M4	M5	M6
1	time (minutes)	0	0	0	0	0	0
	activity (MBq)	58.1	66.2	63.3	61.8	64.8	57.7
	mass (nmol)	2.4	0.5	0.8	0.8	1.2	0.6
2	time (minutes)	91	90	90	90	91	90
	activity (MBq)	60.3	61.0	57.4	60.0	51.4	58.8
	mass (nmol)	19.2	30.6	175.5	164.1	141.1	134.6
3	time (minutes)	150	120	130	130	131	130
	activity (MBq)	46.3	65.9	61.0	55.1	59.6	58.1
	mass (nmol)	113.6	1.1	1.7	1.5	2.4	1.4

5.3.2. Measurement of k_{on}, k_{off}, and B_{max}

The parameter estimates for all of the subjects are given in Table 2, including a single estimate for k_{on}, k_{off}, and V_{ND} across all regions and individual ROI estimates for K_1 and B_{max} in the MTC, sTC, PC, dACC, and RN. For these regions, the highest 5-HT_{1A} receptor density was found in the MTC and dACC, with intermediate levels in the sTC and RN, and lower receptor expression in the PC. The average (over brain regions) *cov* in B_{max} was 17.9% across the 6 subjects. Of the estimated parameters, k_{on} displayed the lowest variability across this group of subjects, with a *cov* of 14%. There was slightly higher variability in k_{off} (*cov* = 17%), which

resulted in a *cov* = 29% in K_{Dapp} due to the propagation of errors. The average K_{Dapp} of [^{18}F]MeFWAY for the 5-HT_{1A} receptor site was 4.3 ± 1.3 pmol/mL.

Figure 5-4 displays the PET measured time courses and the model output for the regions of the MTC, dACC, sTC, RN, PC, and CB in one subject. The CB is also displayed separately in Figure 5-5 to illustrate the absence of measurable 5-HT_{1A} binding in this region, with each of the three injections superimposed over a single time course after correction for residual activity from previous injection(s).

Table 5-2: Parameter measurements across regions.

Region	Parameter	Units	M1	M2	M3	M4	M5	M6	**Mean**	**SD**
all ROIs excluding CB	k_{on}	mL/pmol/min	0.0082	0.0066	0.006	0.0079	0.0076	0.006	**0.0070**	**0.0010**
	k_{off}	min^{-1}	0.024	0.028	0.029	0.024	0.028	0.039	**0.029**	**0.005**
	K_D	pmol/mL	3.0	4.2	5.1	3.1	3.6	6.6	**4.3**	**1.3**
all ROIs	V_{ND}	unitless	3.7	3.3	3.5	2.4	2.2	2.2	**2.9**	**0.6**
CB	K_1	mL/mL/min	0.62	0.36	0.68	0.28	0.80	0.29	**0.50**	**0.20**
MTC	K_1	mL/mL/min	0.70	0.59	0.83	0.50	0.46	0.55	**0.60**	**0.13**
	B_{max}	pmol/mL	42.3	29.3	54.8	36.6	38.0	47.8	**41.5**	**8.2**
sTC	K_1	mL/mL/min	1.01	0.67	0.95	0.51	0.51	0.48	**0.69**	**0.22**
	B_{max}	pmol/mL	21.6	21.0	29.8	21.3	20.2	28.1	**23.7**	**3.8**
PC	K_1	mL/mL/min	1.03	0.65	0.69	0.40	0.47	0.35	**0.60**	**0.23**
	B_{max}	pmol/mL	14.2	11.2	13.3	11.7	10.9	15.5	**12.8**	**1.7**
dACC	K_1	mL/mL/min	1.16	0.68	1.01	0.48	0.50	0.42	**0.71**	**0.28**
	B_{max}	pmol/mL	33.8	30.4	50.1	30.1	28.6	43.9	**36.1**	**8.0**
RN	K_1	mL/mL/min	1.00	0.80	1.05	0.51	0.48	0.63	**0.74**	**0.22**
	B_{max}	pmol/mL	18.8	17.6	18.2	14.8	19.0	26.6	**19.2**	**3.6**

*The coefficients of variation (*cov=s.d./mean*100*) for each estimated parameter found using Monte Carlo methods, resulted in uncertainties of: k_{on} (4%), k_{off} (4%), K_D (6%), V_{ND} (2%), K_1 in the CB (4%), MTC (4%), sTC (4%), PC (5%), dACC (4%), RN (4%), B_{max} in the MTC (3%), sTC (4%), PC (4%), dACC (3%) and RN (4%)

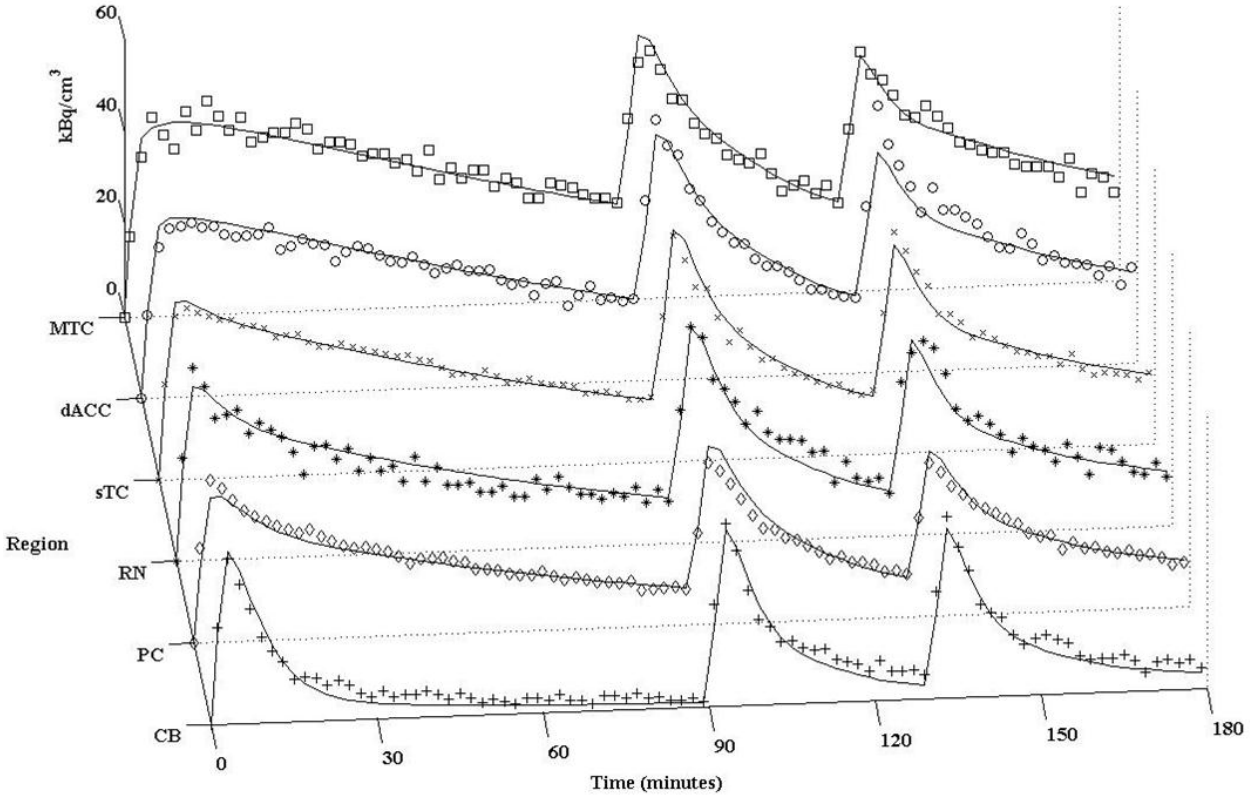

Figure 5-4: Measured time-activity curves (not corrected for decay) and model predictions (solid line) for subject M4 in the regions of the MTC (□), dACC (o), sTC (x), RN (*), PC (◊), and CB(+).

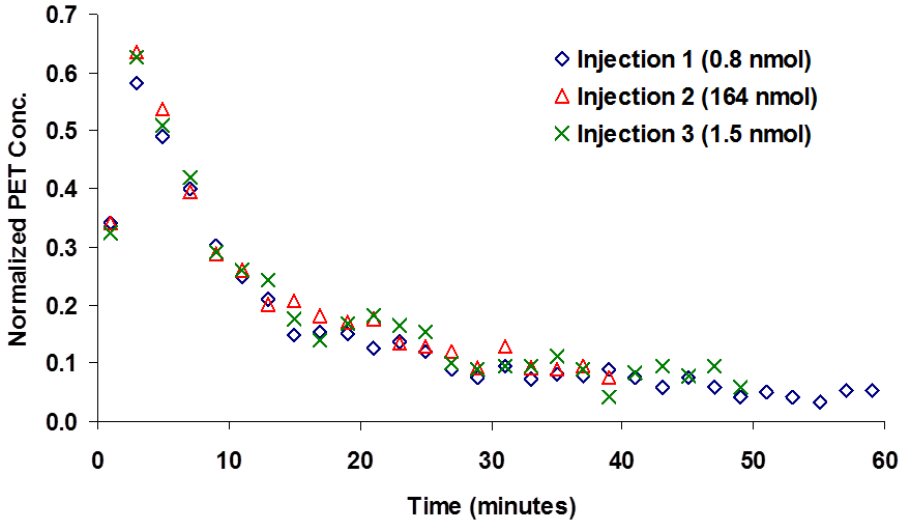

Figure 5-5: Cerebellum TACs (not corrected for decay) for three injections in subject M4 (Bq/cc/i.d. x 1000). The data for injection 2 and injection 3 were corrected for residual activity present from the previous injection(s) by subtracting the extrapolated activity using a bi-exponential function.

5.4. Discussion

In Chapter 2, a direct comparison of the in vivo behavior of [^{18}F]MeFWAY with two other 5-HT_{1A} receptor antagonists, [^{11}C]WAY-100635 and [^{18}F]MPPF, under single-bolus injection conditions (see Wooten et al., 2011a). These experiments were therefore not designed for the direct measurement of K_D. In the work presented in this chapter, a K_{Dapp} of 4.3 ± 1.3 nM was measured when averaged over the six subjects, which is similar to in vivo measures for other related 5-HT_{1A} PET antagonists. Farde and colleagues (1997) performed a PET study of [^{11}C]WAY-100635 in a single cynomolgus monkey using varying mass injections with competing drug and reported a K_{Dapp} of approximately 1-2 nM (estimated from figure). A recent study was conducted using [^{18}F]FPWAY in 21 rhesus monkeys and reported apparent K_{Dapp} values ranging from 1-4 nM (*cov*~30% using SEM) in rhesus monkeys (Spinelli et al., 2010). For [^{18}F]MPPF, MI studies were performed in humans (n = 5) and reported K_{Dapp} = 2.8 nM (*cov*~50%) (Costes et al., 2002), yielding comparable results with [^{18}F]MeFWAY. This similarity in the 5-HT_{1A} affinity of [^{18}F]MPPF and [^{18}F]MeFWAY is not consistent with our previous results, which suggested the K_{Dapp} for [^{18}F]MeFWAY is approximately 3-fold lower compared to [^{18}F]MPPF based upon BP_{ND} comparisons (Wooten et al., 2011a) and in vitro measures (Saigal et al., 2006; Khawaja et al, 1995). This discrepancy in magnitude between the compounds may be due to differences in species, nonspecific binding in the brain (f_{ND}), or experimental design. However, the lower K_{Dapp} values reported for [^{18}F]MPPF were accompanied by reduced estimates of B_{max} (discussed below), indicating a degree of compatibility with these results within the context of the ratio of B_{max}/K_{Dapp}.

5.4.1. Considerations in In vivo measurement of 5-HT_{1A} B_{max}

The highest values of B_{max} were measured in the regions of the MTC and dACC. Due to the limited resolution of PET assay and the lack of accompanying MRI scans, only large areas with uniform binding of each specific brain region were selected for analysis. In vitro autoradiography measurements in the hippocampus of the cynomolgus monkey reveals a heterogeneous distribution of 5-HT_{1A} receptors across the hippocampal subfields, with highest binding in the area dentata, subiculum and parasubiculum in the range of 50-100 fmol/mg of protein (Köhler et al, 1986). In humans, post mortem in vitro studies using [^{3}H]WAY-100635 have shown high levels of receptor density in the hippocampus areas ranging from 31 fmol/mg of wet tissue in the parahippocampus to 113 fmol/mg of wet tissue in the hippocampus CA1 pyrimidal layer (Hall et al., 1997). A separate study also using [^{3}H]WAY-100635 found 5-HT_{1A} receptor densities of 200-300 fmol/mg of wet tissue in the CA1 of the hippocampus (Burnet et al, 1997). This work measured an average B_{max} value of approximately 40 pmol/mL in the MTC, which included regions of the hippocampus. These in vivo measurements of B_{max} are significantly lower than those obtained with in vitro assay. The direct comparison of in vitro and in vivo PET assay is challenging due to high degree of spatial averaging with PET, which will result in an underestimation of B_{max} for structures with cross-sectional areas that are comparable to the scanner resolution (<2-4mm). An example of this effect is most profound when considering the small focal structure of the RN. Reported in vitro receptor densities in the dorsal raphe in humans range from 50 fmol/mg of wet tissue to 230 fmol/mg of wet tissue (Burnet et al., 1997; Hall et al., 1997) compared to measured densities reported herein in the raphe of 18.1 ± 4.3 pmol/mL. The in vivo measurements reported are not specific to just the dorsal region of the raphe nuclei, but selected as the focal region in the superior PET images of the midbrain region. There was no attempt to correct for the resolution related partial volume effects of this region

and the reported B_{max} in the RN are likely underestimates of those that would be obtained with autoradiography. However, this does not necessarily invalidate an intersubject comparison of (in vivo) PET measures in the region of the RN, assuming the partial volume correction is consistent for all subjects. Because this correction accounts not only for regional size of brain structures but also for the spill over (and spill in) of the radioligand signal from surrounding regions, consideration must be given to variations in brain and body size of the subjects being compared. The subjects in this work were all fully grown adults of comparable weight (8.2 ± 1.6 kg) and age (13.0 ± 3.9 y), however, partial volume correction may be needed in experimental designs having greater variability in brain size (e.g. comparing early adolescent with adults subjects).

There have been several studies reporting in vivo PET measures of 5-HT_{1A} receptor densities using a variety of equilibrium and MI techniques with PET radioligands. In a cynomolgus monkey, B_{max} values of approximately 16 pmol/mL and 5 pmol/mL were found in the neocortex and raphe nuclei, respectively, using a 2-injection procotol with [^{11}C]WAY-100635 (Farde et al., 1997). A more recent study in juvenile rhesus monkeys (n=21) found B_{max} values of 5-13 pmol/mL (*cov*~26% using SEM) and 1-2 pmol/mL (*cov*~34% using SEM) in the hippocampus and raphe nuclei, respectively, using a 2-point bolus plus constant infusion equilibrium protocol with [^{18}F]FPWAY (Spinelli et al., 2010). Both of these previous studies used scatchard graphical analysis to estimate B_{max}, which has been demonstrated to be a valid technique with PET measurements, although high uncertainty in B_{max} estimation can be seen if there is insufficient receptor occupancy for the partial saturation injection (Holden and Doudet, 2004). This may explain some of the variation between results, with experiments using [^{18}F]FPWAY achieving only 40% occupancy. In humans, MI PET studies were performed with [^{18}F]MPPF, finding B_{max} values of 2.9 pmol/mL (*cov*~50%) in the hippocampus (Costes et al., 2002) using a 2-injection

(nonequilibrium) protocol. This is a 10-fold difference in measured B_{max} compared to the values reported herein. This discrepancy in B_{max} may be attributed in part to species differences, however, it may also be the result of methodological differences with the level of receptor saturation achieved for the experiments, which is discussed in the section below.

5.4.2. Considerations in experimental design

Careful attention must be given to the experimental design in MI studies to ensure identifiability of each individual parameter, particularly between k_{on} and B_{max}. Generally, parameter estimation algorithms will yield combinations of B_{max} and k_{on} estimates that accurately model the experimental data, even in the case of a faulty experimental MI design. In such situations, it is the product, $k_{on} \cdot B_{max}$, that is identified and not the independent measures of either parameter. For this work, the D-optimal criterion (which minimizes the indifference region and increases parameter precision) was used to assess the measured precision of the binding parameters k_{on}, B_{max}, and k_{off} and to determine the required experimental design for identifying each. It should be noted that the 3-injection design implemented in this protocol was not selected based upon the criteria of experimental simplicity (i.e., the shortest scan with fewest injections). The requirement was enforced that the first injection of each study consist of high specific activity [^{18}F]MeFWAY and 90 minutes of scanning. It has been shown that for other applications, it is possible to measure B_{max} with a 2-injection protocol with partial saturating doses of the ligand for the first injection (Salinas et al., 2007). Such a design foregoes the ability to measure BP_{ND} for comparison with radiotracer-only scans and was therefore not investigated for this work. Figure 5-3 illustrates the relation between one of the experimental variables (unlabeled MeFWAY mass for the second injection) with the D-optimal metric and the effects on the

measured output parameters and sensitivity curves. The correlation of k_{off} with B_{max} $\left(\rho_{k_{off},B_{max}}\right)$ remains small (<0.3) across all values of injected mass, suggesting their relation is not exclusively dependent on the MeFWAY dose, but improvement in decoupling these parameters could be achieved over a range of competing doses of MeFWAY. The variability of the measure k_{off} across subjects was relatively low, 0.030±0.005 min^{-1} (*cov*=17%), which is attributed to its high identifiability for this experimental design. The correlation between k_{on} and B_{max} $\left(\rho_{k_{on},B_{max}}\right)$ revealed much greater dependence on the amount of competing MeFWAY. As expected from radiotracer studies and illustrated in Figure 5-3, there is complete correlation between the parameters $\left(\rho_{k_{on},B_{max}} = -1\right)$in the absence of significant MeFWAY dose. This correlation can be significantly reduced by increasing the competing MeFWAY in the second injection, with a minima in correlation corresponding to receptor occupancy of ~75%.

An examination of the sensitivity curves, $\partial PET(t)/\partial\theta_i$, where θ_i represents an estimated parameter, graphically illustrates the decoupling of the parameters. Figure 5-3 shows the scaled sensitivity curves for B_{max}, k_{on}, and k_{off}. Complete coupling between k_{on} and B_{max} can be seen in the sensitivity curves prior to injection 2 where curves overlay. In the case where partial receptor saturation occurs (receptor occupancy ~75%), there is a divergence of the sensitivity curves for k_{on} and B_{max}, indicating a reduction in the covariance. The sensitivity curves illustrate that identification of k_{on} and B_{max} comes primarily from injection 2, and additional decoupling of k_{off} from k_{on} and B_{max} comes from the third injection.

Examination of the D-optimal criteria, as seen in Figure 5-3, shows that the decoupling of k_{on} and B_{max} is increased with increasing MeFWAY mass (up to a limit) with an occupancy range optimal for decoupling being 50-96% of the 5-HT_{1A} receptor sites. This finding that higher

receptor occupancy is optimal to uncouple k_{on} and B_{max} is comparable to that of a previous 2-injection MI study using [^{18}F]-(S)-fluorcarazalol for measuring B_{max} of myocardial β-adrenergic receptors, which found receptor occupancies of ~90% were optimal for precise estimation of receptor concentration (Salinas et al., 2007). For implementation with 3-injections, maximum decoupling of k_{on} and B_{max} was found to occur with a saturating dose of ~75% receptor occupancy, corresponding to a dose, averaged over the 6 subjects, of approximately 12 nmol/kg. The peak occupancies observed for subjects M1-M6 were: 95%, 43%, 93%, 93%, 91%, and 73% respectively, from the high dose MeFWAY injections. These occupancies can be compared with an MI study in humans using [^{18}F]MPPF (Costes et al., 2002), which administered MPPF doses of approximately 20-fold (estimated) lower than doses used in this work. Based on simulations with MeFWAY, unlabeled dose at this level would not be adequate to decouple k_{on}, k_{off}, and B_{max}, resulting in instability of the parameter estimates. This large difference in occupancy levels may explain the discrepancies in the 5-HT_{1A} B_{max} estimates between methods.

The peak transient occupancy of the 5-HT_{1A} receptors as a function of MeFWAY dose is shown in Figure 5-6. This relation is based upon the measured in vivo parameters of the six subjects and the error bars represent the s.d. accounting for the variations in the parameters as well as the differences in [^{18}F]MeFWAY observed in the measured input function. This information can be used as a guide for examining mass effects in radiotracer-only studies. For a [^{18}F]MeFWAY synthesis yielding a specific activity of 111-185 GBq/μmol (3000-5000 mCi/μmol) and a 111 MBq (3 mCi) injection (typical of tracer-only single bolus injection studies), the 5-HT_{1A} receptor occupancy will range from 1.0-1.6%. Under these conditions it will be possible to perform two sequential radiotracer studies on different subjects, from the same

batch (i.e. synthesis) of [^{18}F]MeFWAY, without exceeding a threshold of 4-5% receptor occupancy from unlabeled MeFWAY at "tracer" levels.

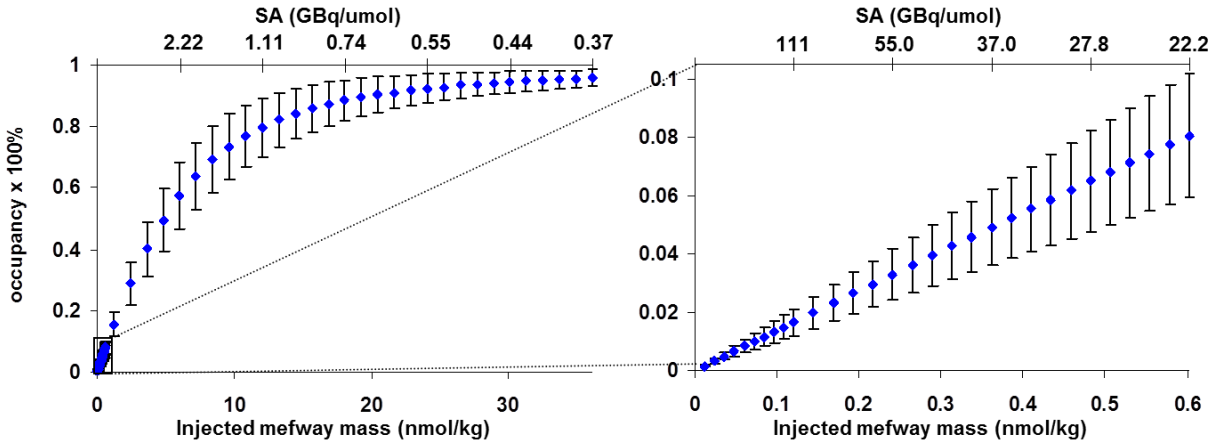

Figure 5-6: Receptor occupancy as a function of injected mass (nmol/kg) and specific activity when using the average parameter values. The inter-subject standard deviation is shown by the error bars which illustrate the difference seen among subjects due to the individual parameters and subject weights. The bottom axis shows the injected mass in nmol/kg and the top axis shows the specific activity in GBq/μmol (assuming a 111 MBq (3 mCi) injection typical to tracer-only single bolus injection studies). The left image shows the receptor occupancy in the full range from high specific activity to near saturation. The right image shows the receptor occupancy in the mass range of a typical high specific activity injection.

The analysis for the parameter estimations involved several assumptions that require consideration. The blood flow was assumed to be constant over the course of the 3 hour experiment. Potential alterations in blood flow would change the rate of MeFWAY delivery (via K_1) and efflux (via k_2) and bias the measurement of these parameters. The heart rates of the subjects were monitored throughout the studies and demonstrated a gradual decreasing trend during the course of the experiment, with a total decrease of approximately 20 ± 5% for the 3 hour scan. There was no observable change in heart rate, SpO_2 levels, or breathing rate when the saturating dose of MeFWAY was delivered. Although this does not discount the possibility of changes to cerebral blood flow, it does alleviate the concern that global changes were induced by the MeFWAY drug. The model included a separate K_1 for each region to account for regional differences in ligand delivery, however, the assumption was made that the nondisplaceable

volume of distribution (V_{ND}) remain constant across all examined brain regions. This assumption is consistent with reference region methods of analysis for single injection PET studies. Further, this constraint can accommodate regional perfusion changes, as it has been demonstrated that V_{ND} remains constant under conditions of changing blood flow (Logan et al., 1994). The assumption of uniform V_{ND} across regions was examined by fitting each region independently and allowing k_2 to float with the other parameters to determine the effects on the resulting B_{max} and V_{ND} estimates. Minimal change in B_{max} (~1%) and V_{ND} (~5%) was observed in the high density 5-HT_{1A} receptor region of the MTC. However, in the lower density 5-HT_{1A} receptor region of the PC, a negative correlation between V_{ND} and B_{max} was observed leading to an increase of ~19% for B_{max} and a decrease of ~18% for V_{ND} when averaged over all subjects. Thus, any potential bias introduced by the assumption of constant V_{ND} would surface primarily in the low 5-HT_{1A} receptor density regions.

As configured, implementation of the MI model required separate arterial input functions for each injection, defined in units of molar concentration of MeFWAY (pmol/mL). Separation of the input functions involved extrapolating data from previous injection(s) and subtracting from the subsequent injection(s), with a bi-exponential function $\left(d_1 e^{-\lambda_1 t} + d_2 e^{-\lambda_2 t}\right)$ used for the extrapolation. This was necessary to account for residual activity from previous injections. At 30 minutes after injection 2, the radioactivity from injection 1 still accounted for approximately 15% of the total parent radioactivity in the plasma and at 30 minutes after injection 3, injections 1 and 2 accounts for approximately 27% of the total plasma activity. The fitting of the second injection to a bi-exponential function was problematic because it consisted of only 40 minutes of arterial sampling time before the administration of the third injection. We initially explored the use of a scaled (by injected activity) version of the first injection for the subsequent injections

based upon the assumption that each injection would have similar a time course. However, close examination of the input functions revealed the second injection possessed a broader peak (i.e. smaller λ_1), suggesting an alteration in the radiotracer delivery between injections. It is speculated that the addition of pharmacological doses of unlabeled MeFWAY increased the bioavailability of [^{18}F]MeFWAY in the system, possibly by releasing previously bound [^{18}F]MeFWAY from the receptors and by preventing new radiotracer from binding. It was initially assumed that small inaccuracies in the extrapolated function fitted to 40 minutes or less of arterial sampling data, coming from the second injection, would result in large variation in the binding parameter estimates due to the presence of the unlabeled MeFWAY in this injection. To examine the effects of potential inaccuracies in the input function of the second injection, the data were analyzed with two different extrapolation schemes. The range of variation was determined from the input function of injection 1, first using the entire 90 minute time course and a secondly using only the data out to 40 minutes. The percent difference in the bi-exponential decay parameters (λ_1 and λ_2) was typically less than 20% between methods, however, in one study, there was a 44% difference in λ_2 (the slow decay term). This difference was then incorporated into the extrapolated data for the second injection to examine the effects of inaccurate extrapolation on the outcome variables B_{max} and K_{Dapp}. It was found that B_{max} varied by less than 1.5% in all areas and K_{Dapp} varied by less than 1.3%, suggesting the experimental design is relatively insensitive to the concentration of MeFWAY and its time course once the third injection is administered, as illustrated by the sensitivity curves for B_{max} and k_{on}.

The unlabeled MeFWAY used in these experiments was a commercially purchased reference standard consisting of an isomeric mixture of *cis*- and *trans*-MeFWAY (15:85). Results

presented in Chapter 3 displayed that *cis*-[^{18}F]MeFWAY exhibits low, but significant 5-HT$_{1A}$ binding compared to *trans*-[^{18}F]MeFWAY, with a BP_{ND} in the MTC of 0.58 and 7.70 for *cis*- and *trans*-[^{18}F]MeFWAY, respectively (see also Wooten et al., 2011b). This profound difference in the binding affinity of isomeric pairs has been reported for other 5-HT$_{1A}$ PET radiotracers (Lang et al., 1999; Wilson et al, 1999). In these studies, the reported injected masses are based only on the measured *trans*-MeFWAY mass and exclude the *cis*-MeFWAY mass fraction. The presence of unlabeled *cis*-MeFWAY in the high dose injections of MeFWAY are assumed to cause negligible effect. It can be approximated, from binding potentials for *cis*- and *trans*-[^{18}F]MeFWAY (Chapter 3), that for equal *cis*- and *trans*- concentrations, the *cis*-MeFWAY would represent 7.6% (0.58/7.70) of the bound MeFWAY, which suggests that only ~1% of the receptor sites are occupied by the *cis*- isomer for the mixture used in these studies.

5.4.3. The use of BP_{ND} as an index of B_{max}

The first 90 minutes of each study was used as a baseline to extract BP_{ND} estimates for comparison with direct measurements of B_{max} and K_{Dapp}. The outer cortex in the lobes of the CB was used as the reference region for the BP_{ND} estimation. Chapter 2 reported on the use of the CB as a region with negligible 5-HT$_{1A}$ binding for radiotracer [^{18}F]MeFWAY studies. The lack of measurable specific binding was confirmed in this study, revealing no measurable displacement of [^{18}F]MeFWAY in the CB as illustrated in Figure 5-5. Shown in Figure 5-7A are scatter plots of the measured B_{max} values with the BP_{ND} for the ROI data across subjects. Regression analysis found no significant correlation between B_{max} and BP_{ND} for any of the regions: MTC (p=0.3), dACC (p=0.98), sTC (p=0.14), PC (p=0.83), RN (p=0.99). However, significant correlation was found between BP_{ND} and B_{max}/K_D in all regions (MTC (p=0.014),

sTC (p=0.017), PC (p=0.0065), RN (p=0.023)) with the exception of the dACC (p=0.15). These data are shown in Figure 5-7B with all of the regions plotted on the same axis (although they were analyzed separately). A similar lack of correlation between the dopamine transporter B_{max} and a composite binding parameter (BP_P) has been reported using [^{11}C]cocaine and serial equilibrium PET studies (Logan et al., 1997). The authors attributed the absence of correlation to a lack of robustness in their estimation of B_{max}. A significant positive correlation has been reported between BP_{ND} and B_{max} values as well as BP_{ND} and B_{max}/K_{Dapp} in extrastriatal dopamine D_2 receptors using [^{11}C]FLB457 and a scatchard type multi-scan session (Olsson et al, 2004). In this particular work, however, a correlation was also observed between B_{max} and K_{Dapp} which may contribute to the correlation observed between B_{max} and BP_{ND}. Additionally, the data were regressed across subjects and across regions whereas our analysis is not regressed across brain regions. It has been suggested that non-equilibrium experiments, such as MI designs which decouple B_{max} and k_{on}, may improve the identifiability of B_{max} (Morris et al., 1999). For the data reported in these six subjects, the mean *cov* of B_{max} across the ROIs was 17.9% which was

similar to the mean *cov* of the BP_{ND} values of 17.3%, suggesting the same variability is seen in the binding indices and neither exhibits an advantage in precision of parameter estimation. The

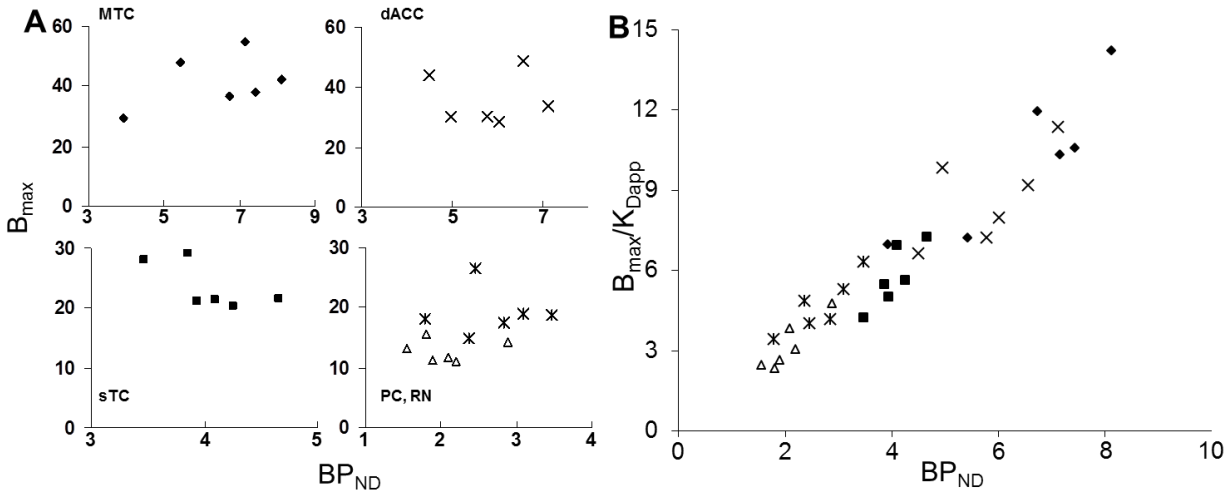

Figure 5-7: A. Comparison of B_{max} with BP_{ND} in the regions of the MTC (♦), dACC(x), sTC(■), RN(Ж), and PC(Δ). B. Comparison of B_{max}/K_{Dapp} with BP_{ND} for all subjects across brain regions.

data in Figure 5-7 suggest that BP_{ND} is not a representative proxy of the receptor density (B_{max}) across subjects, but can serve as an index of B_{max}/K_{Dapp}. Generalization of this statement cannot be assumed for all PET neuroligands and neuroreceptor systems from these six studies. Additionally, attempts to explain the relation of B_{max} and BP_{ND} based upon the methodological approaches that were utilized in these studies are not being discussed, as these issues have been discussed in the literature (Morris et al., 1999; Olsson et al., 2004) and remain largely unresolved.

All in vivo PET methods for B_{max} and K_{Dapp} measurement, equilibrium and non-equilibrium, employ assumptions that can potentially bias the outcome measures. In this work, K_{Dapp} was fixed as a constant across all ROIs by estimating only a single k_{on} and k_{off} for each subject. This was done primarily to reduce the number of estimated parameters and in turn, enhance the identifiability of the others. K_{Dapp} is sensitive to several factors that may challenge this

assumption, such as endogenous 5-HT competition within the vicinity of the receptors. The effects of competing neurotransmitter on the measured K_{Dapp} is given as: $(K_{Dapp})^{est} = (K_{Dapp})^{0}(1 + F_{5HT}/K_D^{en})$, where $(K_{Dapp})^{est}$ is the measured K_{Dapp} in the presence of endogenous 5-HT (as measured in these experiments), $(K_{Dapp})^{0}$ is the measured K_{Dapp} in the absence of 5-HT, F_{5HT} is the synaptic concentration of 5-HT, and K_D^{en} is the equilibrium dissociation constant of 5-HT (Delforge et al, 2001). This relation suggests that 50% occupancy of the receptors by endogenous 5-HT will result in a doubling of $(K_{Dapp})^{est}$ compared to conditions under 5-HT depletion. By imposing a single K_{Dapp} across all brain regions (i.e. ROIs) for each subject, uniform 5-HT occupancy is assumed across regions. No temporal change in endogenous 5-HT due to anesthesia during the course of the experiments is also assumed. Although no effects on endogenous 5-HT due to ketamine have been measured (Bacopoulos, Redmond et al, 1979), isoflurane has been shown to reduce endogenous 5-HT levels (Tokugawa et al., 2007). To minimize potential variations in 5-HT across the cohort, all subjects were anesthetized with the same methodology and consistent timing was used for the injections. The vital signs were examined for evidence of physiological changes. SpO_2 levels remained constant throughout the scanning procedure and were relatively similar between subjects with mean and standard deviation of 98.6 ± 0.6% saturation. Breathing rate was within a range of 10-20 breaths/minute, and did not reveal a noticeable trend in variation from beginning to end of the scanning procedure. The average breathing rate among all subjects was 15.1±2.3 breaths/minute.

Further 5-HT depletion and/or competition experiments will be required to fully validate the use of a uniform K_{Dapp} and the potential effects of isoflurane. Similar studies with PET ligands have been performed for the dopamine system to closely examine the effects of endogenous

neurotransmitter on radioligand binding (Delforge et al., 2001). Without these experiments, it can only be speculated that the effects of competing 5-HT will induce only small changes in these results based upon the similarities in in vivo behavior between [^{18}F]MeFWAY with [^{11}C]WAY-100635 (Wooten et al., 2011a). Studies with [^{11}C]WAY-100635 and [^{3}H]WAY-100635 have shown negligible changes in binding due to increases and decreases in endogenous serotonin levels (Maeda J et al., 2001; Rice et al., 2001). Further, previous in vitro work revealed that inhibition by 5-HT was similar for MeFWAY (Saigal et al., 2006) and WAY-100635 (Khawaja et al, 1995).

5.5. Summary

To summarize, in vivo measurements of K_1, V_{ND}, k_{on}, k_{off}, and B_{max} have been made for [^{18}F]MeFWAY in various 5-HT_{1A} regions of the rhesus monkey brain using PET. Experiment design optimized the identifiability of the binding parameters k_{on}, k_{off}, and B_{max} to improve precision in parameter estimates. These results show that MI [^{18}F]MeFWAY PET experiments can be used to measure 5-HT_{1A} receptor density across the regions of the brain.

5.6. References

Bacopoulos, N.G., Redmond, D.E., Roth, R.H., 1979. Serotonin and dopamine metabolites in brain regions and cerebrospinal fluid of a primate species: effects of ketamine and fluphenazine. Journal of Neurochemistry 32, 1215–8.

Burnet, P.W., Eastwood, S.L., Harrison, P.J., 1997. [^{3}H]WAY-100635 for 5-HT1A receptor autoradiography in human brain: a comparison with [^{3}H]8-OH-DPAT and demonstration of increased binding in the frontal cortex in schizophrenia. Neurochemistry International 30, 565–74.

Christian, B.T., Narayanan, T., Shi, B., Morris, E.D., Mantil, J., Mukherjee, J., 2004. Measuring the in vivo binding parameters of [^{18}F]-fallypride in monkeys using a PET multiple-injection protocol. Journal of Cerebral Blood Flow and Metabolism 24, 309–322.

Christian, B.T., Vandehey, N.T., Floberg, J.M., Mistretta, C.A., 2010. Dynamic PET Denoising with HYPR Processing. Journal of Nuclear Medicine 51, 1147–54.

Costes, N., Merlet, I., Zimmer, L., Lavenne, F., Cinotti, L., Delforge, J., Luxen, A., Pujol, J.-F., Le Bars, D., 2002. Modeling [^{18}F]MPPF positron emission tomography kinetics for the determination of 5-hydroxytryptamine$_{1A}$ receptor concentration with multiinjection. Journal of Cerebral Blood Flow and Metabolism 22, 753–65.

Delforge, J., Bottlaender, M., Loc'h, C., Guenther, I., Fuseau, C., Bendriem, B., Syrota, A., Mazière, B., 1999. Quantitation of extrastriatal D_2 receptors using a very high-affinity ligand (FLB 457) and the multi-injection approach. Journal of Cerebral Blood Flow and Metabolism 19, 533–46.

Delforge, J., Bottlaender, M., Pappata, S., Loc'h, C., Syrota, A., 2001. Absolute quantification by positron emission tomography of the endogenous ligand. Journal of Cerebral Blood Flow and Metabolism 21, 613–30.

Delforge, J., Spelle, L., Bendriem, B., Samson, Y., Bottlaender, M., Papageorgiou, S., Syrota, A., 1996. Quantitation of benzodiazepine receptors in human brain using the partial saturation method. Journal of Nuclear Medicine 37, 5–11.

Delforge, J., Syrota, A., Mazoyer, B.M., 1990. Identifiability analysis and parameter identification of an in vivo ligand-receptor model from PET data. IEEE Transactions on Bio-Medical Engineering 37, 653–61.

Gallezot, J.-D., Bottlaender, M.A., Delforge, J., Valette, H., Saba, W., Dollé, F., Coulon, C.M., Ottaviani, M.P., Hinnen, F., Syrota, A., Grégoire, M.-C., 2008. Quantification of cerebral nicotinic acetylcholine receptors by PET using 2-[^{18}F]fluoro-A-85380 and the multiinjection approach. Journal of Cerebral Blood Flow and Metabolism 28, 172–89.

Gunn, R.N., Sargent, P.A., Bench, C.J., Rabiner, E.A., Osman, S., Pike, V.W., Hume, S.P., Grasby, P.M., Lammertsma, A.A., 1998. Tracer kinetic modeling of the 5-HT_{1A} receptor ligand [carbonyl-^{11}C]WAY-100635 for PET. NeuroImage 8, 426–40.

Gweltas Mauger, Wadad Saba, Philippe Hantraye, Frédéric Dolle, Christine Coulon, Yann Bramoulle, Sylvie Chalon, Marie-Claude Gregoire, 2005. Multiinjection approach for D_2 receptor binding quantification in living rats using [^{11}C]raclopride and the b-microprobe: crossvalidation with in vitro binding data. Journal of Cerebral Blood Flow and Metabolism 25, 1517–27.

Hall, H., Lundkvist, C., Halldin, C., Farde, L., Pike, V.., McCarron, J.., Fletcher, A., Cliffe, I.., Barf, T., Wikström, H., Sedvall, G., 1997. Autoradiographic localization of 5-HT_{1A} receptors in the post-mortem human brain using [^{3}H]WAY-100635 and [^{11}C]WAY-100635. Brain Research 745, 96–108.

Holden, J.E., Doudet, D.J., 2004. Positron emission tomography receptor assay with multiple ligand concentrations: an equilibrium approach. Methods in Enzymology 385, 169–84.

Innis, R.B., Cunningham, V.J., Delforge, J., Fujita, M., Gjedde, A., Gunn, R.N., Holden, J., Houle, S., Huang, S.-C., Ichise, M., Iida, H., Ito, H., Kimura, Y., Koeppe, R.A., Knudsen, G.M., Knuuti, J., Lammertsma, A.A., Laruelle, M., Logan, J., Maguire, R.P., Mintun, M.A., Morris, E.D., Parsey, R., Price, J.C., Slifstein, M., Sossi, V., Suhara, T., Votaw, J.R., Wong, D.F., Carson, R.E., 2007. Consensus nomenclature for in vivo imaging of reversibly binding radioligands. Journal of Cerebral Blood Flow and Metabolism 27, 1533–9.

Farde, L., Ginovart, N., Ito, H., Lundkvist, C., Pike, V.W., McCarron, J.A., Halldin, C., 1997. PET-characterization of [carbonyl-^{11}C]WAY-100635 binding to 5-HT_{1A} receptors in the primate brain. Psychopharmacology 133, 196–202.

Lang, L., Jagoda, E., Schmall, B., Sassaman, M., Magata, Y., Eckelman, W.C., 1999. Comparison of ^{18}F labeled *cis* and *trans* 4-fluorocyclohexane derivatives of WAY-100635. Journal of Nuclear Medicine 40, 37P–38P.

Logan, J., Volkow, N.D., Fowler, J.S., Wang, G.J., Dewey, S.L., MacGregor, R., Schlyer, D., Gatley, S.J., Pappas, N., King, P., 1994. Effects of blood flow on [^{11}C]raclopride binding in the brain: model simulations and kinetic analysis of PET data. Journal of Cerebral Blood Flow and Metabolism 14, 995–1010.

Logan, J., Fowler, J., Volkow, N., 1996. Distribution volume ratios without blood sampling from graphical analysis of PET data. Journal of Cerebral Blood Flow and Metabolism 16, 834–40.

Logan, J., Fowler, J.S., Volkow, N.D., Ding, Y.S., Wang, G.J., Alexoff, D.L., 2001. A strategy for removing the bias in the graphical analysis method. Journal of Cerebral Blood Flow and Metabolism 21, 307–20.

Logan, J., Volkow, N.D., Fowler, J.S., Wang, G.J., Fischman, M.W., Foltin, R.W., Abumrad, N.N., Vitkun, S., Gatley, S.J., Pappas, N., Hitzemann, R., Shea, C.E., 1997. Concentration and occupancy of dopamine transporters in cocaine abusers with [^{11}C]cocaine and PET. Synapse 27, 347–56.

Maeda J, Suhara T, Ogawa M, Okauchi T, Kawabe K, Zhang MR, Semba J, Suzuki K, 2001. In vivo binding properties of [carbonyl-^{11}C]WAY-100635: effect of endogenous serotonin. Synapse 40, 122–9.

Morris, E.D., Babich, J.W., Alpert, N.M., Bonab, A.A., Livni, E., Weise, S., Hsu, H., Christian, B.T., Madras, B.K., Fischman, A.J., 1996. Quantification of dopamine transporter density in monkeys by dynamic PET imaging of multiple injections of ^{11}C-CFT. Synapse 24, 262–72.

Morris, E.D., Bonab, A.A., Alpert, N.M., Fischman, A.J., Madras, B.K., Christian, B.T., 1999. Concentration of dopamine transporters: to B_{max} or not to B_{max}? Synapse 32, 136–40.

Morris, E.D., Christian, B.T., Yoder, K.K., Muzic, R.F.J., 2004. Estimation of local receptor density, B_{max}, and other parameters via multiple-injection positron emission tomography experiments. Methods in Enzymology 385, 184–213.

Muzic, R., Saidel, G., Zhu, N., Nelson, A., Zheng, L., Berridge, M., 2000. Iterative optimal design of PET experiments for estimating β-adrenergic receptor concentration. Medical and Biological Engineering and Computing 38, 593–602.

Muzic, R.F., Cornelius, S., 2001. COMKAT: Compartment model kinetic analysis tool. Journal of Nuclear Medicine 42, 636–45.

Muzic, R.F.J., Christian, B.T., 2006. Evaluation of objective functions for estimation of kinetic parameters. Medical Physics 33, 342–53.

Olsson, H., Halldin, C., Farde, L., 2004. Differentiation of extrastriatal dopamine D_2 receptor density and affinity in the human brain using PET. NeuroImage 22, 794–803.

Poyot, T., Condé, F., Grégoire, M.C., Frouin, V., Coulon, C., Fuseau, C., Hinnen, F., Dollé, F., Hantraye, P., Bottlaender, M., 2001. Anatomic and biochemical correlates of the dopamine transporter ligand ^{11}C-PE2I in normal and parkinsonian primates: comparison with 6-[^{18}F]fluoro-L-dopa. Journal of Cerebral Blood Flow and Metabolism 21, 782–92.

Rice, O. V, Gatley, S.J., Shen, J., Huemmer, C.L., Rogoz, R., DeJesus, O.T., Volkow, N.D., Gifford, A.N., 2001. Effects of Endogenous Neurotransmitters on the in vivo Binding of Dopamine and 5-HT Radiotracers in Mice. Neuropsychopharmacology 25, 679–89.

Saigal, N., Pichika, R., Easwaramoorthy, B., Collins, D., Christian, B.T., Shi, B., Narayanan, T.K., Potkin, S.G., Mukherjee, J., 2006. Synthesis and biologic evaluation of a novel

serotonin 5-HT_{1A} receptor radioligand, ^{18}F-labeled MeFWAY, in rodents and imaging by PET in a nonhuman primate. Journal of nuclear medicine 47, 1697–706.

Salinas, C., Muzic, R.F.J., Ernsberger, P., Saidel, G.M., 2007. Robust experiment design for estimating myocardial beta adrenergic receptor concentration using PET. Medical Physics 34, 151–65.

Spinelli, S., Chefer, S., Carson, R.E., Jagoda, E., Lang, L., Heilig, M., Barr, C.S., Suomi, S.J., Higley, J.D., Stein, E.A., 2010. Effects of early-life stress on serotonin$_{1A}$ receptors in juvenile Rhesus monkeys measured by positron emission tomography. Biological psychiatry 67, 1146–53.

Tai, C., Chatziioannou, A., Siegel, S., Young, J., Newport, D., Goble, R.N., Nutt, R.E., Cherry, S.R., 2001. Performance evaluation of the microPET P4: a PET system dedicated to animal imaging. Physics in Medicine and Biology 46, 1845–62.

Tokugawa, J., Ravasi, L., Nakayama, T., Lang, L., Schmidt, K.C., Seidel, J., Green, M. V, Sokoloff, L., Eckelman, W.C., 2007. Distribution of the 5-HT_{1A} receptor antagonist [^{18}F]FPWAY in blood and brain of the rat with and without isoflurane anesthesia. European Journal of Nuclear Medicine and Molecular Imaging 34, 259–266.

Vandehey, N.T., Moirano, J.M., Converse, A.K., Holden, J.E., Mukherjee, J., Murali, D., Nickles, R.J., Davidson, R.J., Schneider, M.L., Christian, B.T., 2010. High-affinity dopamine D_2/D_3 PET radioligands ^{18}F-fallypride and ^{11}C-FLB457: A comparison of kinetics in extrastriatal regions using a multiple-injection protocol. Journal of Cerebral Blood Flow and Metabolism 30, 994–1007.

Wilson, A.A., Garcia, A., Li, J., Dasilva, J.N., Houle, S., 1999. Analogues of WAY-100635 as radiotracers for in vivo imaging of 5-HT_{1A} receptors. Journal of Labelled Compounds and Radiopharmaceuticals 42, 611–20.

Wooten, D., Hillmer, A., Murali, D., Barnhart, T., Schneider, M.L., Mukherjee, J., Christian, B.T., 2011b. An in vivo comparison of *cis*- and *trans*-[^{18}F]MeFWAY in the nonhuman primate. Nuclear Medicine and Biology 38, 925–32.

Wooten, D.W., Moraino, J.D., Hillmer, A.T., Engle, J.W., Dejesus, O.J., Murali, D., Barnhart, T.E., Nickles, R.J., Davidson, R.J., Schneider, M.L., Mukherjee, J., Christian, B.T., 2011a. In vivo kinetics of [^{18}F]MEFWAY: a comparison with [^{11}C]WAY100635 and [^{18}F]MPPF in the nonhuman primate. Synapse 65, 592–600.

Khawaja, X., Evans, N., Reilly, Y., Ennis, C., Minchin, M.C.W., 1995. Characterisation of the Binding of [^{3}H]WAY-100635, a Novel 5-Hydroxytryptamine$_{1A}$ Receptor Antagonist, to Rat Brain. Journal of Neurochemistry 64, 2716–26.

Chapter 6 5-HT_{1A} sex based differences in B_{max}, K_{Dapp}, and BP_{ND} in the nonhuman primate

6.1. Introduction

Sex differences in 5-HT_{1A} function could contribute to the higher prevalence of depression among females, a disorder often attributed to the serotonin system (Cahill, 2006; Cosgrove et al, 2007). The biological bases for sex-specific functional dissimilarities in the 5-HT system remain unclear, however, could be attributed to gonadal hormones that affect the serotonin system. Variations in sex-dependent 5-HT function have been shown for blood serotonin levels (Ortiz et al, 1988), serotonin synthesis rates (Nishizawa et al., 1997; Sakai et al., 2006), serotonin transporter binding levels, and 5-HT neuroreceptor-ligand binding (Biver et al., 1996; Meltzer et al., 2001; Parsey et al., 2002; Jovanovic et al., 2008; Maron et al., 2011).

A critical regulator of the 5-HT system, 5-HT_{1A} receptors have been a central focus of research in sex-specific function. In vitro studies examining sex-based differences in the 5-HT_{1A} system have been inconclusive. Using [^{3}H]8-OH-DPAT, a 5-HT_{1A} agonist, in vitro binding assays showed similar measures of receptor density (B_{max}) and equilibrium dissociation (K_D) between the sexes (Dillon et al, 1991; Matsubara et al, 1991). Postmortem studies comparing receptor densities in suicide victims and controls showed higher [^{3}H]8-OH-DPAT binding in females (Arango et al, 1995). The effects of age on the 5-HT_{1A} system have been reported to alter B_{max} in the parietal cortex, occipital cortex, and hippocampus of females and K_{Dapp} in the occipital cortex of males (Palego et al., 1997). Positron emission tomography (PET) imaging may provide an opportunity to more closely characterize in vivo sex-specific differences in B_{max} and K_D.

The binding metric frequently used for PET studies examining sex differences in 5-HT_{1A} expression is the binding potential (BP), representing a composite parameter proportional to B_{max}/K_{Dapp} (Meltzer et al., 2001; Parsey et al., 2002; Jovanovic et al., 2008; Innis et al., 2007). In addition to serving as an index of B_{max}, the BP_{ND} ratio can be influenced by the receptor affinity state and endogenous neurotransmitter competition at the receptor site via K_{Dapp}. In this chapter, the MI technique is used with the 5-HT_{1A} receptor antagonist [^{18}F]MeFWAY to uncouple the binding parameters K_{Dapp} and B_{max}. Chapter 4 involved the use of [^{18}F]MeFWAY to measure B_{max} across the regions of the brain to enhance parameter identifiability in the brain regions with low 5-HT_{1A} receptor binding. In this chapter, the assumption has been removed to allow separate estimates of k_{on} in each brain region, focusing on high 5-HT_{1A} B_{max} regions, to account for variations in competing endogenous 5-HT. The additional detail of 5-HT_{1A} function beyond the BP_{ND} measurement will assist in clarifying the differences in the 5-HT system between the sexes and may ultimately provide insight into 5-HT disruption present in neuropsychiatric illnesses such as depression.

6.2. Methods

6.2.1. Radiosynthesis

The radiosynthesis of *trans*-[^{18}F]MeFWAY (N-{2-[4-(2-methoxyphenyl)-piperazinyl]ethyl}-N-(2-pyridyl)-N-(4-*trans*-[^{18}F]-fluoromethylcyclohexane)carboxamide) was performed similar to the method described in Chapter 2. Typical batch yields were between 1.5–3.0 GBq. At time of first injection, the average specific activity was 124 ± 55 GBq/μmol. The unlabeled MeFWAY used for the partial saturation doses was purchased from a commercial vendor (Huayi Isotopes, Toronto, ON, Canada) as an 85:15 isomeric mixture of *trans*-MeFWAY to *cis*-MeFWAY. As

discussed in Chapter 3, the *cis*-MeFWAY component of the mixture offers negligible competition to *trans*-MeFWAY 5-HT_{1A} binding and was therefore omitted from the calculation of injected mass for compartmental modeling purposes (Wooten et al., 2011b).

6.2.2. PET scans

6.2.2.1. Subjects

MI PET experiments were completed on a total of 17 *Macaca mulatta* (rhesus) subjects (6 male, 11 female; 10.4 ± 1.7 kg; 16.4 ± 1.2 years). The subjects were selected from an ongoing research program investigating the role of prenatal stressors on neurodevelopment (see Schneider et al, 1999 for details). For this work, subjects were drawn from a group receiving prenatal acoustic stress (N=10; 4 male, 6 female) and a group of age and sex matched controls (N=7; 2 male, 5 female). Following birth, all subjects were mother reared for the first 6 months of life. The subjects were then housed with peer groups until 30 months of age and then in pairs of similar age, sex, and prenatal condition. Subject care, preparation, and anesthetization was performed similar to methods explained in Section 2.2.2.

6.2.2.2. Scanning protocol

The three-injection scanning protocol including injection times and specific activities were based upon optimizations, performed to increase identifiability of K_{Dapp} and B_{max}, as described in our Chapter 4. Injection times, average specific activities, and average injected activities for males and females are shown in Table 1. To allow estimation of BP_{ND}, the first injection consisted of high specific activity [^{18}F]MeFWAY with a 90 minute scanning duration. For the second (partial saturation) injection, the average unlabeled MeFWAY mass per subject weight was 12 ± 4 nmol/kg and 12 ± 5 nmol/kg for male and female subjects, respectively. Work described in

Chapter 4 demonstrated 12 nmol/kg of MeFWAY corresponded to a peak transient occupancy of approximately 75%. The third injection was administered at 130 minutes and a total scanning duration of 180 minutes was acquired.

Table 6-1: Injection parameters

		Male		Female	
Injection #	Time (minutes)	Activity (MBq)	Mass (nmol/kg)	Activity (MBq)	Mass (nmol/kg)
1	0	58 ± 5	0.05 ± 0.01	60 ± 4	0.07 ± 0.03
2	90	61 ± 5	12 ± 4	58 ± 4	12 ± 5
3	130	60 ± 3	0.11 ± 0.04	60 ± 3	0.15 ± 0.07

A Concorde microPET P4 scanner was used for the scanning procedures similar to methods described in Section 2.2.3 (Tai et al., 2001).

6.2.2.3. Arterial Plasma Sampling

Arterial plasma sampling of [^{18}F]MeFWAY was performed to provide an input function for compartmental modeling. At the time of first injection, arterial sampling was initiated with sampling intervals of approximately 10 seconds for the first 2 minutes, then increasing to every 10 minutes by the end of an injection duration. In the case that arterial sampling was not performed, late venous samples were obtained at 10 minute intervals beginning at 20 minutes after an injection to allow adequate time for [^{18}F]MeFWAY concentration to equilibrate between arterial and venous pools. Whole blood samples were assayed for plasma radioactivity concentration of [^{18}F]MeFWAY in units of kBq/mL using similar methods described in Section 2.2.3. The same method of [^{18}F]MeFWAY radioactivity concentration assay was used for the venous samples. The unlabeled MeFWAY concentration, in units of pmol/mL, was then obtained after dividing by the injected specific activity.

6.2.3. Data analysis

6.2.3.1. Image reconstruction

Dynamic list mode emission data were reconstructed into 90 x 2 minute image frames using methods described in Section 2.2.4.

6.2.3.2. Regions of interest

A standard space template of [^{18}F]MeFWAY binding was created using a population-average MRI-based atlas of the rhesus macaque (McLaren et al., 2009). The reconstructed PET images were spatially normalized to the [^{18}F]MeFWAY template volume. Only brain regions with high 5-HT$_{1A}$ receptor density were chosen for this analysis to maximize the precision of the binding parameter estimates (discussed in section 2.3.4). Regions of interest (ROIs) were generated from a rhesus atlas developed in house which was based upon Paxinos et al (1999). ROIs (shown in Figure 6-1) were placed in the areas of the hippocampus (Hp: 1.6 cm^3), dorsal anterior cingulate cortex (dACC: 0.8 cm^3), amygdala (Am: 0.2 cm^3), and raphe nuclei (RN: 0.1 cm^3) to allow the

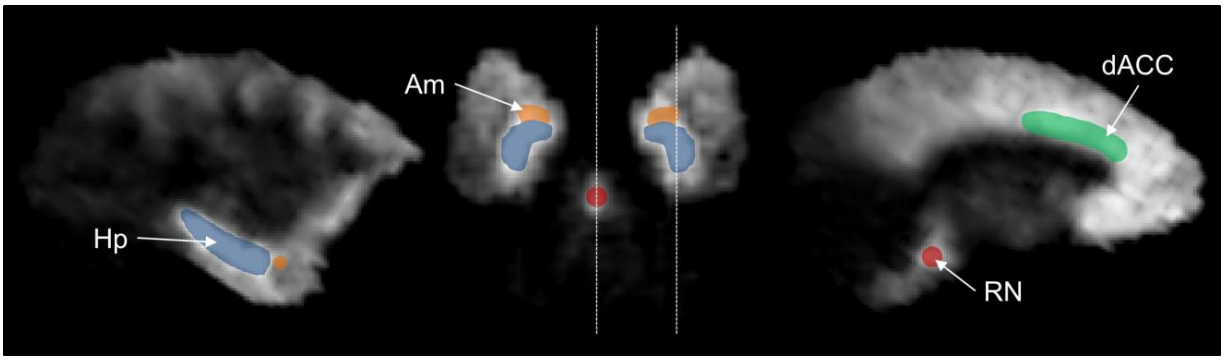

Figure 6-1: Regions of interest (ROIs) in the hippocampus (Hp, blue), amygdala (Am, orange), dorsal anterior cingulate cortex (dACC, green), and raphe nuclei (RN, red). PET images show sagittal (left and right) and transverse (middle) BP_{ND} images with ROIs overlaid. Dashed lines indicate planes shown in sagittal images.

extraction of time activity curves (TACs). A rigid body coregistration was used to align ROIs (Hp, dACC, Am) to each individual subject and the coregistered ROIs from each subject visually inspected. To minimize variability of ROI positioning in the RN, spherical fixed volume

(0.1cm^3) ROIs were manually centered over the high focal binding area which included portions of the dorsal and medial regions. ROIs were also drawn in the cerebellum (CB: 1.0 cm^3) including both gray and white matter avoiding the vermis (similar to Wooten et al, 2011b). Exclusion of the venous sinus in the CB ROI by a margin of several mm was carefully verified by examining ROI placement on the early and late PET frames. TACs were then extracted to serve as a reference for BP_{ND} estimation.

6.2.3.3. Group input function

6.2.3.3.1. Construction of group input function

The MI compartmental modeling requires each arterial input function to be uniquely defined for every injection. The residual activity from prior injections must be mathematically removed from subsequent injections. Starting with arterial plasma sampling data of [^{18}F]MeFWAY in units of kBq/mL., a bi-exponential function $\left(a_1 e^{-\lambda_1 t} + a_2 e^{-\lambda_2 t}\right)$ was fit to times > 5 minutes after a bolus injection to permit extrapolation of [^{18}F]MeFWAY clearance from the plasma which allows its subtraction from later injections. Full arterial sampling over the entire 3-injection 180 minute PET scan was performed in 7 out of the 17 total subjects in this study. A group input function (GIF) was constructed using 11 full arterial data sets (3 male, 8 female; 7 stress, 4 controls) which included 7 from this study and 4 additional data sets not included in the sex-based comparisons due to unsatisfactory experimental design. The 4 additional data sets were from subjects in the same cohort and were age-matched. First, the data sets were normalized by subject mass and injected activity. The normalized arterial time courses for each of three injections from each subject were then averaged together and fit to a 3-exponential function (Feng et al, 1993) to form separate arterial functions. These functions (one for each of three

injections) were then corrected for each subject using their own mass, injected activities, and specific activities (at the time of each injection) resulting in the subject specific GIF in units of pmol/mL of MeFWAY.

6.2.3.3.2. Validation of group input function

To test the validity of the GIF, parameter estimates found using the GIF were compared to parameter estimates obtained using the 7 subject specific input functions. Estimates found using the two different input functions were compared using total least squares regression analysis and the mean absolute percentage error (MAPE): $\mathrm{MAPE}=\left(\frac{1}{N}\sum_{n=1}^{N}\left|\frac{\theta_{P(n)}-\theta_{GIF(n)}}{\theta_{P(n)}}\right|\times 100\right)$ where n = 1 to N and N(=7) is the total number of subjects, θ represents the subject's parameter estimate found using the individual input function (θ_P) and GIF (θ_{GIF}).

Additional validation of the group input function included sex-specific comparison of male and female [^{18}F]MeFWAY plasma time courses and comparisons with late venous samples. Sex-based differences were carefully examined in the arterial blood time course and metabolism profile. An analytic function was fit to averaged male (N=3) and female (N=8) [^{18}F]MeFWAY plasma time course curves to allow a comparison of initial fast washout and late washout rates. In studies without arterial data (N=10), venous data was compared to arterial data for the identification of outliers or subjects with drastically different rates of MeFWAY clearance or blood scaling. Venous data, however, was not incorporated into the modeling procedure.

The use of a GIF has the potential to introduce bias in the parameter estimates if it is not an accurate representation of an individual's input function. To explore the extent of bias caused by misrepresentative input functions, an examination of the sensitivity of two GIF characteristics on the outcome parameter estimates was conducted; 1) overall scaling changes in the arterial time course and 2) clearance rate differences of [^{18}F]MeFWAY from the plasma. As implemented, the GIF was calculated by scaling the individual arterial samples by subject mass and injected activity. In these studies, body fat percentage was not taken into account and has the potential to introduce blood scaling errors due to a lack of linearity between blood volume and subject mass. Similarly, the clearance rate of tracer from the individual subjects caused by differences in tracer metabolism could lead to error in the GIF. Simulated error in the group input functions is shown in Figure 6-2 corresponding to either scaling (left) or clearance rate (right) error. The left panel

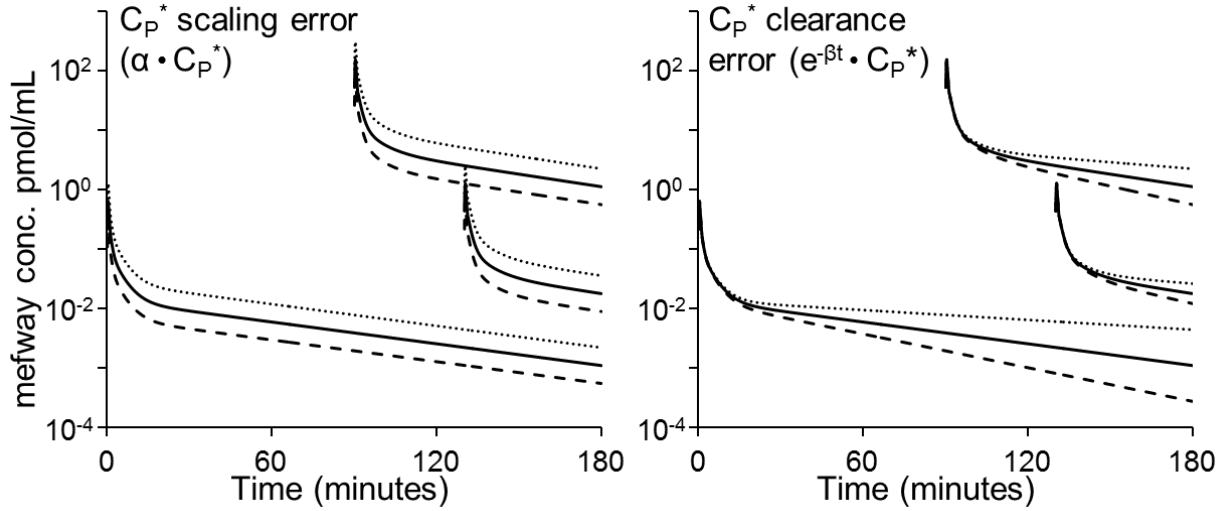

Figure 6-2: Original GIF (solid lines) for injections 1-3 and altered GIFs (dashed and dotted lines) that result from systematic error in scaling of magnitude by α (left) or applying a clearance rate error $e^{-\beta t}$ (right). The dashed and dotted time courses represent the variation in GIF by the application of α or β.

of Figure 6-2 (top) shows the scaling error that applied to the GIF $\left(\alpha \times C^*_{P(i=1-3)}\right)$ where the scaling error (α) ranged between 0.5 – 2.0 representing 50% to 200% of the true value. Figure 4A (top

right panel) also displays the first order clearance error $\left(e^{-\beta t} \times C^{*}_{P(i=1-3)}\right)$ that was applied to the GIF which is similar to methods reported in the literature (Normandin and Morris, 2008). The effects of the input function error on the parameter estimates for V_{ND}, K_{Dapp}, and B_{max} were then examined.

6.2.3.4. Parameter estimation

Compartmental modeling was performed to acquire region specific parameter estimates of receptor density (B_{max}), bidirectional rate constants of tracer across the blood brain barrier K_1 (mL/min/mL) and k_2 (min^{-1}), association rate constant (k_{on}) (mL/pmol/min), and dissociation rate constant (k_{off}) (min^{-1}). Our model did not attempt to measure differences in endogenous 5-HT, which are inherent to k_{on} through the relation:

$$\textbf{(6-1)} \quad k_{on} = (k_{on})^{0} / \left(1 + [5HT] / K_D^{en}\right)$$

where k_{on} represents the association constant in the presence of endogenous 5-HT (as measured in these experiments), $(k_{on})^0$ is the association rate resulting in the absence of endogenous 5-HT, [5-HT] is the synaptic concentration of 5-HT, and K_D^{en} is the equilibrium dissociation constant of 5-HT (Delforge et al., 2001).

A two compartment model was used to account for ligand in free (F) (including nondisplaceably bound) and specifically bound (B) compartments, both in units of pmol/mL. The state equations describing the time dependent molar concentrations in each compartment are given by:

$$\textbf{(6-2)} \quad \frac{dF_i}{dt} = K_1 C^{*}_{p_i} - k_2 F_i + k_{off} B_i - k_{on} F_i \left(B_{max} - \sum_i B_i \right)$$

$$\textbf{(6-3)} \quad \frac{dB_i}{dt} = k_{on} F_i \left(B_{max} - \sum_i B_i \right) - k_{off} B_i$$

where $C_{p_i}^{*}$ represents the GIF for each injection (i = 1 to 3). The time course of the F and B compartment concentrations can then be summed to model the data as acquired by the PET scanner, given by the equation:

$$\textbf{(6-4)}\quad PET_{model}(t)=\frac{1}{t_j-t_{j-1}}\int_{t_{j-1}}^{t_j}\left\{\sum_i sa_i(t)\left[(1-f_V)(F_i(t)+B_i(t))+f_V A_i\right]\right\}dt$$

where t_j represents the end time of each PET frame, $(sa_i(t))$ is the time decaying specific activities, f_v is the fractional blood volume $(f_V = 0.04)$ and A_i is the arterial whole blood concentration.

Compartmental modeling and parameter estimation was performed using COMKAT (Muzic and Cornelius, 2001). Parameter estimates (K_1, k_2, k_{on}, k_{off}, and B_{max}) were made separately for each region (Hp, dACC, Am, RN) and used to calculate the nondisplaceable distribution volume, $V_{ND} = K_1/k_2$ and $K_{Dapp} = k_{off}/k_{on}$. This is distinct from our previous work which assumed K_{Dapp} was constant across all regions. Parameter estimates were obtained by minimizing the least squares objective function (o.f.) between measured ROI PET data (PET_{meas}) and modeled PET data (PET_{model}) over each frame (j), using uniform weighting (w_j), as described:

$$\textbf{(6-5)}\quad o.f.=\sum_{j=1}^{J} w_j\left(PET_{modelj}-PET_{measj}\right)^2$$

Parameter uncertainties were estimated using Monte Carlo methods (similar to: Salinas et al, 2007; Vandehey et al., 2010). In short, noise free PET data was simulated using parameter estimates and $C_{p_i}^{*}$. Gaussian noise realizations (50) were generated and added to the noise free PET data to simulate noise observed in measured PET data. Parameter estimates for the 50 noise realizations were then obtained to acquire coefficients of variation $(CV = 100 \times s.d./mean)$.

6.2.3.5. Estimation of Binding Potential

The nondisplaceable binding potential (BP_{ND}) (Innis et al., 2007) was calculated using radioactive decay corrected data from the first injection duration (high specific activity 90 minute duration). The BP_{ND} was estimated using the multilinear reference tissue model (MRTM) (Ichise et al., 1996) to calculate the distribution volume ratio (DVR). The CB was used as a reference region and BP_{ND} was calculated as: $BP_{ND} = DVR - 1$.

6.2.3.6. Statistical Analysis

The Wilcoxon's rank-sum test was used to test the null hypothesis of no difference between the distribution of the males and females populations. Sex differences were considered significant for *p-values < 0.05 and were checked for multiple comparisons using Holm's method (Holm, 1979). Differences between the treatment (prenatal stress) and control groups were tested using Wilcoxon's rank-sum prior to performing the analysis between males and females. No statistically significant differences were found between the two treatment groups (prenatal stress and controls) for the regions examined and these groups were therefore combined in the statistical model.

6.3. Results

6.3.1. Group input function

The comparison of in vivo binding parameter estimates using C_P^* versus C_P revealed MAPEs of less than 10% in the Hp, dACC, and Am (B_{max}: 7%, 5%, 8%; K_{Dapp}: 7%, 9%, 9%) and slightly higher MAPE in the RN (B_{max}: 15%; K_{Dapp}: 12%). Total least squares regression performed between C_P or C_P* derived estimates of B_{max} and K_{Dapp} over all the reigons are displayed in Figure 6-3, resulting in slopes of 0.95 and 0.97 for B_{max} and K_{Dapp}, respectively.

Male and female separated plasma time courses are shown in Figure 6-4A. No statistically significant differences in [^{18}F]MeFWAY arterial plasma clearance were observed between the

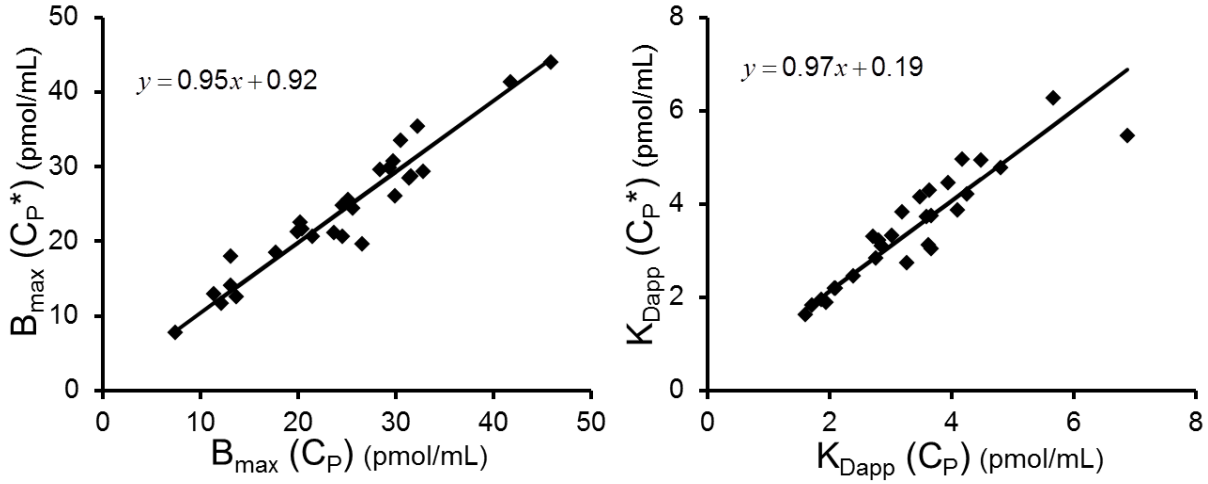

Figure 6-3: Group input function (C_P*) estimates for B_{max} and K_{Dapp} vs individual input (C_p) estimates for B_{max} and K_{Dapp} over all regions.

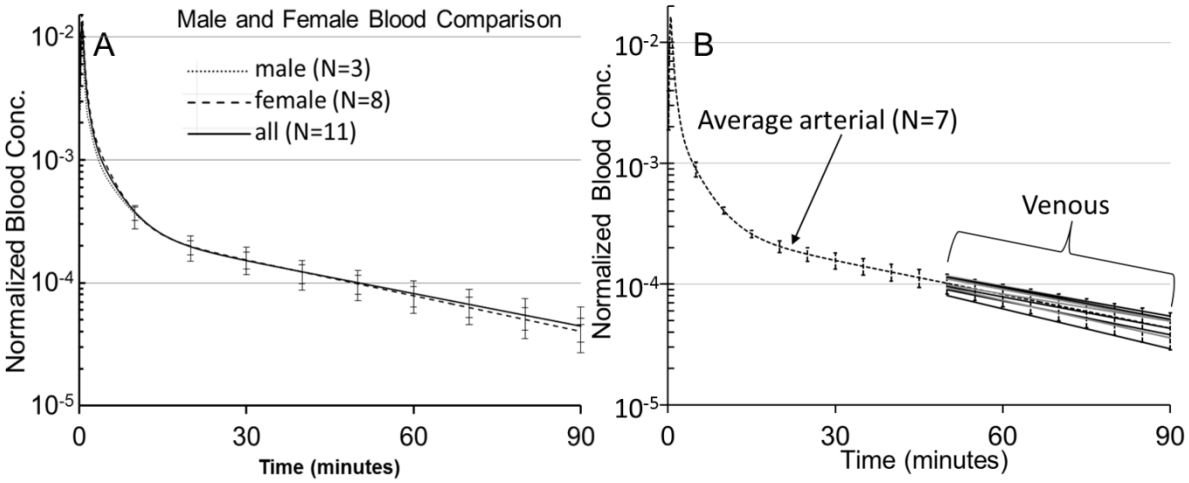

Figure 6-4: (A) Averaged arterial plasma [^{18}F]MeFWAY time courses for injection 1 over male (dotted line), female (dashed line), and all (solid line) subjects. (B) Averaged arterial plasma (dashed line) and individual late venous plasma (solid lines) [^{18}F]MeFWAY time courses for injection 1. Arterial data was fit to a three exponential and venous data was fit to a one exponential function for times 50-90 minutes.

sexes. The separated male and female averaged arterial functions had similar initial, fast components of [^{18}F]MeFWAY clearance $\left(\lambda_1^{male} = 1.7\,\mathrm{min}^{-1}; \lambda_1^{female} = 1.9\,\mathrm{min}^{-1}\right)$. A non-significant difference of <3% in the slow clearance term (λ_3) was observed, indicating similar

slow washout between male and female subjects. A comparison of the late venous plasma [^{18}F]MeFWAY time course with the arterial sampling data is shown in Figure 6-4B. The late (t>50 minutes) venous measured concentrations are generally within the variation seen in arterial time courses, indicating no significant outliers.

6.3.2. Male and female binding parameter estimates

The results of the sex-based differences for K_{Dapp}, B_{max}, and BP_{ND} are shown in Table 6-2 and graphically presented in Figure 6-5. Median K_{Dapp} values were lower for female subjects in all regions. Significant sex differences in K_{Dapp} were found in: Hp (-32%, p=0.014), Am (-38%, p=0.020), and RN (-37%, p=0.007) and a trend was seen in the dACC (-27%, p=0.06). In all regions, B_{max} was higher in males than females. However, the sex differences in B_{max} measurements were only significant in the Hp with a difference of -29% (p=0.027). The BP_{ND} measure showed significant differences in the Am (14%, p=0.047) and RN (23%, p=0.014), however, this was not found in the Hp or dACC. Across the regions, the average intersubject CV(=s.d./mean) was 31%, 26%, and 21% for K_{Dapp}, B_{max}, and BP_{ND}, respectively, suggesting K_{Dapp} and B_{max} show only slightly higher variation than BP_{ND}. Uncertainties in parameter estimates found using Monte Carlo methods, given as CV, were 5.7% and 6.6% for K_{Dapp} and B_{max}, respectively, averaged across all regions.

Table 6-2: Regional results for KD_{app}, B_{max}, and BP_{ND}

		male (N=6; l/l=3; s-carriers=3)	female (N=11; l/l=7; s-carriers=4)		
Parameter	ROI	median (IQR)	median (IQR)	difference	p-value
K_{Dapp} (pmol/mL)	Hp	4.8 (1.3)	3.5 (1.5)	-32%	** 0.014
	dACC	4.2 (1.3)	3.2 (1.4)	-27%	0.061
	Am	4.1 (0.6)	2.8 (0.9)	-38%	** 0.020
	RN	5.9 (1.4)	4.1 (1.3)	-37%	** 0.007
B_{max} (pmol/mL)	Hp	38.3 (7.2)	28.4 (7.5)	-29%	* 0.027
	dACC	34.4 (16.9)	30.3 (6.0)	-13%	0.574
	Am	25.8 (7.8)	21.0 (4.9)	-20%	0.182
	RN	33.2 (10.9)	23.9 (8.2)	-33%	0.098
BP_{ND}	Hp	3.9 (0.9)	4.8 (1.1)	19%	0.122
	dACC	3.9 (1.0)	4.8 (1.2)	22%	0.149
	Am	4.0 (0.6)	4.7 (0.9)	14%	* 0.047
	RN	2.7 (0.5)	3.4 (0.8)	23%	* 0.014

Data are median and interquartile range (IQR) for each ROI by parameter and sex. Percent differences between male and female groups along with Wilcoxon's rank-sum adjusted p-values are shown. *p-values < 0.05 are considered statistically significant. **p-values survived adjustment using Holm's procedure. hippocampus (Hp), dorsal anterior cingulate cortex (dACC), amygdala (Am), raphe nuclei (RN)

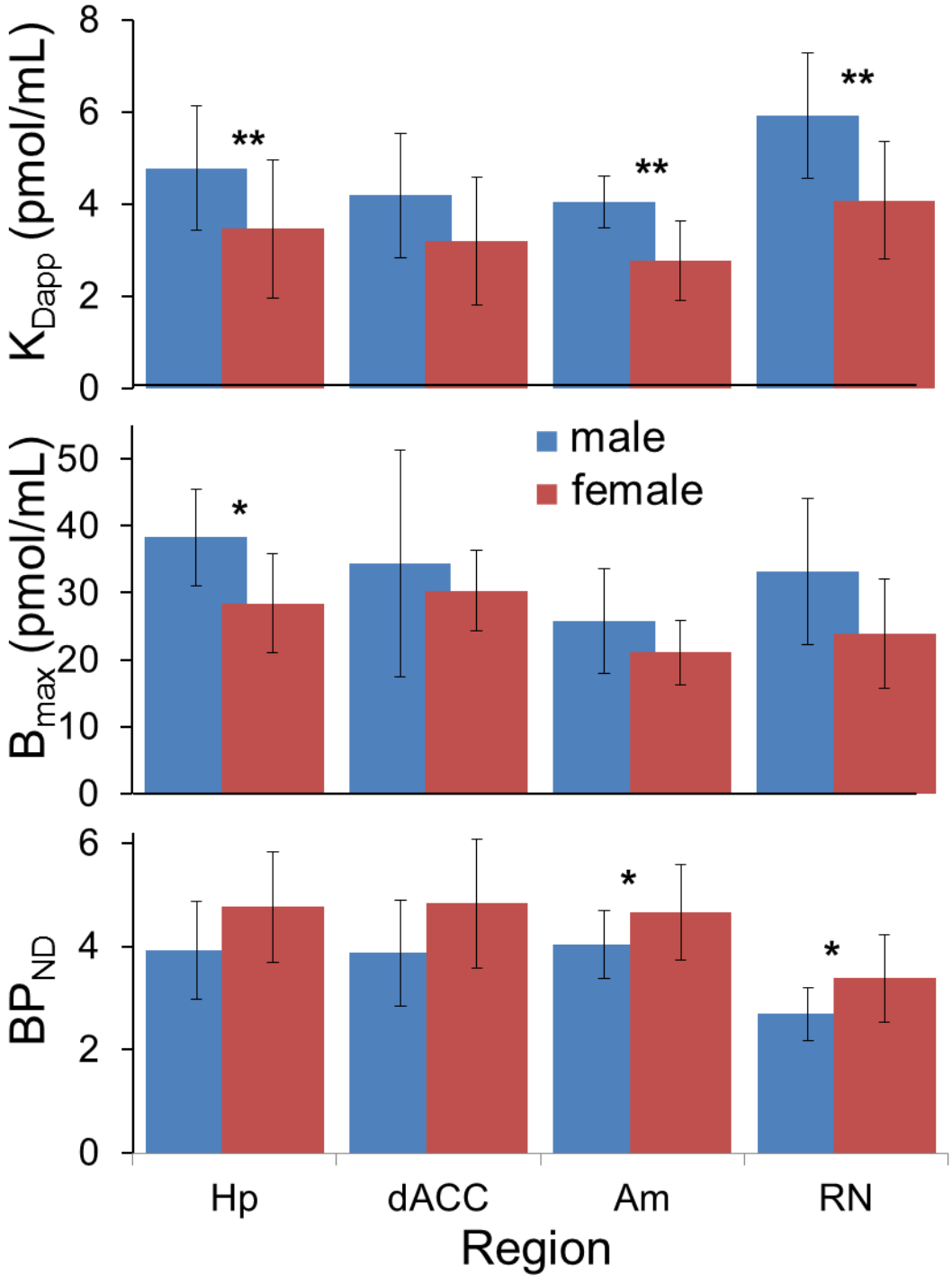

Figure 6-5: K_{Dapp}, B_{max}, and BP_{ND} medians and interquartile ranges for male and female subjects in the hippocampus (Hp), dorsal anterior cingulate cortex (dACC), amygdala (AM), and raphe nuclei (RN).

6.4. Discussion

The 5-HT_{1A} receptor plays an important role in regulating the 5-HT system. Sex-dependent variations in the 5-HT_{1A} system may be a source of the functional differences in the 5-HT system between males and females. In this work, sex-specific differences of in vivo 5-HT_{1A} receptor density (B_{max}), ligand-receptor dissociation constant (K_{Dapp}), and [^{18}F]MeFWAY BP_{ND} are reported. Knowledge of these characteristics and the methodologies developed for their measurement may ultimately aid in examining the underlying causes of 5-HT_{1A} dysfunction and their contribution to neuropsychiatric illnesses.

6.4.1. Considerations in B_{max} and K_{Dapp} Estimation

A significant saturation of receptors must be achieved to effectively uncouple the binding parameters k_{on} and B_{max} (Salinas et al, 2007; Wooten et al., 2012). Our previous work indicated receptor occupancy of ~75% was optimal for uncoupling the binding parameters, corresponding to a dose of approximately 12 nmol/kg of MeFWAY. In this study, roughly equal doses of MeFWAY were given to the male and female subjects in injection 2, 12 ± 4 and 12 ± 5 nmol/kg, respectively.

The estimated uncertainties derived from Monte Carlo methods in our previous work were 6% for K_{Dapp} and 3-4% for B_{max} (Wooten et al., 2012). The estimated uncertainties in K_{Dapp} were similar in this work, however, uncertainties in B_{max} were slightly higher at 6.6% due to the estimation strategies implemented. In our previous work, the parameters were estimated using a constant K_{Dapp} across regions, thus constraining the ratio k_{on} and k_{off} in all brain areas (Wooten et al., 2012). This constraint was enforced to reduce the number of estimated parameters and increase identifiability in the lower receptor density regions. Because the focus of this current

work was to compare both 5-HT_{1A} receptor density and the effects of endogenous 5-HT competition between sexes, the constraint of a constant K_{Dapp} throughout brain regions was removed. As a result, the low 5-HT_{1A} receptor density regions were not analyzed because identifiability of B_{max} and K_{Dapp} was limited in these regions. The K_1, k_2, k_{on}, k_{off}, and B_{max} parameters could be accurately identified in the high binding regions to provide regionally independent measures.

In Chapter 5 a lack of correlation between [^{18}F]MeFWAY BP_{ND} and 5-HT_{1A} B_{max} indicating BP_{ND} is not necessarily an accurate proxy of B_{max} alone (see also Wooten et al., 2012). Similarly in this work, no correlation was found (in any ROI) between B_{max} and BP_{ND} across all of the subjects. Correlations, however, were found between reference region based BP_{ND} and the compartmental model based BP: $\left(BP_{model} = B_{max}/K_{Dapp}\right)$ across all subjects in all ROIs. Further, no correlation was found between K_{Dapp} and B_{max} when examined within the male and female groups separately. In agreement with our earlier findings, these results suggest [^{18}F]MeFWAY BP_{ND} is a representative metric for B_{max}/K_D.

MI studies alter the number of receptors available for binding, permitting an uncoupling of k_{on} and B_{max}. Figure 6-6 illustrates the sensitivity of the MI technique to variations in the radiotracer kinetic behavior. Simulations were performed to examine the effects of changes in K_{Dapp} (via k_{on} and k_{off}) and B_{max} on the PET response curves. Our results indicated sex-specific differences in K_{Dapp} of $\geq$ 30%, which could be the consequence of a ± 30% difference in either k_{on}, k_{off} or a combination of the two. As seen in the figure, a 30% reduction in k_{on} is indistinguishable from a 30% reduction in B_{max} during the first injection period (time = 0-90 minutes). It is not until the second injection of partial saturating dose (time > 90 minutes) that k_{on} and B_{max} become distinguishable. The first 90 minutes of data illustrate the complete coupling of k_{on} and B_{max},

similar to all high-specific activity single injection PET studies. A partial saturating dose of MeFWAY in the second injection changes the number of receptors available for binding as seen

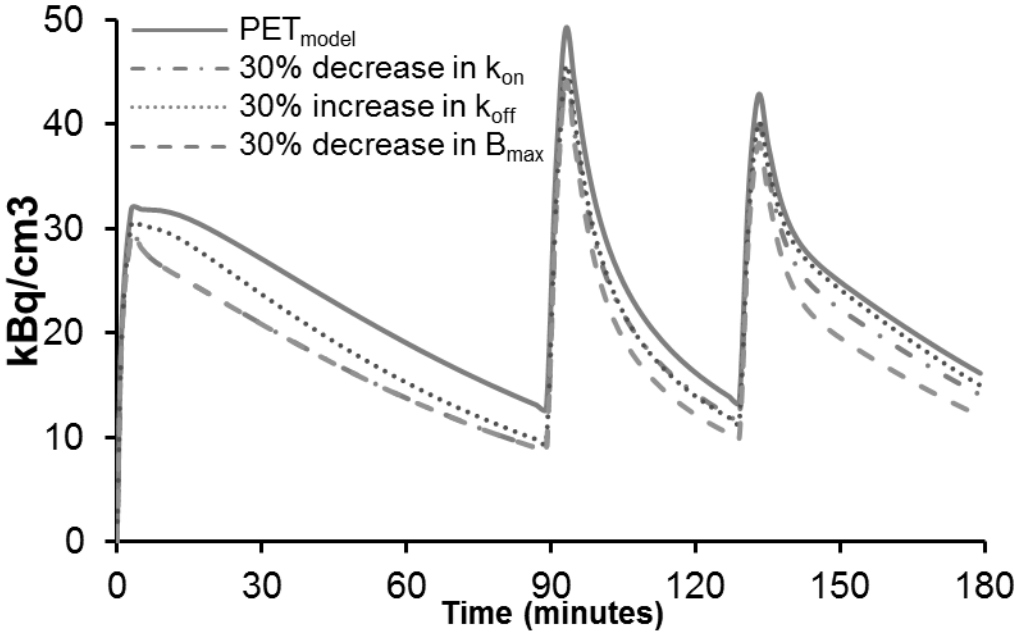

Figure 6-6: Simulated time activity curves (TACs) in the hippocampus. The TACs illustrate situations of no change in parameters (solid line), 30% decrease in k_{on} (dash dotted line) and B_{max} (dashed line), and 30% increase in k_{off} (dotted line).

in the curves for time greater than 90 minutes. After injection 3 (high specific activity), the number of receptors available for binding are beginning to recover as illustrated by the decreased slope in the PET curves. The increase in k_{off} is observed immediately in the first injection period as it is distinguishable from PET_{model} because it represents a faster dissociation rate after the first bolus injection.

6.4.2. Sex differences in 5-HT_{1A} B_{max}, K_{Dapp}, and BP_{ND}

These results with [^{18}F]MeFWAY are similar to previously reported studies finding higher BP_{ND} values in female subjects (Parsey et al, 2002; Jovanovic et al, 2008). However, the higher BP_{ND} was not due to larger B_{max} values in female subjects, as could be suggested by the relation:

$BP_{ND} \propto B_{max}/K_{Dapp}$. Instead, our results indicate K_{Dapp} is the primary source of the higher BP_{ND} for female subjects. Our results are similar to a previous study using a two-injection scatchard method which revealed higher B_{max} and K_D estimates in male subjects, however, due to high variance across the subjects the differences did not reach significance (Spinelli et al, 2010). Knowing that K_{Dapp} is a function of both k_{on} and k_{off}, further examination of these parameters revealed female subjects to have significantly higher k_{on} than male subjects in all areas (Hp: p=0.005; dACC: p=0.047; Am: p=0.002; RN: p=0.005) and no significant differences in k_{off} in any brain regions. Higher k_{on} estimates in female subjects could be due to higher receptor-ligand affinity or lower levels of endogenous serotonin competition at the receptor site (equation 1) when compared to male subjects. However, previous studies using [^{11}C]WAY-100635 to examine changes in 5-HT levels have been inconclusive (Paterson et al, 2010). Because the in vivo kinetics of [^{18}F]MeFWAY and [^{11}C]WAY-100635 are similar (Wooten et al, 2011a), we cannot conclude that the differences are exclusively due to endogenous 5-HT competition. Reported extracellular basal levels of 5-HT as measured with microdialysis are 0.04-3.9 nM (Paterson et al, 2010). Interpolating the inhibition curve of [^{18}F]MeFWAY (Saigal et al, 2006), a 4 nM concentration of serotonin would cause a roughly 10% reduction in [^{18}F]MeFWAY binding. Additionally, lower concentrations of 5-HT at the 5-HT_{1A} autoreceptor sites in the RN should result in higher 5-HT synthesis. Studies designed to measure effects in changes in endogenous 5-HT on binding of [^{18}F]MeFWAY are needed to fully characterize the sensitivity of [^{18}F]MeFWAY to these changes and to identify the mechanism behind these sex-based differences in K_{Dapp}. Although male and female differences in arterial [^{18}F]MeFWAY clearance were not observed in our subjects, the possibility of effects from sex based differences in the

plasma free fraction (f_P) or tissue free fraction (f_{ND}) on these results must also be acknowledged. Further studies will be needed to examine differences in f_P between male and female subjects.

6.4.3. Validation of the group input function for estimation of B_{max} and K_{Dapp}

The high level of consistency of [^{18}F]MeFWAY plasma time course observed in the initial subjects led to exploration of the use of a group input function. Analysis showed that use of the GIF in place of an individual subject's input function yielded reliable results as indicated by the low MAPE and the high consistency of parameter estimates shown in Figure 6-3. The relatively small y-intercept and slopes close to unity in Figure 6-3 indicate high levels of uniformity between the two methods. Although the y-intercept of B_{max} was within the uncertainty of the fit, the y-intercept of K_{Dapp} wasn't, indicating a small bias caused by the GIF. Additionally, male and female [^{18}F]MeFWAY plasma time course exhibited similar profies. A non-significant difference of <3% in the slow clearance term (λ_3) was observed, indicating similar slow washout between male and female subjects. By simulating comparable changes in the arterial input function, it was found that a 3% percent change in λ_3 results in approximately a 1% change in B_{max} and a 2% change in K_{Dapp}.

Effects of changes in scaling and clearance rates in the GIF are shown in Figure 6-7. Errors from scaling the GIF have a large effect on V_{ND}, but negligible influence on K_{Dapp} and B_{max}, whereas inaccuracies in the clearance rate of the GIF have a more profound effect on K_{Dapp} and B_{max} estimates. For the 7 subjects reported herein, the average parent [^{18}F]MeFWAY fraction in plasma at 90 minutes was 15%, and ranged from 10% to 22% (represented by the dashed lines in Figure 6-7). This range of clearance error would lead to a -7% to +3% error in K_{Dapp} and -3% to +6% error in B_{max}. The scaling and clearance terms do not address all of the potential uncertainty

in the GIF, however, these analyses illustrate that the variations present in our measured input functions do not propagate into large uncertainties in our outcome measures of K_{Dapp} and B_{max}.

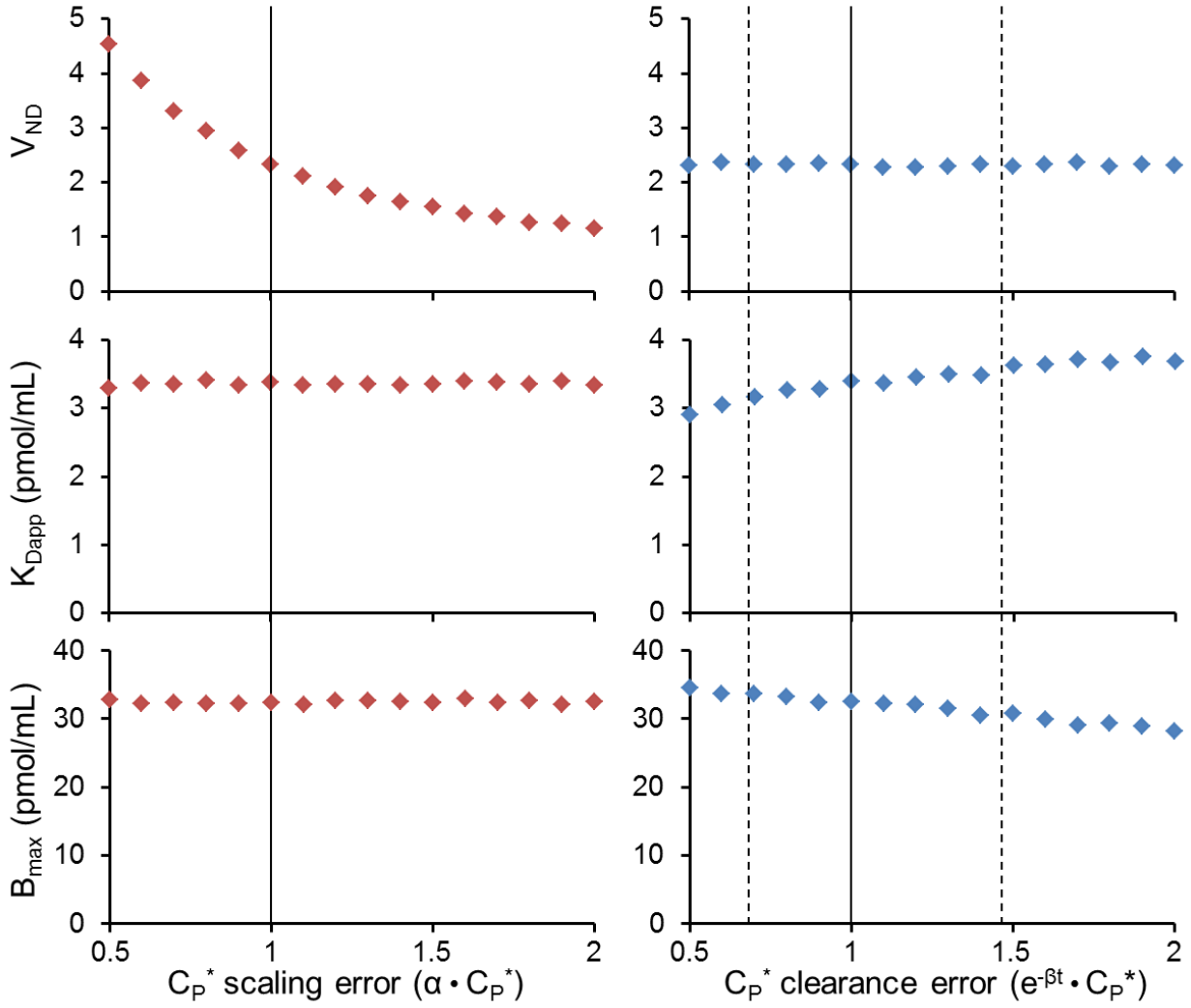

Figure 6-7: Effects on V_{ND} (top row), K_{Dapp} (middle row), and B_{max} (bottom row) caused by the simulated error in the GIF. α was varied between 0.5 – 2.0 and the clearance rate ($e^{-\beta t}$) between 0.5 – 2.0 at t = 90 minutes. The vertical solid lines at 1 represents the original GIF parameter estimates and the dashed lines in the right column represents the range of variation in parent [^{18}F]MeFWAY radioactivity as observed in the subjects in this study.

6.5. Summary

This chapter presents measurements of K_{Dapp}, B_{max}, and BP_{ND} in both male and female rhesus subjects to allow parameter comparisons between the sexes. Results indicate that differences in BP_{ND} are primarily due to differences in K_{Dapp}, which could be an effect of radioligand receptor affinity or sex-specific differences in 5-HT levels. Further endogenous 5-HT depletion or competition studies are needed to determine its effect on the measurement of K_{Dapp} B_{max}, and BP_{ND}. However, this work further demonstrates [^{18}F]MeFWAY's utility for measuring 5-HT_{1A} receptor density and affinity. Moreover, this study suggests measurements of B_{max} and K_{Dapp} separately are more sensitive to detecting changes and group differences in 5-HT_{1A} function over binding potential.

6.6. References

Arango, V., Underwood, M.D., Gubbi, A. V, Mann, J.J., 1995. Localized alterations in pre- and postsynaptic serotonin binding sites in the ventrolateral prefrontal cortex of suicide victims. Brain research 688, 121–33.

Biver, F., Lotstra, F., Monclus, M., Wikler, D., Damhaut, P., Mendlewicz, J., Goldman, S., 1996. Sex difference in 5-HT_2 receptor in the living human brain. Neuroscience Letters 204, 25–8.

Cahill, L., 2006. Why sex matters for neuroscience. Nature Reviews. Neuroscience 7, 477–84.

Cosgrove, K.P., Mazure, C.M., Staley, J.K., 2007. Evolving Knowledge of Sex Differences in Brain Structure, Function and Chemistry. Biological psychiatry 62, 847–55.

Delforge, J., Bottlaender, M., Pappata, S., Loc'h, C., Syrota, A., 2001. Absolute quantification by positron emission tomography of the endogenous ligand. Journal of Cerebral Blood Flow and Metabolism 21, 613–30.

Feng, D., Huang, S.C., Wang, X., 1993. Models for computer simulation studies of input functions for tracer kinetic modeling with positron emission tomography. International Journal of Bio-Medical Computing 32, 95–110.

Holm, S., 1979. A simple sequentially rejective multiple test procedure. Scand J Statist, 6, 65–70.

Ichise, M., Ballinger, J.R., Golan, H., Vines, D., Luong, A., Tsai, S., Kung, H.F., 1996. Noninvasive quantification of dopamine D_2 receptors with iodine-123-IBF SPECT. Journal of Nuclear Medicine 37, 513–520.

Innis, R.B., Cunningham, V.J., Delforge, J., Fujita, M., Gjedde, A., Gunn, R.N., Holden, J., Houle, S., Huang, S.-C., Ichise, M., Iida, H., Ito, H., Kimura, Y., Koeppe, R.A., Knudsen, G.M., Knuuti, J., Lammertsma, A.A., Laruelle, M., Logan, J., Maguire, R.P., Mintun, M.A., Morris, E.D., Parsey, R., Price, J.C., Slifstein, M., Sossi, V., Suhara, T., Votaw, J.R., Wong, D.F., Carson, R.E., 2007. Consensus nomenclature for in vivo imaging of reversibly binding radioligands. Journal of Cerebral Blood Flow and Metabolism 27, 1533–9.

Jovanovic, H., Lundberg, J., Karlsson, P., Cerin, A., Saijo, T., Varrone, A., Halldin, C., Nordström, A.-L., 2008. Sex differences in the serotonin$_{1A}$ receptor and serotonin transporter binding in the human brain measured by PET. NeuroImage 39, 1408–19.

Dillon, K.A., Gross-Isseroff, R., Israeli, M., Biegon, A., 1991. Autoradiographic analysis of serotonin 5-HT_{1A} receptor binding in the human brain postmortem: effects of age and alcohol. Brain Research 554, 56–64.

Maron, E., Tõru, I., Hirvonen, J., Tuominen, L., Lumme, V., Vasar, V., Shlik, J., Nutt, D.J., Helin, S., Någren, K., Tiihonen, J., Hietala, J., 2011. Gender differences in brain serotonin transporter availability in panic disorder. Journal of Psychopharmacology 25, 952–59.

Matsubara, S., Arora, R.C., Meltzer, H.Y., 1991. Serotonergic measures in suicide brain: 5-HT_{1A} binding sites in frontal cortex of suicide victims. Journal of Neural Transmission. General Section 85, 181–94.

McLaren, D.G., Kosmatka, K.J., Oakes, T.R., Kroenke, C.D., Kohama, S.G., Matochik, J.A., Ingram, D.K., Johnson, S.C., 2009. A population-average MRI-based atlas collection of the rhesus macaque. NeuroImage 45, 52–9.

Meltzer, C.C., Drevets, W.C., Price, J.C., Mathis, C.A., Lopresti, B., Greer, P.J., Villemagne, V.L., Holt, D., Mason, N.S., Houck, P.R., Reynolds III, C.F., DeKosky, S.T., 2001. Gender-specific aging effects on the serotonin$_{1A}$ receptor. Brain Research 895, 9–17.

Muzic, R.F., Cornelius, S., 2001. COMKAT: Compartment model kinetic analysis tool. Journal of Nuclear Medicine 42, 636–45.

Normandin, M.D., Morris, E.D., 2008. Estimating neurotransmitter kinetics with ntPET: a simulation study of temporal precision and effects of biased data. NeuroImage 39, 1162–79.

Ortiz, J., Artigas, F., Gelpí, E., 1988. Serotonergic status in human blood. Life Sciences 43, 983–90.

Palego L, Marazziti D, Rossi A, Giannaccini G, Naccarato AG, Lucacchini A, Cassano GB, 1997. Apparent absence of aging and gender effects on serotonin$_{1A}$ receptors in human neocortex and hippocampus. Brain Research 758, 26–32.

Parsey, R. V, Oquendo, M.A., Simpson, N.R., Ogden, R.T., Van Heertum, R., Arango, V., Mann, J.J., 2002. Effects of sex, age, and aggressive traits in man on brain serotonin 5-HT1A receptor binding potential measured by PET using [^{11}C]WAY-100635. Brain Research 954, 173–182.

Paterson, L.M., Tyacke, R.J., Nutt, D.J., Knudsen, G.M., 2010. Measuring endogenous 5-HT release by emission tomography: promises and pitfalls. J. Cereb. Blood Flow Metab. 30, 1682–1706.

Paxinos, G., 2009. The Rhesus Monkey Brain: In Stereotaxic Coordinates. Academic Press.

Nishizawa, S., Benkelfat, C., Young, S.N., Leyton, M., Mzengeza, S., de Montigny, C., Blier, P., Diksic, M., 1997. Differences between males and females in rates of serotonin synthesis in human brain. PNAS 94, 5308–13.

Salinas, C., Muzic, R.F.J., Ernsberger, P., Saidel, G.M., 2007. Robust experiment design for estimating myocardial beta adrenergic receptor concentration using PET. Medical Physics 34, 151–65.

Schneider, M.L., Roughton, E.C., Koehler, A.J., Lubach, G.R., 1999. Growth and development following prenatal stress exposure in primates: an examination of ontogenetic vulnerability. Child Development 70, 263–74.

Spinelli, S., Chefer, S., Carson, R.E., Jagoda, E., Lang, L., Heilig, M., Barr, C.S., Suomi, S.J., Higley, J.D., Stein, E.A., 2010. Effects of early-life stress on serotonin$_{1A}$ receptors in juvenile Rhesus monkeys measured by positron emission tomography. Biological Psychiatry 67, 1146–1153.

Tai, C., Chatziioannou, A., Siegel, S., Young, J., Newport, D., Goble, R.N., Nutt, R.E., Cherry, S.R., 2001. Performance evaluation of the microPET P4: a PET system dedicated to animal imaging. Physics in Medicine and Biology 46, 1845–62.

Vandehey, N.T., Moirano, J.M., Converse, A.K., Holden, J.E., Mukherjee, J., Murali, D., Nickles, R.J., Davidson, R.J., Schneider, M.L., Christian, B.T., 2010. High-affinity dopamine D_2/D_3 PET radioligands ^{18}F-fallypride and ^{11}C-FLB457: A comparison of kinetics in extrastriatal regions using a multiple-injection protocol. Journal of Cerebral Blood Flow and Metabolism 30, 994–1007.

Wooten, D.W., Hillmer, A.T., Murali, D., Barnhart, T.E., Schneider, M.L., Mukherjee, J., Christian, B.T., 2011. An in vivo comparison of *cis*- and *trans*-[^{18}F]MeFWAY in the nonhuman primate. Nuclear Medicine and Biology 38, 925–32.

Wooten, D.W., Hillmer, A.T., Moirano, J.M., Ahlers, E.O., Slesarev, M., Barnhart, T.E., Mukherjee, J., Schneider, M.L., Christian, B.T., 2012. Measurement of 5-HT$_{1A}$ receptor density and in-vivo binding parameters of [^{18}F]MeFWAY in the nonhuman primate. Journal of Cerebral Blood Flow and Metabolism 32, 1546–58.

Wooten, D.W., Moraino, J.D., Hillmer, A.T., Engle, J.W., Dejesus, O.J., Murali, D., Barnhart, T.E., Nickles, R.J., Davidson, R.J., Schneider, M.L., Mukherjee, J., Christian, B.T., 2011. In vivo kinetics of [^{18}F]MEFWAY: a comparison with [^{11}C]WAY100635 and [^{18}F]MPPF in the nonhuman primate. Synapse 65, 592–600.

Y. Sakai, M. Nishikawa, M. Leyton, C. Benkelfat, S.N. Young, M. Diksic, 2006. Cortical trapping of α-[11C]methyl-l-tryptophan, an index of serotonin synthesis, is lower in females than males. NeuroImage 33, 815–24.

Chapter 7 Conclusions

The work presented in this thesis focused on the development of tools and techniques to study the 5-HT_{1A} system using PET. The techniques of 5-HT_{1A} assay developed will assist in future work examining the fundamental characteristics of 5-HT_{1A} expression and its influence on functions of the 5-HT system. Additionally, [^{18}F]MeFWAY will assist in the characterization of the 5-HT_{1A} system's role in neuropsychiatric illness.

The characterization and development of [^{18}F]MeFWAY for in vivo measurement of 5-HT_{1A} expression was performed over multiple experiments. First, *trans*-[^{18}F]MeFWAY was compared with two other commonly used 5-HT_{1A} PET antagonist to validate its use in PET studies. The validation studies revealed that [^{18}F]MeFWAY had similar in vivo kinetics to the commonly used [^{11}C]WAY-100635 and higher binding potentials than [^{18}F]MPPF. Furthermore, these studies established [^{18}F]MeFWAY's potential for use in PET studies as a substitute of [^{11}C]WAY-100635. Next, 4-*trans*-[^{18}F]MeFWAY, 4-*cis*-[^{18}F]MeFWAY, and 3-[^{18}F]MeFWAY were examined to allow a comparison of their kinetic properties. The results revealed that 4-*cis*-[^{18}F]MeFWAY and 3-[^{18}F]MeFWAY have lower affinity than 4-*trans*-[^{18}F]MeFWAY, however, both suffer from a lower binding potential. A 5-HT_{1A} radioligand with lower affinity may be susceptible to changes in endogenous 5-HT concentrations providing a useful tool to test pharmaceuticals that influence 5-HT levels. Next, MI studies were developed to estimate 5-HT_{1A} B_{max} and other kinetic parameters of [^{18}F]MeFWAY beyond a simple binding potential estimate. The studies showed that [^{18}F]MeFWAY could be used in properly designed MI studies to make high precision in vivo estimates of 5-HT_{1A} B_{max}. Studies such as these allow an examination of pathologies inherent to either B_{max} or affinity independent from one another. Finally, the use of a group input function was validated for the measurement of 5-HT_{1A} B_{max} and [^{18}F]MeFWAY

K_{Dapp} in a cohort of rhesus monkeys to allow an examination of sex-specific differences in 5-HT_{1A} B_{max} and K_{Dapp}. The results indicated that high female binding potentials found in previously reported literature were due to affinity effects, possibly a result of endogenous 5-HT competition, and not higher B_{max} in female subjects. In any case, these studies suggest measurements of B_{max} and K_{Dapp} separately are more sensitive to detecting changes and group differences in 5-HT_{1A} function.

The similar in vivo kinetics of [^{18}F]MeFWAY and [^{11}C]WAY-100635 provide neuro-PET researchers with an excellent alternative to the commonly used [^{11}C]WAY-100635. With the preliminary analysis of [^{18}F]MeFWAY complete, the next step is to move [^{18}F]MeFWAY PET imaging into humans. Preliminary biodistribution studies in rats have already been performed using [^{18}F]MeFWAY showing biodistribution is similar to [^{11}C]WAY-100635 leading to an injectable dose, limited by dosimetry, of around 1500 MBq (40 mCi) of [^{18}F]MeFWAY (Constantinescu et al, Mol. Imaging Biol., 2013). [^{18}F]MeFWAY would provide many advantages over [^{11}C]WAY-100635. First, the one-step radiochemistry of [^{18}F]MeFWAY is much simpler than the multi-step radiosynthesis of [^{11}C]WAY-100635. Next, the long radioactive half-life of [^{18}F]MeFWAY provides the benefit of higher counting statistics toward the end of a PET scanning procedure. Additionally, the longer half-life also offers the opportunity of distribution to multiple PET imaging sites from single batch synthesis. These characteristics make [^{18}F]MeFWAY advantageous over [^{11}C]WAY-100635 for use in human research for the study of the involvement of gene, environment, sex, and neuropsychiatric illness on function of the 5-HT system.

Preliminary work has been performed to examine the in vivo kinetics of 4-*cis*-[^{18}F]MeFWAY and 3-[^{18}F]MeFWAY. The low affinity of 4-*cis*- and 3- [^{18}F]MeFWAY are desired

characteristics in radiotracers used for examination of changes in endogenous neurotransmitter levels. Additional studies are needed with both 4-*cis*- and 3- [^{18}F]MeFWAY to determine if binding of these radioligands to 5-HT$_{1A}$ receptors are sensitive to changes in endogenous 5-HT concentrations altered by pharmaceutical manipulation; e.g., (±)fenfluramine.

Finally, with the dawn of PET/MR scanners, it is now possible to obtain quantitative physiological information provided by PET simultaneously with structural and functional information provided by MRI and fMRI. A particularly exciting use of PET/MR imaging is in neurology such as imaging 5-HT function. Beyond the advantages of the structural regional definitions provided by the MR T1 image, fMRI could be used synergistically with PET to measure effects of drug interactions. Studies using radiotracers such as 3- and 4-*cis*-[^{18}F]MeFWAY that possess the characteristics necessary for detection of changes in endogenous neurotransmitter concentration would gain benefit from temporal resolution of drug interaction provided by fMRI. Additionally, techniques such as diffusion tensor imaging (DTI) MRI which provide information about connectivity in the brain may combine with PET receptor imaging with radiotracers such as [^{18}F]MeFWAY to advance knowledge of projections within the brain. For example, 5-HT binding to 5-HT$_{1A}$ autoreceptors in the raphe nuclei is responsible for reduced 5-HT synthesis in the cortex. Information of disruptions in connectivity between the raphe nuclei and cortical regions provided by DTI may offer insight into illnesses associated with 5-HT synthesis. These are just a few of the advancements for studying the 5-HT system provided by simultaneous PET/MR, however, the opportunities are widespread.